Disturbance Robustness Measures and Wrench-Feasibile Workspace Generation Techniques for Cable-Driven Robots

A Thesis
Presented to
The Academic Faculty

by

Paul M. Bosscher

In Partial Fulfillment
of the Requirements for the Degree of
Doctor of Philosophy in Mechanical Engineering

George W. Woodruff School of Mechanical Engineering
Georgia Institute of Technology
November 2004

Disturbance Robustness Measures and Wrench-Feasibile Workspace Generation Techniques for Cable-Driven Robots

Approved by:

Dr. Imme Ebert-Uphoff, Advisor

Dr. Magnus Egerstedt

Dr. Harvey Lipkin

Dr. Jarek Rossignac

Dr. William Singhose

Date Approved: 17 November 2004

ACKNOWLEDGEMENTS

First of all I would like to thank my wife Elise for her unfailing encouragement, love and patience. Thank you for all the times you pretended to understand what I was talking about...this thesis could not have happened without your support. I would like to thank my family for loving me whether I succeed or not. Your support of me is a true constant in my life. Most of all I thank God for blessing me with this opportunity and putting the right people in my life to make this possible.

I would like to thank my advisor, Dr. Imme Ebert-Uphoff. Her ideas, feedback and guidance kept me focused and challenged me to always push to see what else can be accomplished. I would like to thank my other committee members, Dr. Harvey Lipkin, Dr. William Singhose, Dr. Magnus Egerstedt and Dr. Jarek Rossignac, for their valuable input on this thesis, with a special thank-you to Dr. Lipkin for his suggestions and opinions on wrench norms.

Lastly, I would like to thank my current and former RML labmates: Phil Voglewede, Kris Kozak, Anh Dang, Sebastien Wolff and Andrew Riechel. They have been some of my best colleagues, critics and friends.

This research was financially supported by a National Defense Science and Engineering Graduate (NDSEG) Fellowship.

TABLE OF CONTENTS

LIST OF TABLES

LIST OF FIGURES

LIST OF SYMBOLS

$\mathbf{0}^{a\times b}$	a by b zero matrix
$\boldsymbol{A}$	Intermediate space mapping matrix for twists
A_{avail}	Available Acceleration Set
$AE(\cdot)$	Acceleration energy
$\overline{a}$	Vector of linear acceleration of the end-effector
$\hat{a}$	Vector of generalized acceleration of the end-effector
a, b, c, d	Constants
$\boldsymbol{B}$	Intermediate space mapping matrix for wrenches
$\overline{c}_i$	Vector from G to the attachment point of cable i on the end-effector
C	Set of critical wrenches
$\hat{C}$	Set of critical wrenches mapped to the intermediate space
CW	Cable wrench set
$\overline{F}_{ee}$	Force at the end effector
$\hat{f}$	Vector of generalized force applied to the end-effector
G	Center of gravity
$\overline{g}$	Gravitational vector
$\boldsymbol{I}^{a\times b}$	a by b identity matrix
$\boldsymbol{In}$	Rotational inertia matrix
i, j, k	Indices
$\boldsymbol{J}$	Jacobian matrix
$KE(\cdot)$	Kinetic energy
$\boldsymbol{M}$	Inertia (mass) matrix
$\overline{M}_{ee}$	Moment at the end-effector
m	Mass of the end-effector
NW_{avail}	Available Net Wrench Set
$\widehat{NW}_{avail}$	Available Net Wrench Set mapped to the intermediate space

NW_{req}	Required Net Wrench Set
$\widehat{NW}_{req}$	Required Net Wrench Set mapped to the intermediate space
n	Dimension of a manipulator's task space
p	Number of cables attached to the end-effector
$\mathbb{P}$	Power
$\mathcal{P}$	The set of principal twists
$\dot{q}_i$	Velocity of cable i being reeled in or out
$\mathcal{R}$	Disturbance robustness measure
$\mathcal{R}_i$	Impulsive disturbance robustness measure
$\mathcal{R}_s$	Static disturbance robustness measure
$\boldsymbol{R}$	Rotation matrix
t	Time
t_i	Cable tension
$\overline{t}$	Vector of cable tensions
U	Set of unconstrained twists
$\overline{u}$	Unit vector along a cable
WFW	Wrench-Feasible Workspace
$\overline{v}$	Vector of translational velocity of the end-effector
$\hat{v}$	Vector of generalized velocity of the end-effector
x, y, z	Cartesian coordinates
$\overline{\alpha}$	Vector of angular acceleration of the end-effector
β, κ	Constants
Δ	Small increment of change
ψ, θ, ϕ	End effector Euler angles
ρ	Radius of gyration
$\overline{\omega}$	Vector of angular velocity of the end-effector
$\$^a$	Acceleration screw vector in axis coordinates
$\$^t$	Twist (screw) vector in axis coordinates

$\$^w$	Wrench (screw) vector in ray coordinates
$\cdot$	Dot product
$\oplus$	Minkowski sum
$\|\| \cdot \|\|$	Euclidian norm
$\|\| \cdot \|\|_a$	Acceleration energy norm

SUMMARY

Cable robots are a type of robotic manipulator that has recently attracted interest for large workspace manipulation tasks. Cable robots are relatively simple in form, with multiple cables attached to a mobile platform or end-effector. The end-effector is manipulated by motors that can extend or retract the cables.

Cable robots have many desirable characteristics, including low inertial properties, high payload-to-weight ratios, potentially vast workspaces, transportability, ease of disassembly/reassembly, reconfigurability and economical construction and maintenance. However, relatively few analytical tools are available for analyzing and designing these manipulators.

This thesis focuses on expanding the existing theoretical framework for the design and analysis of cable robots in two areas: disturbance robustness and workspace generation. Underconstrained cable robots cannot resist arbitrary external disturbances acting on the end-effector. Thus a disturbance robustness measure for general underconstrained single-body and multi-body cable robots is presented. This measure captures the robustness of the manipulator to both static and impulsive disturbances. Additionally, a wrench-based method of analyzing cable robots has been developed and is used to formulate a method of generating the Wrench-Feasible Workspace of cable robots. This workspace consists of the set of all poses of the manipulator where a specified set of wrenches (force/moment combinations) can be exerted. For many applications the Wrench-Feasible Workspace constitutes the set of all usable poses. The concepts of robustness and workspace generation are then combined to introduce a new workspace: the Specified Robustness Workspace. This workspace consists of the set of all poses of the manipulator that meet or exceed a specified robustness value.

CHAPTER 1

INTRODUCTION

This research addresses the analysis and design of cable-driven robots. Cable-driven robots have many desirable attributes, particularly for large workspace manipulation tasks. However, much of the existing research on cable-driven robots only applies to a class of cable-driven robots known as fully constrained manipulators. The research presented in this thesis focuses on extending the existing theoretical framework of cable-driven robots to include analysis techniques for underconstrained cable-driven robots. Specifically, this thesis presents disturbance robustness measures for underconstrained cable-driven robots and Wrench-Feasible Workspace generation techniques for general cable-driven robots.

1.1 Cable Robots

Cable-driven robots, referred to as *cable robots* in this thesis, are a type of robotic manipulator that has recently attracted interest for large workspace manipulation tasks. Cable robots are relatively simple in form, with multiple cables attached to a mobile platform or end-effector as illustrated in Figure 1. The end-effector is manipulated by motors that can extend or retract the cables. These motors may be in fixed locations or mounted to mobile bases. The end-effector may be equipped with various attachments, including hooks, cameras, electromagnets and robotic grippers. Figures 1(a), 1(b) and 1(c) illustrate cable robots with eight, four and three cables, respectively, each equipped with a robotic gripping tool grasping a barrel.

Cable robots possess a number of desirable characteristics, including: 1) stationary heavy components and few moving parts, resulting in low inertial properties and high

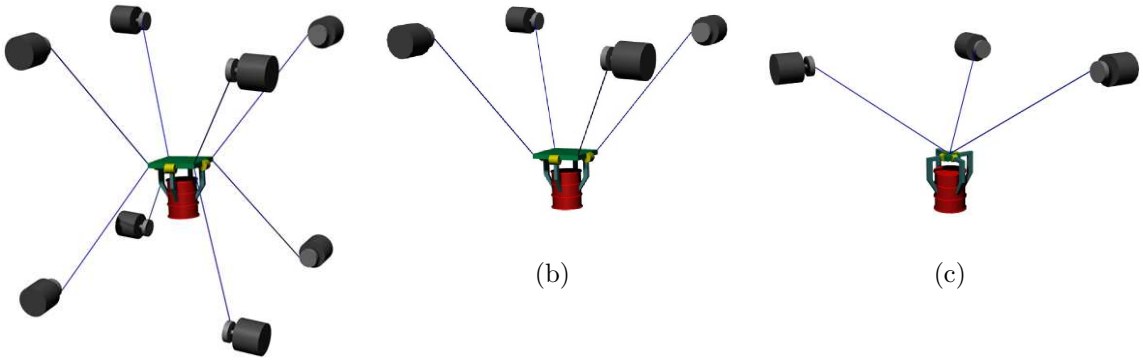

(a) (b) (c)

Figure 1: Example cable robots: a) fully constrained, b) underconstrained and c) underconstrained point-mass.

payload-to-weight ratios, 2) potentially vast workspaces, limited mostly by cable lengths, interference with surroundings, and force/moment exertion requirements, 3) transportability and ease of disassembly/reassembly, 4) reconfigurability by simply relocating the motors and updating the control system accordingly, and 5) economical construction and maintenance due to few moving parts and relatively simple components.

Consequently, cable robots are exceptionally well suited for many applications such as material handling, manipulation of heavy payloads, high-speed manipulation (with fully constrained manipulators), rapidly deployable rescue robots, cleanup of disaster sites, access to remote areas and interaction with hazardous environments. On the other hand, cable robots do sacrifice some accuracy due to cable sag and stretch. Additionally, traditional methods of robot analysis and control do not apply to cable robots due to the unidirectional cable forces.

Current research challenges for cable robots include the optimization of workspace properties, maintenance of positive cable tensions, resisting external disturbances, design of suitable control algorithms, sensing of end-effector motion and avoidance of cable interference. Workspace issues are particularly important, as many large-scale

applications require the end-effector to operate in regions of a particular shape and to exert certain minimum force/moment combinations (or *wrenches*) throughout those regions.

1.2 Classification of Cable Robots

In this thesis, different analysis techniques will be applied to different manipulators depending on characteristics of the manipulator. Thus in order to properly present and discuss these techniques the pertinent classifications of cable robots must be detailed.

1.2.1 Fully Constrained and Underconstrained Cable Robots

Cable robots can be classified as *fully constrained* or *underconstrained* [49] based on the degree to which the cables determine the pose of the manipulator. In the fully constrained case the pose (position and/or orientation) of the end-effector can be completely determined given the current lengths of the cables. An example of a fully constrained cable robot is shown in Figure 1(a). In addition to providing exact knowledge of the end-effector pose, these manipulators can have very high stiffness by pretensioning the cables. However, these manipulators may not always be practical because of the relatively large number of motors necessary and the possibility of cables interfering with the end-effector, surroundings and each other.

In contrast, underconstrained manipulators use fewer cables than fully constrained manipulators and thus the pose of the end-effector is not completely determined by the lengths of the cables. Instead, these manipulators rely on the presence of gravity to determine the resulting pose of the end-effector. While this complicates the forward kinematics of underconstrained cable robots (in fact it causes it to become a "forward statics" problem), it decreases problems with cable interference. For example, the manipulator in Figure 1(b) is underconstrained. Because underconstrained cable

robots are not fully constrained and must rely on gravity to determine the pose of the end-effector, it is possible for the pose of the end-effector to be changed by the presence of external disturbances. This motivates a study of the robustness of underconstrained cable robots to disturbances.

1.2.2 Point-Mass Cable Robots

An additional classification of cable robots are point-mass cable robots. In these manipulators all cables attach to a single point on the end-effector and can change lengths to control the position of the end-effector. Typically the end-effector is modeled as a lumped mass located at the point of intersection of the cables. As an example, the manipulator in Figure 1(c) is a 3-cable point-mass cable robot. Although in many cases the center of mass of the end-effector is not truly located at the point of intersection of the cables, the distance of this offset is assumed small in comparison to the scale of the manipulator. In addition, in order to avoid interference between the cables and the surroundings most point-mass cable robots are underconstrained.

Point-mass cable robots are well suited to perform operations similar to those of construction cranes – positioning an end-effector but not controlling its orientation. However, a cable robot has significantly less swaying of the payload than a crane in performing the same operation due to its parallel architecture. This class of robots is also useful for camera positioning operations [5] and is a promising candidate for rapidly-deployable manipulators for disaster relief.

1.3 Research Focus

Given the potential for cable robots to be used in a variety of applications, it is important to have tools for analyzing and designing such manipulators. The goal of this research is to expand the theoretical framework for cable robots. As Chapter 2 details, most of the existing theory that has been developed for cable robots applies

only to fully constrained cable robots. Thus the aim of this research is to develop analysis techniques that apply to underconstrained (and potentially fully constrained) cable robots.

Towards that end, two main areas of research are presented in this thesis:

1. **Disturbance robustness of underconstrained cable robots.** Robustness to disturbances is an important concern for underconstrained cable robots as they have a limited ability to resist unknown external disturbances. This ability to resist external disturbances is quantified by a disturbance robustness measure.

2. **Wrench-Feasible Workspace generation for underconstrained and fully constrained cable robots.** For many manipulators the most appropriate workspace to consider is the *Wrench-Feasible Workspace*, which represents the set of end-effector poses where the end-effector can exert a user-specified minimum set of force/moment combinations. The Wrench-Feasible Workspace therefore constitutes the "usable" workspace of the manipulator. While this workspace has been described in general terms by previous researchers, no tools exist to date for analytically calculating the Wrench-Feasible Workspace. A method is presented in this thesis for analytically forming this workspace for both underconstrained and fully constrained cable robots.

1.4 Thesis Organization

The remainder of this thesis is organized as follows. Chapter 2 reviews the relevant literature. This includes not only literature on cable robot design and control, but also relevant literature from problems in parallel robots and grasping.

Much of the work presented in this thesis relies on concepts from screw theory and parallel robots. As such, Chapter 3 provides an introduction to the basics and

relevant concepts in screw theory as well as an introduction to relevant topics in parallel robots, such as Jacobian matrix relationships and manipulator redundancy.

Chapter 4 then presents an analysis of the robustness of unconstrained cable robots to external disturbances. The problem is split into two cases: static disturbances and impulsive disturbances, resulting in two measures of disturbance robustness. These measures are related to each other and combined to form a single measure of disturbance robustness.

In Chapter 5 the issue of workspace generation is addressed. Specifically, a method is developed for forming the Wrench-Feasible Workspace of both underconstrained and fully constrained cable robots. Building on the concepts presented in Chapter 3, geometric conditions are formulated for analytically finding the workspace boundaries. The concepts developed in Chapters 4 and 5 are combined in Section 5.6 to create the Specified Robustness Workspace. This workspace consists of the set of all manipulator poses that meet or exceed a specified robustness value.

Lastly, Chapter 6 concludes the thesis, discusses the contributions of this work and presents possibilities for future continuations of this work.

CHAPTER 2

LITERATURE REVIEW

There have been a number of researchers who have developed analytical tools for cable robots that relate to the analyses presented here. Related work is first presented in the areas of existing manipulators, control, and parallel robots and grasping, followed by the areas most closely related to this thesis: disturbance robustness and workspace generation.

2.1 Existing Manipulators

Existing cable robots can be divided into fully constrained manipulators and underconstrained manipulators.

Fully Constrained Cable Robots

Fully constrained cable robots have often been designed for applications that require high speed/acceleration or high stiffness. High speed cable robots include the WARP manipulator [42] which uses 8 cables and the FALCON [34], a 7-cable manipulator (shown in Figure 2) that was able to achieve accelerations up to $43g$. The Charlotte robot is an 8-cable manipulator designed for use inside space structures, where the motors that control the cables are located inside the end-effector [71]. High stiffness fully-constrained cable robots have been designed for applications in teleoperation [35], haptics [52], [81], and virtual reality rides [67]. The planar cable robot haptic device developed in [81], termed the Cable-Suspended Haptic Interface, is shown in Figure 3.

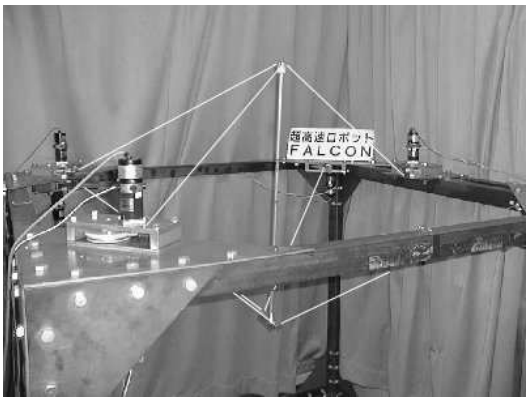

(a) A prototype of the FALCON.

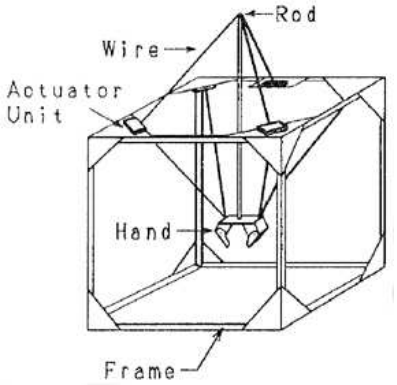

(b) A diagram of the FALCON.

Figure 2: The FALCON [31].

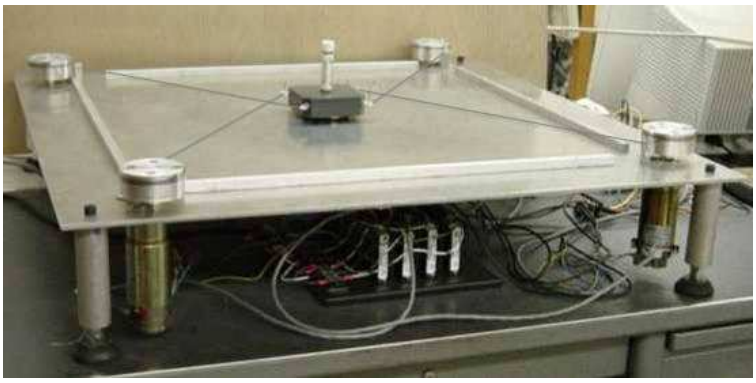

Figure 3: The Cable-Suspended Haptic Interface [27].

Underconstrained Cable Robots

Underconstrained manipulators have more typically been designed for applications where large workspaces are required. The NIST ROBOCRANE [1] is a six-cable, six degree-of-freedom cable robot designed for use in tasks such as material handling, inspection, pipe/beam fitting and manufacturing operations such as welding, sawing and grinding [13], [14]. Several versions of the ROBOCRANE are shown in Figure 4, including a ROBOCRANE mounted to a mobile base (Figure 4(a)), a ROBOCRANE used as a gantry crane (Figure 4(b)) and a ROBOCRANE modified to handle pallets of munitions (Figure 4(c)). Cable robots such as the ROBOCRANE have also been

(a) A scale model of the ROBOCRANE mounted to mobile bases.

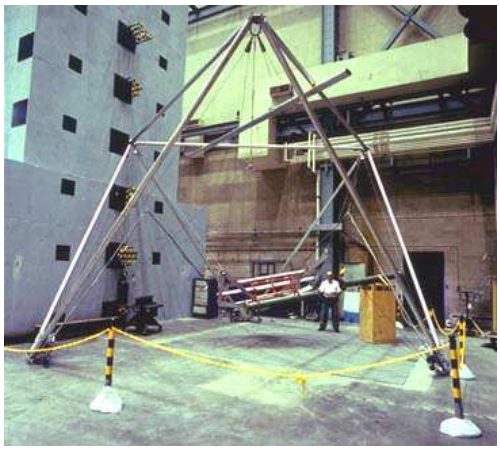

(b) A 1/3 scale model of the ROBOCRANE used as a gantry crane.

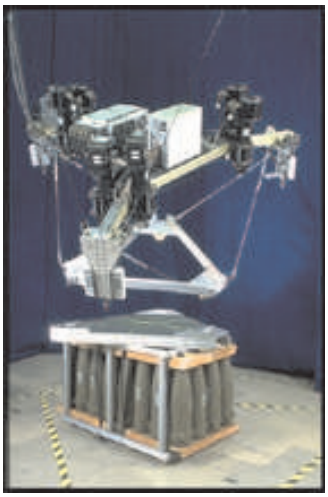

(c) The ROBOCRANE modified to handle munitions.

Figure 4: The ROBOCRANE [29].

used as motion bases on which serial robots are mounted [13], [57].

Cable robots have also been proposed for use in transferring cargo to and from ships. One such system is the Automated All-Weather Cargo Transfer System (AACTS) [6] made by August Design and shown in Figure 5. The system utilizes a large SCARA robotic arm (shown in Figure 5(a)) combined with a rigid hoist

(a) The AACTS unloading cargo from a ship [6].

(b) Closeup of the ISB [4].

Figure 5: The Automated All-Weather Cargo Transfer System (AACTS) and Intelligent Spreader Bar (ISB).

to position a six-cable, six degree-of-freedom spreader bar cable robot [4] (shown in Figure 5(b)) that will pick up freight containers from cargo ships in high sea states. Another manipulator designed for transferring cargo to and from ships is the Cable Array Robot [22], [66]. The Cable Array Robot was developed at the Pennsylvania State University and is a 4-cable point-mass cable robot. Figure 6(a) shows a prototype of the Cable Array Robot and Figure 6(b) shows a diagram of the Cable Array Robot being used to load containers onto a ship.

Another point-mass manipulator is the SkyCam [5], made by August Design. SkyCam is a cable robot that positions a video camera for use in stadiums and indoor arenas (shown in Figure 7). The use of underconstrained cable robots has also been proposed for search and rescue in the event of urban earthquakes [68], haptics [11], [46], [47] and pose-measurement systems [33], [70]. Cable robots have even been proposed as bathroom cleaning robots [69].

(a) Prototype of the Cable Array Robot.

(b) Diagram of the Cable Array Robot used for loading containers onto a ship.

Figure 6: The Cable Array Robot [28].

(a) A closeup of the SkyCam end-effector [26].

(b) The SkyCam in use at a stadium [30].

Figure 7: The SkyCam.

2.2 Control

Because the robot's cables can pull but not push, traditional robot control strategies often cannot be used for cable robots. One of the major issues with control of cable robots is maintaining positive cable tensions [2], [3], [36], [66], [76], [83]. Some work has been done in trajectory generation for underconstrained cable robots [85].

Nonlinear control schemes such as feedback linearization and sliding mode control have also been applied to cable robots [2], [3], [22], [37], [43], [50], [86]. Another major issue in cable robot control is reduction of the vibration caused by the flexibility of the cables. Anti-sway control schemes have been proposed [84], [86] and observer based optimal control [38] and input-shaping techniques [32] have been used to reduce residual vibrations after movement of the end-effector.

2.3 Parallel Robots and Grasping

Some researchers have also pointed out the similarity of cable robots to parallel robots and multi-fingered grasps [18], [34], [35]. The similarity to parallel robots allows the use of the forward and inverse kinematic relationships and Jacobian relationships of parallel robots (described in [48]) to analyze cable robots, provided all cables remain in tension. However, the uni-directional forces provided by the cables prevent many of the more advanced analysis tools from being applied to cable robots. Some researchers have attempted to extend the concept of manipulability (originally formulated for traditional robots [17][1], [47], [48], [88]) to apply to cable robots [21], [39], [64], [65].

The similarity between cable robots and problems in fixturing and grasping arises because cables can pull but not push on the end-effector, while fixture contacts and robot finger contacts can push but not pull on an object. Grasping and fixturing have been studied in great detail (for example [9], [16], [44], [45], [51], [54], [55], [56]). The grasp map, which defines the relationship between finger forces and the resulting wrench on the grasped body, is analogous to the transpose of the Jacobian matrix for cable robots. The application of the concept of grasp stability to cable robots is discussed in the following section.

[1]Note that a common problem with manipulability measures is that they do not appropriately take into account mixed dimensional task spaces. In [17] this is remedied by using the inertia matrix of the end-effector as a weighting matrix, similar to what is done in Chapter 4.

2.4 Disturbance Robustness

The robustness of cable robots to external disturbances has not been addressed at all by the existing literature. The most closely related concept is that of stability. Stability of a particular cable robot was investigated in [87]. A condition for stability of a spatial 3-cable crane was developed based on the curvature of the path of the center of gravity. The approach does generate a test for stability, but does not develop an adequate quantification of stability because the approach does not appropriately handle the mixed-dimensions of the task space.

The only other closely related area of existing research is grasp stability. Grasp stability has been studied by a number of researchers (for example [24], [25], [62]), [72], [73], [74]. However, these studies have often included the effects of friction, soft fingers and curvature of the grasped object. Because a cable cannot exert forces perpendicular to the direction of the cable, there is no analogy to friction for cable robots. Likewise, a cable cannot exert a moment about the axis along the cable, thus there is no analogy to soft finger contacts for cable robots. There is also no analogy in cable robots to the curvature of a grasped object. This is detailed in [18], but essentially stems from the fact that in a frictionless grasp the direction of applied force is always normal to the object and thus translates and rotates with the object during manipulation, while in a cable robot the direction of applied force is dependent upon the cable direction, which changes with respect to the end-effector during manipulation. The remaining studies of grasp stability typically focus on fixtures or grasps that fully constrain the object, which are analogous to fully constrained cable robots. Thus the majority of the research to date on fixture and grasp stability does not transfer easily to the stability/disturbance robustness of underconstrained cable robots.

The disturbance robustness analysis presented in Chapter 4 also defines norms for twists (combinations of linear and/or angular velocities) and wrenches (combinations

of forces and/or moments). Defining norms for twists and wrenches is a form of creating a metric on $SE(3)$ (the set of all rigid-body motions). Existing literature for metrics on $SE(3)$ tells us that any distance metric on $SE(3)$ must necessarily be parameterized by a choice of length scale (i.e. characteristic lengths) [59]. In this thesis the radii of gyration are used as characteristic lengths, resulting in a frame-invariant, objective metric [40].

2.5 Workspace Generation

Several different workspaces have been addressed previously. A number of researchers have investigated the set of all poses that the end-effector can attain statically (with no external forces or moments acting besides gravity) [1], [2], [3], [19], [20], [50], [63], [67]. A variety of terms have been used to refer to this workspace, but in this thesis the term Static Equilibrium Workspace is used to denote this workspace.

In most cases formulation of the Static Equilibrium Workspace has been done numerically via "brute force" methods, where the entire taskspace is discretized and exhaustively searched to find the statically reachable poses. One exception is in [20], where the boundaries of the Static Equilibrium Workspace were defined analytically for an underconstrained and fully-constrained planar cable robot. However, this was done for a special geometry end-effector and does not generalize to other geometries. The second exception is in [1], where the Static Equilibrium Workspace of the ROBOCRANE was found analytically, but again this formulation relied on the special geometry of the manipulator and does not generalize to other geometries.

Another workspace that has been researched is the "dynamic workspace," defined in [8] as the set of all poses where the end-effector can be given a specific acceleration. This workspace was determined for a planar cable robot by analytically forming the workspace boundaries.

The Wrench-Feasible Workspace is defined as the set of poses where the

manipulator can counteract a specified set of wrenches. For many applications the Wrench-Feasible Workspace constitutes the "usable" workspace of the manipulator and is thus one of the main considerations in this thesis. While the Wrench-Feasible Workspace has been defined in general terms [18], [78], it has generally been formed numerically using an exhaustive search approach [42], [75], [77], [78]. The boundaries of the Wrench-Feasible Workspace were determined analytically for planar 4-cable fully-constrained cable robots in [23], assuming infinite upper tension limits.

Some additional workspaces that are very similar to the Wrench-Feasible Workspace have also been defined. In [23] the "force-closure workspace" was introduced, which is a special case of the Wrench-Feasible Workspace where only forces are considered. The "workspace with tension conditions" [78] is defined similarly to the Wrench-Feasible Workspace with the additional constraint that all cable tensions must remain above a minimum tension value and below a maximum tension value. The "workspace with stiffness conditions" [78] is defined similar to the Wrench-Feasible Workspace with the additional constraint that the stiffness of the end-effector is above a threshold value. Some researchers have also incorporated workspace limits based on cable interference, but these workspace limits were determined either experimentally [42] or numerically [82]. In addition, the workspace generation technique presented in this thesis has been applied to planar and spatial cable robots with point-mass end-effectors [61], [60], as is discussed in Section 5.4.

In formulating the Wrench-Feasible Workspace and performing the disturbance robustness analysis, this thesis uses a construction called the Available Net Wrench Set, the set of all forces and moments that the manipulator can exert without violating cable tension limits. There are several similar concepts that have been developed by other researchers. The "capable force region" is defined in [57] as the set of forces that the manipulator can exert without consideration for the associated moments. In [65] a 3-cable planar cable robot with point-mass end-effector was examined and a

"set of manipulating forces" was formed. This is the set of all forces that the 3 cables could exert on the end-effector. A similar set of wrenches was also defined in [8] and termed a "pseudo-pyramid." This pseudo-pyramid includes the set of all wrenches (force/moment combinations) that the cables could apply to the end-effector at a pose if the cables have no upper tension limits.

2.6 Summary

In summary, in nearly all of these theoretical studies the cable robots have been assumed to be fully constrained. Thus there is a serious need to extend the existing theoretical framework for cable robots to include underconstrained robots. The issues of disturbance robustness and Wrench-Feasible Workspace generation are two of the most important issues for these manipulators, and the existing literature does not adequately address these issues.

CHAPTER 3

SCREW THEORY AND WRENCH ANALYSIS

This chapter introduces some of the fundamental concepts that are used throughout this thesis. Specifically, this chapter discusses some of the basics of screw theory, shows how Jacobian relationships apply to cable robots, and introduces the Available Net Wrench Set. Note that the introduction to screw theory relies primarily on the screw theory overview presented in [41].

3.1 Introduction to Screw Theory

In the analysis of rigid body motion and the dynamics of moving bodies, both linear and angular quantities are used. For example, consider a rigid body and a coordinate frame x-y-z. The linear velocity of a point, P, on the body can be written as:

$$\overline{v}_P = \begin{pmatrix} \dot{x}_P \\ \dot{y}_P \\ \dot{z}_P \end{pmatrix} \tag{1}$$

and the angular velocity of the body can be written as:

$$\overline{\omega} = \begin{pmatrix} \omega_x \\ \omega_y \\ \omega_z \end{pmatrix}. \tag{2}$$

If a force and moment are applied to the body at point P, the force applied to the body can be written as:

$$\overline{F} = \begin{pmatrix} F_x \\ F_y \\ F_z \end{pmatrix} \tag{3}$$

and the moment about point P can be written as:

$$\overline{M}_P = \begin{pmatrix} M_{P,x} \\ M_{P,y} \\ M_{P,z} \end{pmatrix}. \tag{4}$$

The screw, first introduced by Ball [7], combines rotational and linear quantities into a single element called a screw. Screw theory is based on two theorems:

- *Chasle's Theorem*: Rigid-body motion is equivalent to a twist on a screw (i.e. a rotation along a unique axis and translation parallel to that axis).
- *Poinsot's Theorem*: Rigid-body action is equivalent to a wrench on a screw (i.e. a force along a unique line and a couple parallel to that line).

The concept of a screw is similar to that of a mechanical screw. When turning a nut on a screw, turning the nut produces rotation about the screw centerline (axis) and any point on the nut has translation along the screw axis proportional to the pitch of the screw and translation perpendicular to the screw axis proportional to the distance of the point from the axis. A *twist*, denoted as $\$^t$, is the velocity form of a screw, describing the simultaneous linear and angular velocity of a body[1], while a *wrench*, denoted as $\$^w$, is the simultaneous force and moment combination acting on a body.

Because screws provide a compact way to describe both motion of a body and action applied to a body, twists and wrenches will be used throughout this thesis. There are several ways to express screw quantities, including vector form (describing the screw axis, pitch and the vector from the axis to the point), dual numbers, Plücker coordinates and Lie algebra. For our purposes, the easiest screw representation is Plücker coordinates.

[1]Note that while it is possible to consider twists in a finite sense (finite displacements), in this thesis twists will be assumed to refer to instantaneous velocities.

In Plücker coordinates a twist $\$^t$ is written[2] as:

$$\$^t = \begin{pmatrix} \overline{v}_O \\ \overline{\omega} \end{pmatrix} \tag{5}$$

where O is the origin of the coordinate frame. Throughout this thesis the origin of the coordinate frame is chosen to coincide with G, the center of gravity of the body, thus without loss of generality $\overline{v}_O$ can be replaced with $\overline{v}_G$. Note that because the origin is placed at G throughout this thesis the subscript will generally be dropped. Similarly, a wrench $\$^w$ in Plücker coordinates is written[3] as:

$$\$^w = \begin{pmatrix} \overline{F} \\ \overline{M}_O \end{pmatrix} \tag{6}$$

where again O is chosen here to be G, thus without loss of generality $\overline{M}_O$ can be replaced with $\overline{M}_G$. Note again that because the origin is placed at G throughout this thesis the subscript will generally be dropped. If it is desired for a wrench or twist to be expressed at a different point on a body a coordinate transformation can be used as described in [7], [41], but these transformations are not used in this thesis and thus are not discussed here. It is also possible to determine for any twist or wrench the corresponding axis, pitch, radius and rotation of the screw, but this will not be necessary for the analysis performed in this thesis.

In addition, if a body undergoes twist $\$^t$ under the action of wrench $\$^w$ then the power generated is:

$$\mathbb{P} = \$^w \cdot \$^t = \begin{pmatrix} \overline{F} \\ \overline{M} \end{pmatrix}^T \begin{pmatrix} \overline{v} \\ \overline{\omega} \end{pmatrix} \tag{7}$$

which is also referred to as the *power product* between a wrench and a twist. When the power product vanishes ($\mathbb{P} = 0$), the twist and wrench are said to be *reciprocal*.

[2]This is also said to be written in *axis* coordinates, where the upper (velocity) component varies depending on which point on the body is considered.

[3]This is also said to be written in *ray* coordinates, where the lower (moment) component varies depending on which point on the body is considered.

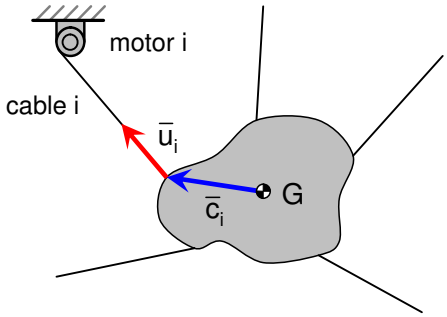

Figure 8: Diagram of kinematic parameters.

3.2 Jacobian Relationships

As Chapter 2 mentioned, there is a structural similarity between cable robots and parallel robots and multi-fingered grasps [34], [35], [18]. This allows the Jacobian relationships of parallel robots [48] and the grasp map for grasps with frictionless contact points [54], [45] to be used in the analogous case of cable robots [63], provided all cables remain in tension.

Note that in the analysis presented in this section it is assumed that the cables have negligible mass and do not stretch or sag, the end-effector is a single rigid body with known cable attachment points on the end-effector relative to the center of gravity, the locations of the attachments of the cables to the motors are known and each motor controls exactly one cable. Cable lengths, the direction of gravity and the resulting pose of the mechanism are also assumed to be known.

Consider the cable robot shown in Figure 8. Let the length of cable i be q_i. Then the velocity of cable i extending or retracting is $\dot{q}_i$, with $\dot{q}_i > 0$ corresponding to cable i being reeled in. Let the number of cables be p and the dimension of the task space (the space in which the end-effector operates) be n. Note that typically $n = 3$ (for point-mass or planar cable robots) or $n = 6$ (for spatial cable robots). Let the twist, $\$^t$, of the end effector be $\$^t = \begin{pmatrix} \overline{v} \\ \overline{\omega} \end{pmatrix}$. The Jacobian matrix, $\boldsymbol{J}$, defines the linear relationship between the velocities of the cables extending or retracting and

the resulting twist of the end-effector assuming all cables are taut:

$$\begin{pmatrix} \dot{q}_1 \\ \vdots \\ \dot{q}_p \end{pmatrix} = \boldsymbol{J}\$^t \tag{8}$$

where

$$\boldsymbol{J} = \left[\$_1^w \ ... \ \$_p^w\right]^T. \tag{9}$$

Here $\$_i^w$ is the wrench[4] along the i^{th} cable:

$$\$_i^w = \begin{pmatrix} \overline{u}_i \\ \overline{c}_i \times \overline{u}_i \end{pmatrix} \tag{10}$$

where $\overline{u}_i$ is the unit vector running along cable i directed from the end-effector towards motor i, $\overline{c}_i$ is the vector from G, the center of gravity of the end-effector, to the point on the end-effector where cable i is connected as illustrated in Figure 8 and there are p cables attached to the end-effector.

A similar relationship can be formed for the statics of the end-effector. Let the tension in cable i be t_i. Let the wrench, $\$^w$, applied to the end effector by the cables be $\$^w = \begin{pmatrix} \overline{F} \\ \overline{M} \end{pmatrix}$. The transpose of the Jacobian matrix, $\boldsymbol{J}^T$, defines the linear relationship between the tensions in the cables and the resulting wrench applied to the end-effector assuming all cables are taut:

$$\$^w = \boldsymbol{J}^T \begin{pmatrix} t_1 \\ \vdots \\ t_p \end{pmatrix}, \quad t_{i,max} \geq t_i \geq 0. \tag{11}$$

The restriction that $t_{i,max} \geq t_i \geq 0$ stems from the fact that each cable can pull but not push (i.e. a cable cannot have negative tension) and is restricted to be less than

[4]Note that $\$_i^w$ does not actually have units of force and moment, but must be multiplied by a scalar force factor in order to take on the standard units of a wrench. $\$_i^w$ can also be thought of as simply a screw in ray coordinates.

or equal to a maximum tension $t_{i,max}$. This maximum tension may be determined by the torque limits of the motor reeling in the cable or by the maximum tension a cable can withstand without breaking.

Note that the vectors $(t_1, \ldots, t_p)^T$ and $(\dot{q}_1, \ldots, \dot{q}_p)^T$ are vectors in the *joint space* of the manipulator (which has purely linear units) and $\$^w$ and $\$^t$ are vectors in the *task space* (which may have both linear and angular units). Note also that the *workspace* of a manipulator is a set of poses in the taskspace.

Redundancy

In this thesis a manipulator is said to be *redundant* if there are more cables than degrees of freedom ($p > n$). Thus the Jacobian matrix is non-square. Note that some researchers do not use this definition, as $p = n + 1$ cables are required to fully constrain a body [49] and thus some researchers define redundancy as when $p > (n+1)$. Redundancy is used here in the force sense, where given the wrench $\$^w$ in (11) there are too many cables to solve uniquely for the resulting cable tensions. Note that (9) and (11) hold for both redundant and non-redundant manipulators. Note also that redundancy does *not* imply full constraint (i.e. a robot may be underconstrained and redundant). On the other hand, every fully constrained robot is redundant as it has at least $n + 1$ cables.

3.3 Wrench Analysis

3.3.1 Available Net Wrench Set

In order to use a cable robot to accomplish desired tasks, the cables driving the end-effector must exert wrenches on the end-effector. Based on the current pose of the robot, the Jacobian transpose relationship in (11) can be used to determine the set of all possible wrenches that the cables can apply to the end-effector and thus the set of all wrenches that the end-effector can apply to its surroundings. Let $\overline{t}$ be the vector of cable tensions, $\overline{t} = (t_1, \ \ldots, t_p)^T$. The set of all wrenches that the cables can exert

on the end-effector is defined as the *cable wrench set*, CW, and is expressed as:

$$CW = \left\{ \$^w \ : \ \$^w = \boldsymbol{J}^T \overline{t} \, ; \ \ t_{i,max} \geq t_i \geq 0 \right\}. \tag{12}$$

We now wish to form the set of wrenches that the end-effector can apply to its surroundings, taking into account the effect of constant external wrenches such as gravity. This set is termed the *Available Net Wrench Set*, abbreviated NW_{avail}. Assuming a constant external wrench $\begin{pmatrix} \overline{F} \\ \overline{M} \end{pmatrix}_{ext}$ is present (typically $\begin{pmatrix} m\overline{g} \\ \overline{0} \end{pmatrix}$), where m is the mass of the end-effector and $\overline{g}$ is the gravitational vector, directed downward), the applied wrench set can be formed by simply shifting the wrench set in the direction of the external wrench:

$$\begin{aligned} NW_{avail} &= CW \oplus \begin{pmatrix} \overline{F} \\ \overline{M} \end{pmatrix}_{ext} \\ &= \left\{ \$^w \ : \ \$^w = \boldsymbol{J}^T \overline{t} + \begin{pmatrix} \overline{F} \\ \overline{M} \end{pmatrix}_{ext} \ ; \ \ t_{i,max} \geq t_i \geq 0 \right\}. \end{aligned} \tag{13}$$

Note that in this thesis $\begin{pmatrix} \overline{F} \\ \overline{M} \end{pmatrix}_{ext}$ will be assumed to be the gravitational wrench $\begin{pmatrix} m\overline{g} \\ \overline{0} \end{pmatrix}$.

3.3.2 Graphical Representation

If the dimension n of the task-space of the robot is less than or equal to three, it is possible to construct a graphical representation of NW_{avail}. As an example, consider the planar manipulator in Figure 9(a). Given the geometry of the manipulator at the current pose, the unit vectors $\overline{u}_1$, $\overline{u}_2$ and $\overline{u}_3$ can be constructed. Applying (10) results in $\$_1^w$, $\$_2^w$ and $\$_3^w$, respectively, which are wrenches along each of the cables. The set NW_{avail} can then be expressed as $NW_{avail} = \{\$^w : \$^w = a_1 t_{1,max} \$_1^w + a_2 t_{2,max} \$_2^w + a_3 t_{3,max} \$_3^w + m\overline{g}; \ \ 0 \leq a_i \leq 1\}$. Figure 9(b) illustrates the resulting set where t_{max}

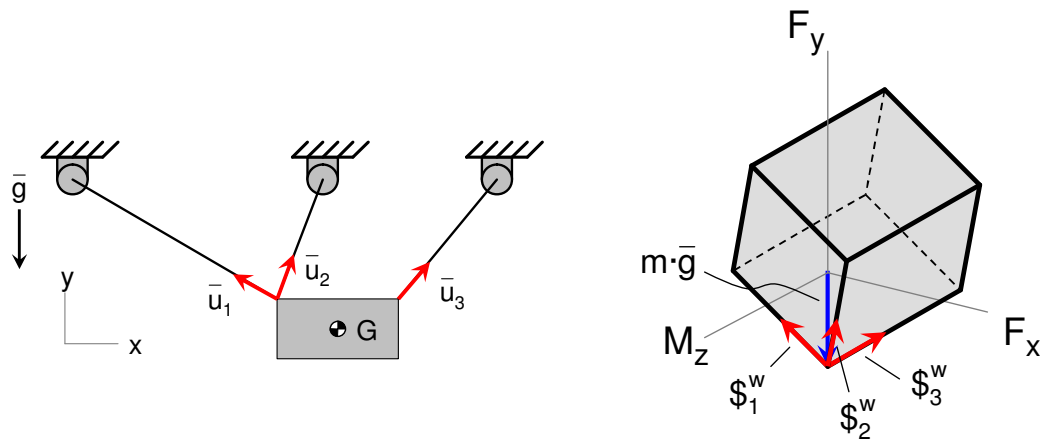

(a) Example planar cable robot.

(b) Available Net Wrench Set.

Figure 9: A planar cable robot and its Available Net Wrench Set.

is assumed to be the same for all three cables. We can see here that NW_{avail} is a parallelepiped. Note that this parallelepiped is defined in the mixed-dimensional space of F_x-F_y-M_z.

As a second illustration, consider the manipulator in Figure 10(a). Here the end-effector is a point-mass suspended from four cables. Because the task space has only linear dimensions, the wrenches $\$_1^w$ through $\$_4^w$ are simply $\overline{u}_1$ through $\overline{u}_4$ (the unit vectors along the cables), respectively, resulting in $NW_{avail} = \{\$^w : \$^w = a_1 t_{1,max}\overline{u}_1 + ... + a_4 t_{4,max}\overline{u}_4 + m\overline{g};\ 0 < a_i \leq 1\}$, shown in Figure 10(b). Note that because t_{max} has been assumed to be the same for all four cables and because this set is defined in the force domain only (F_x-F_y-F_z), the length of every edge of NW_{avail} is t_{max}. Also, the geometry of the set is somewhat altered here due to the fact that the number of cables is larger than the degrees of freedom of the task space (i.e. the manipulator is redundant). In this case NW_{avail} is the projection of a four-dimensional hyper-parallelepiped onto three-dimensional space.

In general it can be seen that NW_{avail} is some form of a parallelogram, parallelepiped or hyper-parallelepiped, depending on the number of cables and the

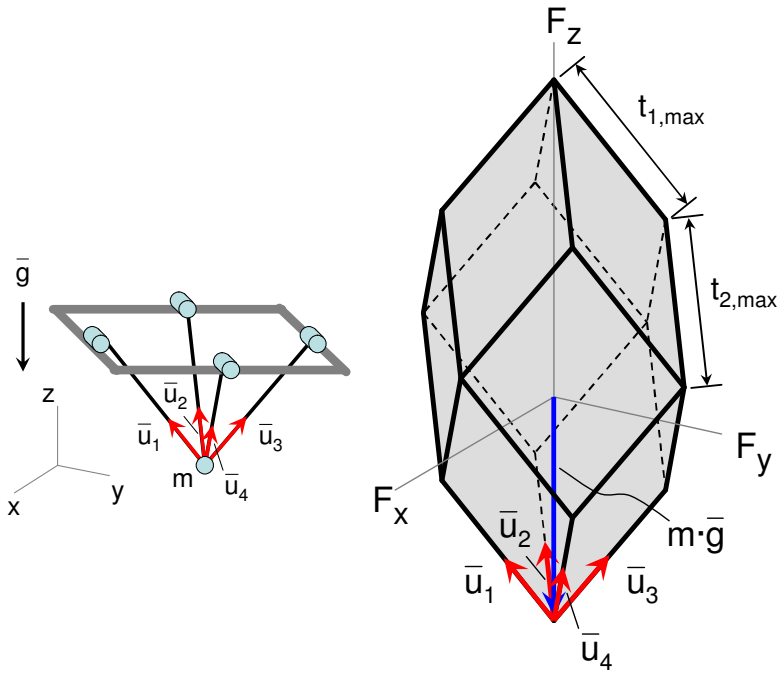

(a) Example manipulator. (b) Available Net Wrench Set.

Figure 10: A 4-cable point-mass cable robot and its Available Net Wrench Set.

dimension of the task-space. In all cases, however, NW_{avail} is a volume bounded by lines (2-D task space), planes (3-D task space) or hyperplanes (task space $>$ 3-D), where the number of boundaries is $2\binom{p}{q-1} = \frac{2p!}{(q-1)!(p-(q-1))!}$, and where p is the number of cables and q is the dimension of the task space.

CHAPTER 4

DISTURBANCE ROBUSTNESS MEASURES FOR UNDERCONSTRAINED CABLE ROBOTS

4.1 Introduction

Because underconstrained cable robots are not fully constrained and must rely on gravity to determine the pose of the end-effector, it is possible for the pose of the end-effector to be changed by external disturbances. Due to the likelihood that these external disturbances cannot be completely predicted, the possibility arises that the resulting pose of the manipulator cannot be known. If external wrenches change the pose of the end-effector, the manipulator is said to have been *disturbed*. Such a situation will cause problems in many applications and thus should be avoided. It is therefore of interest to investigate the ability of the manipulator to resist external disturbances. In this chapter a *Disturbance Robustness Measure* is developed to describe how much the manipulator is affected by disturbances.

4.1.1 Organization

In the analysis presented in this chapter, two types of disturbances will be considered: static disturbance wrenches and impulsive disturbance wrenches. Static disturbance wrenches are constant external wrenches applied to the end-effector by things such as a steady wind, a steady flow of water past an underwater end-effector, magnetic attraction, etc. Impulsive disturbance wrenches, in contrast, are brief impulses that impart a velocity (and corresponding kinetic energy) to the end-effector. Impulsive disturbance wrenches may be the result of a gust of wind or a collision between the end-effector and another object. These two types of disturbances are important to

consider because most disturbances that a cable robot encounters can be modeled as one of these two types of disturbances. In addition Section 4.5.1 briefly discusses how the robustness analysis can be extended to other types of disturbances.

Analysis of static and impulsive disturbances leads to two measures, *Static Disturbance Robustness* and *Impulsive Disturbance Robustness*, respectively. Both of these analyses are facilitated by the construction of a vector space referred to here as the *intermediate space*. Section 4.2 describes a mapping of twists and wrenches to this intermediate space as well as the properties of this space.

Section 4.3 presents the static disturbance analysis, which is primarily concerned with the question of what is the "smallest" static wrench that will disturb the end-effector. Because wrenches include both forces and moments, the standard Euclidean norm is not defined. Thus it is necessary to develop a physically meaningful wrench norm in order to define what the smallest static disturbance wrench is. This analysis also uses some of the wrench analysis described in Chapter 3. A measure of *Static Disturbance Robustness* is then presented.

Next Section 4.4 presents the impulsive disturbance analysis, which aims to quantify the degree to which an impulsive wrench disturbs the end-effector. Specifically, the acceleration of the end-effector back toward the equilibrium pose is found. This is accomplished by using the uni-directional constraints imposed by the cables to form the set of all twists that the end-effector can undergo. The concept of slope is then generalized to mixed dimensions (via the intermediate space) and then used to determine the worst-case acceleration of the end-effector back to its equilibrium pose. Based on these results, a measure of *Impulsive Disturbance Robustness* is presented. Section 4.5 then uses the intermediate space to show that the Static Disturbance Robustness Measure and Impulsive Disturbance Robustness Measure are equal, leading to a single measure, the *Disturbance Robustness Measure*.

After a discussion of the Disturbance Robustness Measure (Section 4.5.1) a

method is presented in Section 4.6 for extending the Disturbance Robustness Measure to manipulators with multi-body end-effectors. This is an important case to consider, as cable robots used in material handling operations frequently carry suspended payloads. This extension of the measure allows for the analysis of such situations. The chapter concludes with some future work that can be done in the area of disturbance robustness analysis (Section 4.8).

4.1.2 Assumptions

For this disturbance robustness analysis it is assumed that the cables have negligible mass and do not stretch or sag, the end-effector is a single rigid body (until Section 4.6) with known cable attachment points on the end-effector relative to the center of gravity, the locations of the attachments of the cables to the motors (or any pulleys the cables are routed through) are known and each motor controls exactly one cable. Cable lengths, the direction of gravity and the resulting pose of the end-effector are also assumed to be known. External disturbances are assumed to be unknown wrenches of unknown magnitudes that act only on the end-effector. Additionally, the lengths of the cables are assumed to be held constant.

4.2 Intermediate Space

In analyzing the robustness of a manipulator to a variety of disturbances it is of interest to talk about the 'magnitude' of a wrench, or a twist and wrench being 'parallel.' However, because twists and wrenches have both linear and angular units, such vector operations are generally not defined. For example, the magnitude (Euclidean norm) of a twist or wrench and parallelism between a twist and a wrench are not defined unless both the twist and wrench have purely linear units or purely angular units. A linear mapping is presented here that maps twists and wrenches to an intermediate space based on the inertial properties of the end-effector. This space

has only linear units, allowing standard vector operations to be defined while at the same time producing results that retain physical significance due to the manner in which the mapping is defined. As a result, examining twists and wrenches in this space is useful for both the static disturbance analysis and impulsive disturbance analysis presented in the following sections.

4.2.1 Mapping

Using the inertial properties of the end-effector, a mapping to an intermediate space can be defined for both twists and wrenches. The mass of the end-effector is m and ρ_i is the radius of gyration of the end-effector about axis i. Any twist, $\$^t$, in the task space of the manipulator can be expressed as:

$$\$^t = \begin{pmatrix} \overline{v} \\ \overline{\omega} \end{pmatrix} \tag{14}$$

and any wrench, $\$^w$, in the task space of the manipulator can be expressed as:

$$\$^w = \begin{pmatrix} \overline{F} \\ \overline{M} \end{pmatrix}. \tag{15}$$

Without loss of generality, the origin of the coordinate frame can be placed at the center of gravity, G, with the axes aligned with the principal axes of the end-effector. A mapping can then be defined between the task space and the intermediate space for both twists and wrenches as follows.

If the dimension of the task space is n and the task space has ℓ linear dimensions and $n - \ell$ angular dimensions, a twist $\$^t$ can be mapped to a generalized velocity $\hat{v}$ by:

$$\hat{v} = \boldsymbol{A}\$^t \tag{16}$$

where

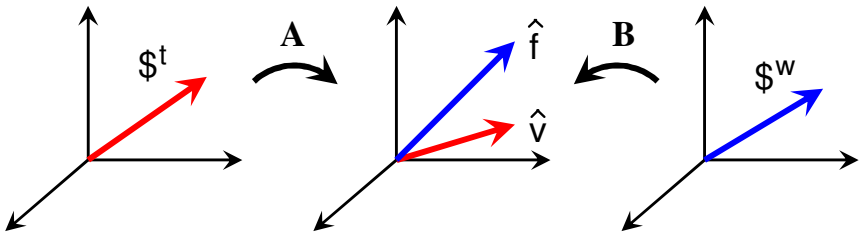

Figure 11: A twist and wrench mapped to a generalized force and velocity in the intermediate space.

$$\boldsymbol{A} = \begin{bmatrix} \boldsymbol{I}^{\ell\times\ell} & 0 & \cdots & 0 \\ 0 & \rho_1 & \cdots & 0 \\ \vdots & \vdots & \ddots & \vdots \\ 0 & 0 & \cdots & \rho_{(n-\ell)} \end{bmatrix} \tag{17}$$

where $\boldsymbol{I}^{\ell\times\ell}$ is the $\ell\times\ell$ identity matrix. Note that $(\hat{})$ is used to denote that the vector is defined in the intermediate space.

A mixed-dimensional wrench $\$^w$ can be mapped to a generalized force $\hat{f}$

$$\hat{f} = \boldsymbol{B}\$^w \tag{18}$$

where

$$\boldsymbol{B} = \boldsymbol{A}^{-1} = \begin{bmatrix} \boldsymbol{I}^{\ell\times\ell} & 0 & \cdots & 0 \\ 0 & \frac{1}{\rho_1} & \cdots & 0 \\ \vdots & \vdots & \ddots & \vdots \\ 0 & 0 & \cdots & \frac{1}{\rho_{(n-\ell)}} \end{bmatrix}. \tag{19}$$

These two mappings produce n-dimensional vectors (usually $n = 3$ or $n = 6$), with consistent units of linear velocity and force, respectively. Figure 11 illustrates the mapping of twists and wrenches to the intermediate space.

4.2.2 Properties

This mapping is using the radii of gyration of the end-effector as characteristic lengths for the corresponding rotation elements of the twists and wrenches. As a result, vector

operations in the intermediate space have physical significance. First, the dot product between a generalized velocity and a generalized force is equal to the power product between the associated twist and wrench:

$$\hat{v}^T \hat{f} = \$^{tT} \boldsymbol{A}^T \boldsymbol{B} \$^w = \$^{tT} \$^w. \tag{20}$$

As a result, perpendicularity between a generalized velocity and a generalized force in the intermediate space implies that the associated twist and wrench are reciprocal (they have a zero power product).

Second, the magnitude of a generalized velocity is proportional to the kinetic energy of the end-effector undergoing the associated twist. For compactness, define the kinetic energy, KE, of a twist $\$^t$ (with respect to the end-effector) as:

$$KE\left(\$^t\right) = \frac{1}{2} \$^{tT} \boldsymbol{M} \$^t \tag{21}$$

where $\boldsymbol{M} = \boldsymbol{A}^2 m$ is the inertia matrix of the end-effector. Then:

$$\begin{aligned} KE\left(\$^t\right) &= \frac{m}{2} \$^{tT} \boldsymbol{A}^2 \$^t \\ &= \frac{m}{2} \$^{tT} \boldsymbol{A}^T \boldsymbol{A} \$^t \\ &= \frac{m}{2} \left(\boldsymbol{A}\$^t\right)^T \left(\boldsymbol{A}\$^t\right) \\ &= \frac{m}{2} \parallel \hat{v} \parallel^2 . \end{aligned} \tag{22}$$

Third, the magnitude of a generalized force is proportional to the acceleration energy of the corresponding wrench with respect to the end-effector. While acceleration energy is not a commonly used quantity, it is closely connected to kinetic energy and will be discussed in more detail in Section 4.3.5. The acceleration energy, AE, of a wrench $\$^w$ (with respect to the end-effector) is defined as:

$$AE\left(\$^w\right) = \frac{1}{2} \$^{wT} \boldsymbol{M}^{-1} \$^w \tag{23}$$

where $\boldsymbol{M}^{-1} = \frac{1}{m}\boldsymbol{A}^{-2} = \frac{1}{m}\boldsymbol{B}^2$. Then:

$$\begin{aligned} AE\left(\$^w\right) &= \frac{1}{2m}\$^{wT}\boldsymbol{B}^2\$^w \\ &= \frac{1}{2m}\$^{wT}\boldsymbol{B}^T\boldsymbol{B}\$^w \\ &= \frac{1}{2m}\left(\boldsymbol{B}\$^w\right)^T\left(\boldsymbol{B}\$^w\right) \\ &= \frac{1}{2m}\parallel \hat{f} \parallel^2 . \end{aligned} \tag{24}$$

Fourth, parallelism between a generalized velocity and a generalized force has physical meaning. This can be interpreted in several different ways. Consider a twist $\$^t$ and a wrench $\$^w$. Let the kinetic energy of $\$^t$ with respect to the end-effector be b and let the acceleration energy of $\$^w$ with respect to the end-effector be c. Let $\$^t$ and $\$^w$ be mapped to the generalized velocity $\hat{v}$ and the generalized force $\hat{f}$. The dot product between the two vectors is then

$$\hat{v}\cdot\hat{f} = \parallel \hat{v} \parallel \parallel \hat{f} \parallel \cos\theta \tag{25}$$

where θ is the angle between the two vectors. If $\hat{v}$ and $\hat{f}$ are parallel and in the same direction, then

$$\hat{v}\cdot\hat{f} = \parallel \hat{v} \parallel \parallel \hat{f} \parallel . \tag{26}$$

Thus if the generalized velocity and generalized force are parallel, the dot product between the two vectors is maximized.

The analogous relationship between the intermediate space and the task space produces the following two interpretations:

1. Given a wrench $\$^w$. Out of all the twists that have an associated kinetic energy of b (with respect to the end-effector), the parallel twist $\$^t_{par}$ has the maximum power product with $\$^w$, i.e.

$$\max_{\frac{1}{2}\$^{tT}\mathbf{M}\$^t = b} \$^{tT}\$^w = \$^t_{par}{}^T\$^w = d. \tag{27}$$

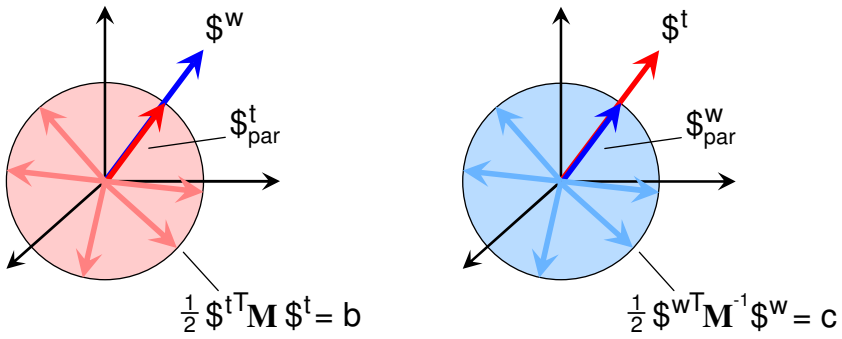

(a) The parallel twist maximizes $\$^{t^T}\$^w$ out of all twists with $KE(\$^t) = b$.

(b) The parallel wrench maximizes $\$^{t^T}\$^w$ out of all wrenches with $AE(\$^w) = c$.

Figure 12: Interpretations of twist and wrench parallelism.

2. Given a twist $\$^t$. Out of all the wrenches that have an associated acceleration energy of c (with respect to the end-effector), the parallel wrench $\$^w_{par}$ has the maximum power product with $\$^t$, i.e.

$$\max_{\frac{1}{2}\$^{w^T}\mathbf{M}^{-1}\$^w = c} \$^{t^T}\$^w = \$^{t^T}\$^w_{par} = d. \tag{28}$$

These two properties are illustrated in Figure 12[1]. Figure 12(a) illustrates the first property, where for a given wrench $\$^w$, out of the set of all twists where $KE(\$^t) = b$, $\$^t_{par}$ maximizes $\$^{t^T}\$^w$. Similarly, Figure 12(b) illustrates the second property, where for a given twist $\$^t$, out of the set of all wrenches where $AE(\$^w) = c$, $\$^w_{par}$ maximizes $\$^{t^T}\$^w$.

Now assume that the dot product between $\hat{v}$ and $\hat{f}$ (which are not assumed parallel) is a known value d. Then given $\hat{v}$ we can find the set of all generalized forces that have the same dot product with $\hat{v}$ as $\hat{f}$. Out of this set of generalized forces, $\hat{f}_{par}$ has the smallest magnitude. In other words, if for some $\hat{f}$

$$\hat{v} \cdot \hat{f} = \| \hat{v} \| \| \hat{f} \| \cos\theta = d \tag{29}$$

[1]Note that twists and wrenches are shown in the same reference frame for illustration only. In general the difference in units between them prevent them from being plotted in the same space.

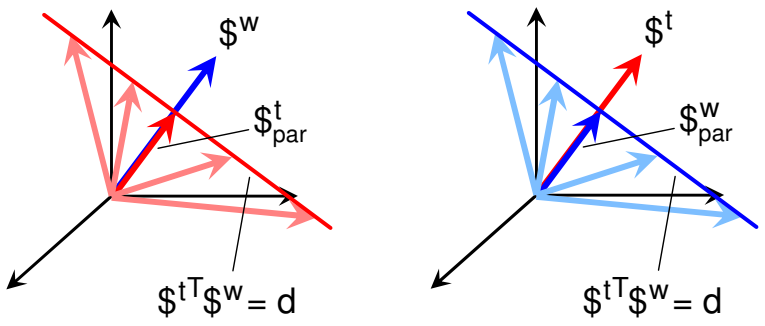

(a) The parallel twist minimizes $KE(\$^t)$ out of all twists where $\$^{t^T}\$^w = d$.

(b) The parallel wrench minimizes $AE(\$^w)$ out of all wrenches where $\$^{t^T}\$^w = d$.

Figure 13: Interpretations of twist and wrench parallelism.

then $\| \hat{f} \|$ is minimized when $\theta = 0$, corresponding to $\hat{f} = \hat{f}_{par}$. The same relationship is true when $\hat{v}$ and $\hat{f}$ are switched (i.e. $\hat{v}_{par}$ is found by considering the set of all generalized velocities where $(\hat{v} \cdot \hat{f}) = d$). The analogous relationship between the intermediate space and the task space produces the following two interpretations:

3 Given a wrench $\$^w$. Out of all the twists that have a power product of d with the wrench, the parallel twist has the smallest associated kinetic energy (with respect to the end-effector)

$$\min_{\$^{t^T}\$^w = d} \frac{1}{2}\$^{t^T}\boldsymbol{M}\$^t = \frac{1}{2}\$^t_{par}{}^T\boldsymbol{M}\$^t_{par} = b. \tag{30}$$

4 Given a twist $\$^t$. Out of all the wrenches that have a certain power product with the twist, the parallel wrench is the one that has the smallest corresponding AE (with respect to the end-effector)

$$\min_{\$^{t^T}\$^w = d} \frac{1}{2}\$^{w^T}\boldsymbol{M}^{-1}\$^w = \frac{1}{2}\$^w_{par}{}^T\boldsymbol{M}^{-1}\$^w_{par} = c. \tag{31}$$

These two properties are illustrated in Figure 13[2]. Figure 13(a) illustrates the third property, where for a given wrench $\$^w$, out of the set of all twists where $\$^{t^T}\$^w = d$,

[2]Note that twists and wrenches are shown in the same reference frame for illustration only. In general the difference in units between them prevent them from being plotted in the same space.

$\$^t_{par}$ minimizes $KE(\$^t)$. Similarly, Figure 13(b) illustrates the fourth property, where for a given twist $\$^t$, out of the set of all wrenches where $\$^{tT}\$^w = d$, $\$^w_{par}$ minimizes $AE(\$^w)$.

Summary

In short, parallelism between a generalized velocity and a generalized force corresponds to a sort of optimal solution to a power product type problem, using acceleration energy or kinetic energy as a norm for the wrench or twist, respectively. If a twist and wrench are parallel when mapped to the intermediate space, they are denoted as a *corresponding* twist and wrench.

4.3 Static Disturbance Analysis

4.3.1 Motivation

This section investigates the effects of static disturbance wrenches on the pose of a cable robot. Specifically, we are concerned with the question of what is the "smallest" static wrench that will disturb the end-effector. This smallest static disturbance wrench represents a sort of "worst-case scenario" for the manipulator, and can be thought of as being applied in the direction of least constraint for the end-effector. By defining the static disturbance robustness measure using this approach, the measure provides a conservative estimate of the static wrenches that can be resisted by the manipulator. However, in order to find the smallest static disturbance wrench it is necessary to define the magnitude of a wrench. In general cable robots have mixed-dimensional task spaces, and thus the magnitude of a wrench in such a space cannot be defined using the Euclidean norm.

In order to find the *smallest* static disturbance wrench, it is first necessary to show how to find the static wrenches that disturb the end-effector (Section 4.3.2). Then three different approaches to defining a physically meaningful wrench norm are investigated. These approaches include: 1) examining pure force disturbances applied

to the end-effector at arbitrary locations (Section 4.3.3), 2) analyzing disturbance wrenches in the tension (joint) space (Section 4.3.4) and 3) analyzing disturbance wrenches using acceleration energy (Section 4.3.5).

4.3.2 Static Disturbance Wrenches

As stated earlier, there is an infinite number of static wrenches that will disturb the end-effector. **However, because we are interested in the smallest static disturbance wrench we only need to consider the set of wrenches that *just begin* to disturb the end-effector.** In order to define this set we can use the Available Net Wrench Set. Recall from Chapter 3 the Available Net Wrench Set, NW_{avail}, is the set of all wrenches that can be exerted by the manipulator, factoring in cable forces and gravity. Define $-NW_{avail}$ as the opposite of NW_{avail}. That is,

$$-NW_{avail} = \{\$^w \ : \ -\$^w \in NW_{avail}\}. \tag{32}$$

$-NW_{avail}$ is the set of external wrenches that can be resisted by the manipulator without violating tension limits. While the boundaries of NW_{avail} represent the limits of the wrenches that the manipulator can exert, the boundaries of $-NW_{avail}$ represent the limits of the wrenches that can be resisted. As an example, consider Figure 14. Figure 14(a) shows an example NW_{avail} and Figure 14(b) shows the corresponding $-NW_{avail}$. Thus any external wrench applied to the manipulator that is not in the $-NW_{avail}$ in Figure 14(b) cannot be resisted by the manipulator.

Let the set of all wrenches on the boundaries of $-NW_{avail}$ constitute the set of all *boundary wrenches*. That is, a wrench $\$^w_{bound}$ is defined as a boundary wrench if and only if for $\alpha \in I\!R$,

$$\begin{aligned} 1 \geq \alpha \geq 0 \ &\Rightarrow \ \alpha\$^w_{bound} \in -NW_{avail} \\ \text{and} \qquad \alpha > 1 \ &\Rightarrow \ \alpha\$^w_{bound} \notin -NW_{avail}. \end{aligned} \tag{33}$$

In other words, the wrench $\alpha\$^w_{bound}$ can be resisted by the manipulator (without

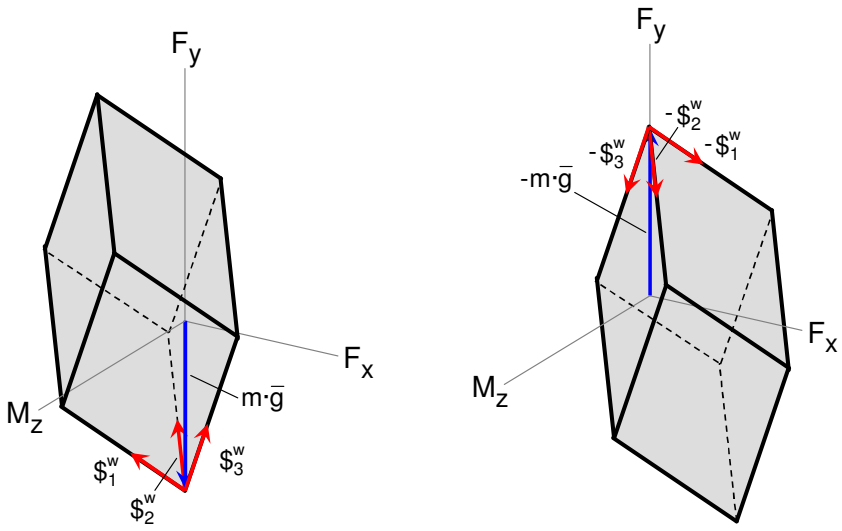

(a) Example NW_{avail}. (b) Example $-NW_{avail}$.

Figure 14: Example NW_{avail} and the corresponding $-NW_{avail}$.

violating tension limits) if $1 \geq \alpha \geq 0$ but cannot be resisted if $\alpha > 1$. These wrenches are the boundary between the set of wrenches that can be resisted by the manipulator and the set of wrenches that can not.

We are now interested in a particular subset of the boundary wrenches. When a disturbance causes the pose of the manipulator to change, this is generally because the disturbance causes one or more of the cables to go slack[3]. While it is important not to exceed upper tension limits in the cables, the upper tension limits are often very large and they can typically be made irrelevant or of little concern by appropriate sizing of the cables and motors and constraining the end-effector to operate in an appropriate workspace (discussed in Chapter 5). Thus for the purpose of this analysis the upper tension limits will be ignored. In the case that this assumption cannot be made and disturbance wrenches cause upper tension limits to be reached, additional considerations must be taken into account as will be discussed in Chapter 4.

[3]In the case where $p < n$, the disturbance can change the pose of the manipulator without causing a cable to go slack or overtensioning the cables. Regardless, the same reasoning applies for neglecting the upper tension limits.

Thus we will focus on the external wrenches that disturb the manipulator by causing one or more of the cables to have zero tension. As was discussed in Chapter 3, the lower sides of NW_{avail} correspond to exerting a wrench while having one or more of the cables have zero tension. Consequently, the upper sides of $-NW_{avail}$ correspond to disturbance wrenches that cause one or more of the cables to have zero tension. Thus in order to find the smallest disturbance wrench, the upper sides of $-NW_{avail}$ is the set of wrenches that will be examined to find the smallest static disturbance wrench[4]. Let us refer to these wrenches as the *critical* wrenches and denote the set of all critical wrenches by C. The critical wrenches are a subset of the boundary wrenches. Specifically, a wrench $\$^w_{crit}$ is defined as a critical wrench if the wrench $\alpha\$^w_{crit}$ ($\alpha \in I\!R$) can be resisted by the manipulator if $1 \geq \alpha \geq 0$ but disturbs the manipulator (i.e. causes a cable to go slack) if $\alpha > 1$.

2-D Test Case

Consider the manipulator in Figure 15(a), which is used in later sections as a test case for different definitions of a wrench norm. The manipulator is a a 2-D underconstrained point-mass cable robot with two cables, the lengths of the cables are not changing and the end-effector is in static equilibrium. The manipulator is assumed to have very large upper tension limits and the end-effector weighs 10 N. Figure 15(b) shows $-NW_{avail}$ for this pose of the manipulator, in which the critical wrenches, C (the two upper sides of $-NW_{avail}$), are highlighted. In order to find the disturbance robustness of this pose of the manipulator we wish to find the smallest wrench in C. In this case the magnitude of a wrench is easily defined because the task space has only linear dimensions, thus the magnitude of the wrench is found using the Euclidean norm. By calculating the shortest distance between the origin

[4]Again, in the case where $p < n$, the disturbance can change the pose of the manipulator without causing a cable to go slack. In this case the dimension of $-NW_{avail}$ is less than n and so $C = -NW_{avail}$.

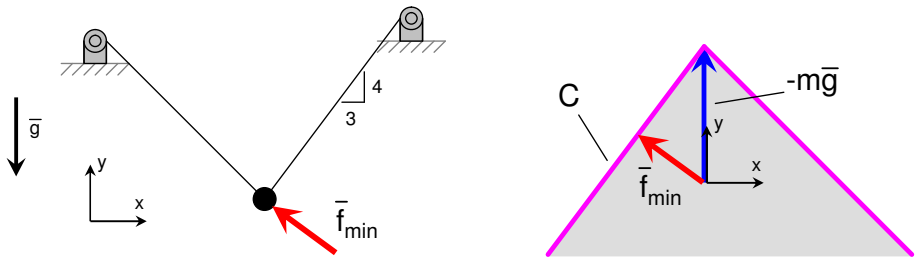

(a) Example manipulator and minimum disturbance force.

(b) $-NW_{avail}$ for this pose of the manipulator.

Figure 15: Minimum disturbance force example.

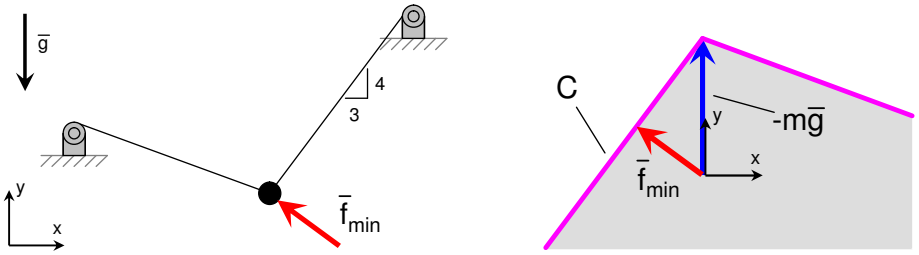

(a) Example manipulator and minimum disturbance force.

(b) $-NW_{avail}$ for this pose of the manipulator.

Figure 16: Minimum disturbance force example.

and C, the smallest wrench in C can be found to be $\overline{f}_{min} = (-\frac{24}{5}\,\text{N}, \frac{18}{5}\,\text{N})^T$, as shown in Figure 15(b).

Consider now the manipulator in Figure 16(a). It is the same manipulator as in Figure 15(a), only the left motor mount location has been lowered, changing the angle of the left cable. Figure 16(b) shows $-NW_{avail}$ for this pose of the manipulator, with the critical wrenches highlighted. In this case the smallest wrench in C is still $\overline{f}_{min} = (-\frac{24}{5}\,\text{N}, \frac{18}{5}\,\text{N})^T$, as shown in Figure 16(b).

In this simple example, the smallest static disturbance that causes a cable to go slack can be found in a straightforward manner because the task space had only linear dimensions, thus the magnitude of the wrench was found using the Euclidean norm. However, this problem is complicated for general underconstrained cable robots by

the fact that the norm of a mixed-dimensional wrench (with forces and moments) is not defined. Thus we must develop some meaningful form of a wrench norm if we are to talk about which is the smallest. This norm should also remain consistent with the simple case of a manipulator with a point-mass end-effector, such as the one discussed above. The following three subsections consider three different approaches to defining a wrench norm. It is shown that the first two approaches in Sections 4.3.3 and 4.3.4 do not produce acceptable wrench norms, while the approach in Section 4.3.5 does.

4.3.3 Pure Force Disturbance Norm

The first approach considered here for defining a wrench norm is to consider only pure-force disturbances applied at arbitrary locations. The magnitude of such wrenches would then be defined by the magnitude of the applied force. That is, if a force $\overline{F}_{dist}$ is applied to the end-effector and $\overline{r}$ is the vector from G to the point at which $\overline{F}_{dist}$ is applied, the disturbance wrenches are modeled as being of the form:

$$\$^w = \begin{pmatrix} \overline{F}_{dist} \\ \overline{M}_{dist} \end{pmatrix} = \begin{pmatrix} \overline{F}_{dist} \\ \overline{F}_{dist} \times \overline{r} \end{pmatrix}. \tag{34}$$

This model of the disturbance essentially removes the possibility of having any moment about the line of action of the force. This appears to be a reasonable model of disturbance wrenches, as it seems that a common scenario would involve a pure force being applied to the end-effector.

If the magnitude of such a wrench is defined as the magnitude of the applied force, the wrench norm is the *pure-force norm*, $\| \$^w \|_f$, defined to be:

$$\| \$^w \|_f = \| \overline{F}_{dist} \| = \sqrt{\$^{w^T} \boldsymbol{W} \$^w} \tag{35}$$

where the weighting matrix $\boldsymbol{W}$ is

$$\boldsymbol{W} = \begin{bmatrix} \boldsymbol{I}^{\ell \times \ell} & \boldsymbol{0}^{\ell \times (n-\ell)} \\ \boldsymbol{0}^{(n-\ell) \times \ell} & \boldsymbol{0}^{(n-\ell) \times (n-\ell)} \end{bmatrix} \tag{36}$$

and where **0** is a zero matrix, the dimension of the task space is n and the task space has ℓ linear dimensions and $n-\ell$ angular dimensions. Using the pure-force norm, the disturbance robustness measure $\mathcal{R}_f$ would be:

$$\mathcal{R}_f = \min_{\$^w \in C} \| \$^w \|_f \ . \tag{37}$$

Comparing this result to the 2-D test case, we see that this norm is consistent with the case of a point-mass end-effector, as $n - \ell = 0$ for such a manipulator and the norm simplifies to be the Euclidean norm.

However, for a general underconstrained manipulator, a pure moment above a certain magnitude cannot be resisted and will cause a cable tension to become zero. Thus a pure force applied at a very large distance (perpendicular to the direction of the force) will result in a very large moment, thus a vanishingly small force will result in a large moment if applied at a distance that approaches infinity. As a result, the smallest pure-force disturbance that causes a cable to have zero tension is a force with magnitude approaching zero. **Thus applying this wrench norm to a general underconstrained manipulator results in the magnitude of the smallest disturbance wrench to approach zero** ($\mathcal{R}_f = 0$)[5]**, regardless of the arrangement of the cables, the end-effector geometry, etc.** Thus this norm is not an appropriate choice. Similarly, a wrench norm based on a pure-moment disturbance would have the same problems and thus will not be considered.

4.3.4 Tension Space Norm

Another approach for constructing a wrench norm would be to map the wrenches to the tension space and defining the magnitude of a wrench as the norm of the resulting cable tensions[6]. The mapping of a disturbance wrench back to the tension space is

[5]Note that the minimum of $\| \$^w \|_f$ is not actually attained in C, but approaches 0 in the limit. Thus the infimum of $\| \$^w \|_f$ is actually used.

[6]This approach was suggested by Dr. Harvey Lipkin.

accomplished using the inverse of the transpose of the Jacobian matrix:

$$\overline{t} = \boldsymbol{J}^{-T} \$^{w} \tag{38}$$

assuming that $\boldsymbol{J}^T$ is invertible. In the case of a redundant manipulator ($p > n$), $\boldsymbol{J}^{-T}$ can be replaced by $\left(\boldsymbol{J}^T\right)^{\dagger}$, the right pseudo-inverse[7] of $\boldsymbol{J}^T$. If the magnitude of the wrench is defined as the Euclidean norm of the resulting tension vector, the wrench norm is called the *tension-space norm*, $\| \$^{w} \|_t$, defined as:

$$\| \$^{w} \|_t = \| \overline{t} \| = \| \boldsymbol{J}^{-T} \$^{w} \| = \sqrt{\$^{w T} \boldsymbol{J}^{-1} \boldsymbol{J}^{-T} \$^{w}} \tag{39}$$

where $\boldsymbol{J}^{-T}$ is replaced by $\left(\boldsymbol{J}^T\right)^{\dagger}$ for redundant manipulators. Using the tension-space norm, the disturbance robustness measure $\mathcal{R}_t$ would be:

$$\mathcal{R}_t = \min_{\$^{w} \in C} \| \$^{w} \|_t \, . \tag{40}$$

Note that if the manipulator is not redundant but is in a particular pose where $\boldsymbol{J}^T$ is singular, the tension-space norm is assumed to equal 0. This is because an infinitesimally small external wrench can disturb the manipulator in such a pose. Additionally, this provides continuity, as $\mathcal{R}_t \rightarrow 0$ as the pose approaches such a configuration.

It is actually fairly simple to find $\mathcal{R}_t$ for a pose of a manipulator. The tensions of the manipulator with no disturbance wrenches present are found by:

$$\overline{t}_{mg} = \boldsymbol{J}^{-T} \left(m\overline{g} \right) . \tag{41}$$

When the disturbance wrench is applied:

$$\$^{w}_{tot} = m\overline{g} + \$^{w}_{dist} = \boldsymbol{J}^T (\overline{t}_{mg} + \overline{t}_{dist}). \tag{42}$$

Thus for cable i to go slack, $t_i = 0 = t_{mg,i} + t_{dist,i}$. Thus $t_{dist,i} = -t_{mg,i}$. If the smallest cable tension $t_{mg,i}$ is $t_{mg,min}$, the resulting robustness measure would be $\mathcal{R}_t = t_{mg,min}$.

[7] $\left(\boldsymbol{J}^T\right)^{\dagger} = \boldsymbol{J} \left(\boldsymbol{J}^T \boldsymbol{J}\right)^{-1}$

By mapping the wrench to the tension space, the issue of mixed-dimensional wrenches is overcome. That is, regardless of the units of the task space, the tension-space norm can be calculated. However, examination of the results of this wrench norm are not consistent with the 2-D test case examined earlier. Consider again the manipulators shown in Figures 15(a) and 16(a). In both cases the smallest external force that caused a cable to go slack was $\overline{f}_{min} = (-\frac{24}{5}\,\mathrm{N}, \frac{18}{5}\,\mathrm{N})^T$. For the first manipulator the slope of the left cable is -1 and the slope of the right cable is $\frac{4}{3}$. The tensions in the left and right cables of the first manipulator are then $\frac{30\sqrt{2}}{7}\,\mathrm{N}$ and $\frac{50}{7}\,\mathrm{N}$, respectively, resulting in $\mathcal{R}_t = \frac{30\sqrt{2}}{7}\,\mathrm{N}$. For the second manipulator the slope of the left cable is $-\frac{1}{3}$ and the slope of the right cable is $\frac{4}{3}$. The tensions in the left and right cables of the second manipulator are $2\sqrt{10}\,\mathrm{N}$ and $10\,\mathrm{N}$, respectively, resulting in $\mathcal{R}_t = 2\sqrt{10}\,\mathrm{N}$. Clearly, this measure produces different results despite the fact that the smallest disturbance force is the same in both cases. As a result, the ability of this approach to deal with mixed-dimensional wrenches is outweighed by the fact that the results do not agree with the natural result for the point-mass case.

4.3.5 Acceleration Energy Norm

The last approach considered here for constructing a wrench norm is to use the acceleration energy associated with a wrench to define its magnitude. While acceleration energy is not a commonly used quantity, it is closely connected to kinetic energy. Therefore, before the wrench norm based on acceleration energy is presented, acceleration energy will be discussed.

4.3.5.1 Acceleration Energy

Let an orthonormal coordinate frame be defined as fixed to the end-effector with its origin at the center of gravity, G. The acceleration energy of the end-effector (also referred to as Appel's function, the Appelian or the Gibbs-Appel function [58]) is defined as:

$$AE = \int_{body} \frac{1}{2} a^2 \mathrm{d}m. \tag{43}$$

Where a is the magnitude of the linear acceleration of the differential mass $\mathrm{d}m$. If the body is a rigid body, $\overline{a}$ is the linear acceleration of the center of gravity, $\overline{r}_{p_i/G}$ is the vector from G to point p_i on the body, $\overline{\omega}$ is the angular velocity of the body and $\overline{\alpha}$ is the angular acceleration of the body, then the acceleration $\overline{a}_{p_i}$ of point p_i on the body is:

$$\overline{a}_{p_i} = \overline{a} + \overline{\alpha} \times \overline{r}_{i/G} + \overline{\omega} \times \left(\overline{\omega} \times \overline{r}_{i/G} \right).$$

In the problem considered here the end-effector is initially at rest before the wrench acts on it. Thus $\overline{a}_{p_i}$ simplifies to:

$$\overline{a}_{p_i} = \overline{a} + \overline{\alpha} \times \overline{r}_{p_i/G}$$

which is a screw quantity. Thus let the acceleration screw $\$^a$ is defined as:

$$\$^a = \begin{pmatrix} \overline{a} \\ \\ \overline{\alpha} \end{pmatrix} = \begin{pmatrix} a_x & a_y & a_z & \alpha_x & \alpha_y & \alpha_z \end{pmatrix}^T \tag{44}$$

where a_x, a_y and a_z are the components of the linear acceleration of the center of gravity and α_x, α_y and α_z are the components of the angular acceleration of the body. The acceleration energy then simplifies[8] to:

$$AE = \int_{body} \frac{1}{2} a^2 \mathrm{d}m = \frac{1}{2} \begin{pmatrix} \overline{a} \\ \\ \overline{\alpha} \end{pmatrix}^T \boldsymbol{M} \begin{pmatrix} \overline{a} \\ \\ \overline{\alpha} \end{pmatrix} = \frac{1}{2} \$^{aT} \boldsymbol{M} \$^a \tag{45}$$

where $\boldsymbol{M}$ is the inertia matrix of the end-effector. Because the end-effector is initially at rest the applied wrench is related to the resulting acceleration screw by:

$$\$^w = \boldsymbol{M} \$^a. \tag{46}$$

[8]The expression in (43) is nearly identical in form to the expression for the kinetic energy of a body, thus the complete derivation of the expression for acceleration energy follows the same steps as the derivation of the kinetic energy expression $KE(\$^t) = \frac{1}{2} \$^{tT} \boldsymbol{M} \$^t$. As such, the complete derivation is not included here.

Noting that $\boldsymbol{M}$ is square, symmetric and invertible, we can see that

$$\$^a = \boldsymbol{M}^{-1}\$^w \tag{47}$$

thus

$$AE = \frac{1}{2}\$^{wT}\boldsymbol{M}^{-1}\boldsymbol{M}\boldsymbol{M}^{-1}\$^w = \frac{1}{2}\$^{wT}\boldsymbol{M}^{-1}\$^w. \tag{48}$$

Thus we define the acceleration energy of a wrench $\$^w$ with respect to the end-effector as

$$AE(\$^w) = \frac{1}{2}\$^{wT}\boldsymbol{M}^{-1}\$^w. \tag{49}$$

At this point we note the similarity of the acceleration energy expression to that of the magnitude of a generalized force in the intermediate space. Recall that in the intermediate space the magnitude of a generalized force is:

$$\parallel \hat{f}_i \parallel = \sqrt{\$_i^{wT}\boldsymbol{B}^2\$_i^w} = \sqrt{2m\, AE\,(\$_i^w)}. \tag{50}$$

Thus the acceleration energy of a wrench can be found directly from the magnitude of the associated generalized force in the intermediate space:

$$AE(\$^w) = \frac{1}{2m} \parallel \hat{f}_i \parallel^2 . \tag{51}$$

4.3.5.2 Correlation of Acceleration Energy to Kinetic Energy

For a wrench applied to a body at rest, the acceleration energy of the wrench with respect to the body is directly proportional to the resulting kinetic energy of the body after a short period of time. If a wrench is applied to the body over a small time Δt (and no other external wrenches are present) the acceleration energy of the wrench relates to the resulting kinetic energy of the body as follows. If we approximate:

$$\$^t \;\approx\; \$^a\Delta t \;=\; \boldsymbol{M}^{-1}\$^w\Delta t$$

then we get the relationship:

$$\begin{aligned} KE(\$^t) &= \frac{1}{2}\$^{t^T}\boldsymbol{M}\$^t && (52)\\ &\approx \frac{1}{2}\$^{w^T}\boldsymbol{M}^{-1}\$^w(\Delta t)^2 && (53)\\ &= AE(\$^w)\Delta t^2 && (54)\end{aligned}$$

where the approximation becomes exact as $\Delta t \to 0$. Equivalently, the wrench can be made impulsive ($\$^w_{dist} = \$^w\delta(t)$), in which case the body will be given an initial velocity (twist) of $\$^t_0$ determined by the impulse-momentum relationship[9]:

$$\begin{aligned} \int_{0^-}^{0^+} \$^w\delta(t)\mathrm{d}t &= \boldsymbol{M}\$^t_{0^+}\\ \$^w sec &= \boldsymbol{M}\$^t_{0^+}\\ \boldsymbol{M}^{-\frac{1}{2}}\$^w sec &= \boldsymbol{M}^{\frac{1}{2}}\$^t_{0^+}\\ \$^{w^T}\boldsymbol{M}^{-1}\$^w sec^2 &= {\$^t_{0^+}}^T\boldsymbol{M}\$^t_{0^+}\\ AE(\$^w)sec^2 &= KE(\$^t_{0^+}) && (55)\end{aligned}$$

As the previous equations demonstrate, **the acceleration energy of a wrench is proportional to the kinetic energy of the resulting twist of the body**. In fact, it can be shown that if the applied wrench and the resulting twist are mapped to the intermediate space they are parallel. Recall

$$\$^w = \boldsymbol{M}\$^a \quad (56)$$

and

$$\$^t \approx \$^a\Delta t. \quad (57)$$

If the wrench is applied over an infinitesimally small period of time and we let $\alpha = \frac{1}{\Delta t}$, the previous expression becomes

$$\alpha\$^t = \$^a. \quad (58)$$

[9]Note that here $\int_{0^-}^{0^+}\delta(t)\mathrm{d}t \equiv 1sec$

Then

$$\$^w = \alpha \boldsymbol{M} \$^t \tag{59}$$

$$= \alpha m \boldsymbol{A}^2 \$^t \tag{60}$$

$$\boldsymbol{B} \$^w = \alpha m \boldsymbol{A} \$^t. \tag{61}$$

Let $\beta = \alpha m$, then

$$\hat{f} = \beta \hat{v}. \tag{62}$$

Thus we can see that the generalized force and generalized velocity associated with the applied wrench and resulting twist are parallel and in the same direction (because $\beta > 0$). An applied wrench and the resulting twist are termed here as a *corresponding* wrench and twist, denoted $\$_c^t$ and $\$_c^w$, respectively. We can now apply the property of parallelism in the intermediate space to make the following claims:

- Given a twist $\$_c^t$, then out of all the wrenches that have the same acceleration energy as $\$_c^w$, $\$_c^w$ has the maximum power product with $\$_c^t$.
- Given a twist $\$_c^t$, then out of all the wrenches that have the same power product with $\$_c^t$ as $\$_c^w$, $\$_c^w$ has the minimum acceleration energy.
- Given a wrench $\$_c^w$, then out of all the twists that have the same kinetic energy as $\$_c^t$, $\$_c^t$ has the maximum power product with $\$_c^w$.
- Given a wrench $\$_c^w$, then out of all the twists that have the same power product with $\$_c^w$ as $\$_c^t$, $\$_c^t$ has the minimum kinetic energy.

These relationships illustrate two things. The first is the unique relationship between an applied wrench and the resulting twist of the manipulator. The relationships show how the corresponding twist and wrench represent solutions to several optimal-value power-product problems. Secondly, these relationships illustrate the symmetry

between acceleration energy and kinetic energy. While acceleration energy may not be as widely used as kinetic energy, it is clear that the two are naturally tied to one another. In fact, Section 4.3.6 will show how acceleration energy can be used to solve initial-value problems for cable robots.

4.3.5.3 Acceleration Energy Norm

Based on the concept of acceleration energy, the *acceleration energy norm*, $\| \$^w \|_a$, is defined as:

$$\| \$^w \|_a = \sqrt{2m\, AE(\$^w)} \tag{63}$$

$$= \sqrt{m \$^{w^T} \boldsymbol{M}^{-1} \$^w} \tag{64}$$

$$= \| \hat{f} \| . \tag{65}$$

Note that the $2m$ term is added such that the acceleration energy norm of a wrench is equal to the magnitude of the associated generalized force. As a result, applying this norm is relatively simple. If all wrenches are mapped to the intermediate space, the magnitudes of the wrenches can be calculated in the same way as they would in a pure-force case. Note also that this norm produces results with units of force. This can be interpreted as the norm producing the magnitude of a pure-force wrench that would have the same acceleration energy with respect to the end-effector as the given wrench.

Comparing this norm to the 2-D test case reveals that it is consistent with the case of a point-mass end-effector, as the norm simplifies to be the Euclidean norm for a task space with only linear units. The significant advantage of this norm over the previously considered norms is that it also accommodates the mixed dimensions of general wrenches and produces results that have physical meaning.

As a side note, a norm similar to the acceleration energy norm can be defined for twists using the kinetic energy associated with the twist. While this norm is not

used in the static disturbance analysis, it will be useful for the impulsive disturbance analysis. The *kinetic energy norm*, $\| \$^t \|_k$, is defined as:

$$\| \$^t \|_k = \sqrt{\frac{2}{m} KE(\$^t)} \tag{66}$$

$$= \sqrt{\frac{1}{m} \$^{t^T} \boldsymbol{M} \$^t} \tag{67}$$

$$= \| \hat{v} \| . \tag{68}$$

Note that the addition of the $\frac{2}{m}$ term is added such that the kinetic energy norm of a twist is equal to the magnitude of the associated generalized velocity. Note also that this norm produces results with units of linear velocity. This can be interpreted as the norm producing the magnitude of a linear velocity that would have the same kinetic energy with respect to the end-effector as the given wrench.

4.3.6 Static Disturbance Robustness Measure

Because the acceleration energy norm provides the most meaningful wrench norm, the proposed static disturbance robustness measure is based on this norm.

Definition: The *static disturbance robustness* measure, $\mathcal{R}_s$, for a pose of a cable robot is:

$$\boxed{\mathcal{R}_s = \frac{1}{mg} \min_{\$^w \in C} \sqrt{\$^{w^T} \boldsymbol{B}^2 \$^w}} \tag{69}$$

$$= \frac{1}{mg} \min_{\hat{f} \in \hat{C}} \| \hat{f} \| \tag{70}$$

$$= \frac{1}{mg} \min_{\$^w \in C} \| \$^w \|_a . \tag{71}$$

where $\boldsymbol{B}$ is the mapping matrix used to map wrenches to the intermediate space and $\hat{C}$ is the set of wrenches in C mapped to the intermediate space.

This measure uses the acceleration energy norm to define the magnitude of a disturbance wrench, which is equivalent to mapping all wrenches to the intermediate space and considering the magnitude of the corresponding generalized forces. **The**

measure then finds the smallest wrench in C, which is the set of all critical wrenches (the static wrenches that just begin to disturb the manipulator). The resulting magnitude is then normalized by the factor $\frac{1}{mg}$. This normalization produces a result between 0 and 1, with 1 corresponding to a manipulator with the highest static disturbance robustness and 0 corresponding to the lowest static disturbance robustness.

As a result of the normalization, the magnitude of this smallest static disturbance wrench is $mg\mathcal{R}_s$. Since $\mathcal{R}_s$ is pose-dependent, $\mathcal{R}_s$ will have different values throughout the workspace of a manipulator. Note that the extension of this measure to include multi-body end-effectors will be discussed in Section 4.6.

4.3.6.1 Calculation and Interpretation

Calculation:

As was discussed in the previous section, the use of acceleration energy to formulate a wrench norm has several advantages, including consistency with the point-mass end-effector case, easy calculation of wrench magnitudes in the intermediate space, and a physically meaningful way of resolving the mixed-dimensionality of the wrenches. The measure is also scale- and frame-invariant. That is, it does not matter where the global coordinate frame is placed or what system of units is used, the result will be the same. The measure also handles redundant manipulators just as easily as it does non-redundant manipulators.

By providing a lower bound on the wrenches that disturb the end-effector, this measure also allows for other types of disturbances to be analyzed. For example, an oscillating disturbance wrench or random wrenches (like white noise) could be applied to the end-effector. If the acceleration energy norm of such a disturbance has a known upper bound that is at or below $mg\mathcal{R}_s$ then the end-effector can resist that disturbance.

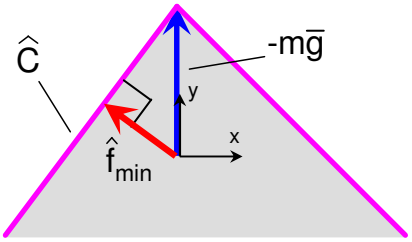

Figure 17: Calculation of the smallest wrench in $\hat{C}$.

Note also that finding the smallest generalized force in $\hat{C}$ in the intermediate space is fairly simple. Consider Figure 17. Because C is made up of planar segments, $\hat{C}$ is made up of planar segments (because the mapping to the intermediate space is linear). From geometry we know that the shortest distance between a point and a plane is along a line perpendicular to the plane. Thus the vector to the smallest generalized force in $\hat{C}$ will be perpendicular to one of these segments. In order to find the smallest generalized force only the forces perpendicular to the planar segments of $\hat{C}$ need to be considered.

The calculation of the smallest wrench in C can also be formulated as an optimization problem. For brevity this will be described here for the non-redundant case of $p = n$. Let a modified Jacobian matrix be defined as $\boldsymbol{J}^T_{mod,i} = \begin{bmatrix} \$^w_1 & \dots & \$^w_{i-1} & \$^w_{i+1} & \dots & \$^w_p \end{bmatrix}$. Note that the columns of $\boldsymbol{J}^T_{mod,i}$ span one of the sides of C. Let us also define $\overline{t}_{mod,i} = (t_1 \ \dots \ t_{i-1} \ t_{i+1} \ \dots \ t_p)^T$. Finding the smallest wrench in one of the sides of C becomes:

$$\begin{aligned} \text{minimize} \quad & \frac{1}{2}\$^{wT}\boldsymbol{M}^{-1}\$^w \\ \text{such that} \quad & \$^w = \boldsymbol{J}^T_{mod,i}\overline{t}_{mod,i} + m\overline{g} \\ \text{and} \quad & \overline{t}_{mod,i} \geq \overline{0} \end{aligned} \tag{72}$$

where $\overline{t}_{mod,i} \geq \overline{0}$ implies that each element of $\overline{t}_{mod,i}$ is nonnegative. The solution (when $\overline{t}_{mod,i} > \overline{0}$) is:

$$\$^w_{min,i} = -m\boldsymbol{J}^T_{mod,i}\left(\boldsymbol{J}_{mod,i}\boldsymbol{M}^{-1}\boldsymbol{J}^T_{mod,i}\right)^{-1}\boldsymbol{J}_{mod,i}\boldsymbol{M}^{-1}\overline{g} + m\overline{g}. \tag{73}$$

Then $\$^w_{min}$, the smallest wrench in C, is found by:

$$\$^w_{min} = \min_{i \in \{1,2,\ldots p\}} \$^w_{min,i}. \tag{74}$$

Interpretation:

In addition, the use of an acceleration energy norm to find the smallest disturbance wrench has another connection to the physical behavior of the system. Consider a general underconstrained cable robot with p cables[10] where $p = n$. Then $\boldsymbol{J}^T = \begin{bmatrix}\$^w_1 & \cdots & \$^w_p\end{bmatrix}$ is $n \times n$, where $\$^w_i$ is the wrench along the i^{th} cable. Assume that $\boldsymbol{J}^T$ is full rank.

Now consider what happens if cable i (which is assumed to have a nonzero tension) is cut. The manipulator cannot counteract the force of gravity and thus the manipulator will begin to accelerate. Let the initial wrench that accelerates the end-effector from its original pose be called $\$^w_{init}$. Note that $\$^w_{init}$ is exerted by gravity and the remaining $p-1$ cables. At this instant the new Jacobian transpose, $\boldsymbol{J}^T_{new}$, will be $\boldsymbol{J}^T = \begin{bmatrix}\$^w_1 & \cdots & \$^w_{i-1} & \$^w_{i+1} & \cdots & \$^w_p\end{bmatrix}$ and is now $n \times (n-1)$. Initially all cables will remain taut, and thus the initial twist of the manipulator $\$^t_{init}$ is reciprocal[11] to the columns of $\boldsymbol{J}^T_{new}$. As we know from discussion of the intermediate space, reciprocality between a twist and a wrench corresponds to perpendicularity between the associated generalized velocity and generalized force. Thus since $\$^t_{init}$ is reciprocal to $\{\$^w_1, \cdots, \$^w_{i-1}, \$^w_{i+1}, \cdots, \$^w_p\}$, it is reciprocal to the hyperplane spanned by these wrenches. In the intermediate space, the generalized velocity is thus perpendicular to the side of $\hat{C}$ corresponding to the hyperplane spanned by those generalized wrenches.

Recall that $\hat{C}$ is the set of upper sides of $-NW_{avail}$ mapped to the intermediate space. Let $-\hat{C}$ be the set of lower sides of NW_{avail} mapped to the intermediate space. Because $\$^w_{init}$ is exerted by gravity and the remaining $p-1$ cables, it must lie

[10]Note that this analysis works equally well for redundant manipulators, but for simplicity of explanation the manipulator is assumed non-redundant

[11]Note that this analysis will be described in greater detail in Section 4.4.2.

on one of the lower boundaries of NW_{avail}. Specifically, it must be on the lower side of NW_{avail} spanned by $\{\$_1^w, \cdots, \$_{i-1}^w, \$_{i+1}^w, \cdots, \$_p^w\}$. Thus in the intermediate space it lies on the corresponding side of $-\hat{C}$. As discussed earlier, the wrench (generalized force) applied to a body is parallel to the resulting twist (generalized velocity) of the body in the intermediate space. From the previous reasoning we know that the vector corresponding to the resulting generalized velocity $\hat{v}_{init}$ is perpendicular to the side of $\hat{C}$ in the intermediate space. The vector to $\hat{f}_{init}$ must therefore also be perpendicular to the corresponding side of $-\hat{C}$. Thus in the intermediate space the generalized force $\hat{f}_{init}$ is parallel to $\hat{v}_{init}$ and thus is also perpendicular to the side of $-\hat{C}$. Therefore we can conclude that $\hat{f}_{init}$ is the smallest generalized force in the side of $-\hat{C}$.

Let us instead consider the side of C that corresponds to the $p-1$ cables that are not cut. If we use the acceleration energy norm to find the smallest wrench in this set, we get a wrench that corresponds to a generalized force with the minimum distance from the origin. The vector to this wrench in $\hat{C}$ is perpendicular to that side of $\hat{C}$, as illustrated in Figure 17. This wrench is the smallest wrench (using the acceleration energy norm) that causes cable i to go slack. Let us call this wrench $\$_{dist,i}^w$ and the corresponding generalized force $\hat{f}_{dist,i}$. Because this wrench is the smallest wrench in the side of C, it must be equal and opposite to $\hat{f}_{init}$. **Thus we can see that the wrench $\$_{dist,i}^w$ is in fact the *exact same wrench* as $\$_{init}^w$, but now in the opposite direction. That is, $\$_{init}^w = -\$_{dist,i}^w$.**

Summary:

Thus we see that using the acceleration energy norm produces a wrench that exactly opposes the wrench exerted on the end-effector if the constraint of a cable is lost. In other words, **out of all the wrenches that could be exerted by the cables and gravity on the end-effector, the manipulator naturally exerts the wrench with the smallest acceleration energy**. If we consider each of the p different cases of a cable being cut, the smallest possible wrench that the robot will

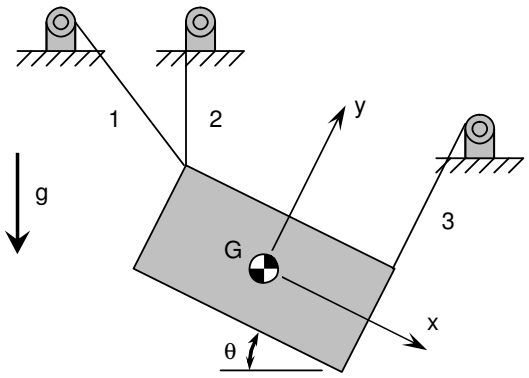

Figure 18: Static robustness measure example.

exert out of these cases has magnitude $mg\mathcal{R}_s$. Thus this measure produces results consistent with the physical behavior of the system.

4.3.6.2 Example

Consider the planar 3-DOF 3-cable manipulator shown in Figure 18. The end-effector is a 2 m $\times$ 4 m rectangle with a mass of 100 kg and rotational inertia of $\frac{500}{3}\text{kg}\cdot\text{m}^2$ ($\rho_z = \sqrt{\frac{5}{3}}\text{m}$). In the given pose the bottom edge has a slope of $-\frac{1}{2}$ with respect to gravity (i.e. $\tan\theta = \frac{1}{2}$), cable 1 is collinear with G, cable 2 is vertical and cable 3 is aligned with the right edge of the end-effector. The origin of the x-y coordinate frame is placed at G, with the axes parallel to the edges of the end-effector. While in a planar problem it would be possible to simply align the y-axis with gravity, the coordinate frame is aligned with the geometry of the end-effector to illustrate how the coordinate frame would align with the principal axes of a spatial end-effector.

Forming $\boldsymbol{J}^T$ results in:

$$\boldsymbol{J}^T = \begin{bmatrix} \frac{-2}{\sqrt{5}} & \frac{-1}{\sqrt{5}} & 0 \\ \frac{1}{\sqrt{5}} & \frac{2}{\sqrt{5}} & 1 \\ 0 & \frac{-3}{\sqrt{5}}\,\text{m} & 2\,\text{m} \end{bmatrix} = \begin{bmatrix} \$_1^w & \$_2^w & \$_3^w \end{bmatrix}.$$

Calculation of the gravitational wrench results in:

$$\$^w_{grav} = \begin{pmatrix} \frac{1}{\sqrt{5}} \\ \frac{-2}{\sqrt{5}} \\ 0 \end{pmatrix} 980\,\mathrm{N}. \tag{75}$$

Mapping the gravitational wrenches and the columns of $\boldsymbol{J}^T$ to the intermediate space results in:

$$\hat{f}_{grav} = \begin{pmatrix} \frac{1}{\sqrt{5}} \\ \frac{-2}{\sqrt{5}} \\ 0 \end{pmatrix} 980\,\mathrm{N} \qquad \hat{f}_1 = \begin{pmatrix} \frac{-2}{\sqrt{5}} \\ \frac{1}{\sqrt{5}} \\ 0 \end{pmatrix} \frac{\mathrm{m}}{\mathrm{s}}$$

$$\hat{f}_2 = \begin{pmatrix} \frac{-1}{\sqrt{5}} \\ \frac{2}{\sqrt{5}} \\ \frac{-3\sqrt{3}}{5} \end{pmatrix} \frac{\mathrm{m}}{\mathrm{s}} \qquad \hat{f}_3 = \begin{pmatrix} 0 \\ 1 \\ \frac{2\sqrt{3}}{\sqrt{5}} \end{pmatrix} \frac{\mathrm{m}}{\mathrm{s}}.$$

In the intermediate space the smallest generalized force in C is perpendicular to a planar side of $\hat{C}$. Thus the smallest generalized force in the side of $\hat{C}$ spanned by $\hat{f}_i$ and $\hat{f}_j$ is perpendicular to both $\hat{f}_i$ and $\hat{f}_j$. Let us construct unit vector $\hat{u}_{i,j}$ perpendicular to $\hat{f}_i$ and $\hat{f}_j$ directed such that $\hat{u}_{i,j} \cdot \hat{f}_{grav} > 0$. This results in:

$$\hat{u}_{1,2} = \begin{pmatrix} \frac{-\sqrt{3}}{2\sqrt{5}} \\ \frac{-\sqrt{3}}{\sqrt{5}} \\ \frac{-1}{2} \end{pmatrix} \qquad \hat{u}_{1,3} = \begin{pmatrix} \frac{-\sqrt{15}}{10} \\ \frac{-\sqrt{15}}{5} \\ \frac{1}{2} \end{pmatrix} \qquad \hat{u}_{2,3} = \begin{pmatrix} \frac{7\sqrt{3}}{2\sqrt{41}} \\ \frac{\sqrt{3}}{\sqrt{41}} \\ \frac{-\sqrt{5}}{2\sqrt{41}} \end{pmatrix}.$$

Note that the smallest wrench in the side of $\hat{C}$ spanned by $\hat{f}_i$ and $\hat{f}_j$ is $\hat{f}_{ij,min} = \| \hat{f}_{i,j,min} \| \hat{u}_{i,j}$. Then using the fact that:

$$\left(\hat{f}_i \times \hat{f}_j\right) \cdot \hat{f}_{grav} = \left(\hat{f}_i \times \hat{f}_j\right) \cdot \hat{f}_{ij,min}$$

we can find the smallest $\| \hat{f}_{i,j,min} \|$:

$$\| \hat{f}_{1,2,min} \| = \frac{\left(\hat{f}_1 \times \hat{f}_2\right) \cdot \hat{f}_{grav}}{\left(\hat{f}_1 \times \hat{f}_2\right) \cdot \hat{u}_{1,2}} = 509.2\,\mathrm{N}$$

$$\| \hat{f}_{1,3,min} \| = \frac{\left(\hat{f}_1 \times \hat{f}_3\right) \cdot \hat{f}_{grav}}{\left(\hat{f}_1 \times \hat{f}_3\right) \cdot \hat{u}_{1,3}} = 509.2\,\mathrm{N}$$

$$\| \hat{f}_{2,3,min} \| = \frac{\left(\hat{f}_2 \times \hat{f}_3\right) \cdot \hat{f}_{grav}}{\left(\hat{f}_2 \times \hat{f}_3\right) \cdot \hat{u}_{2,3}} = 177.8\,\mathrm{N}.$$

Thus the smallest static disturbance wrench has a magnitude of 177.8 N (using the acceleration energy norm). The corresponding static robustness measure is $\mathcal{R}_s = \frac{\|\hat{f}_{2,3,min}\|}{mg} = \frac{177.8\,\mathrm{N}}{980\,\mathrm{N}} = 0.1815$. Note that the calculation of the smallest static disturbance wrench has also been verified using computer simulation, as discussed in Appendix B.

4.4 Impulsive Disturbance Analysis

4.4.1 Motivation

In contrast to the previous section, which focused on static disturbance wrenches, this section will examine the effect of impulsive disturbance wrenches. Whereas some static wrenches will disturb a manipulator and some will not, all[12] impulsive disturbance wrenches disturb the end-effector. This is because all impulsive wrenches have an infinite magnitude (theoretically), albeit acting over an infinitesimally small period of time.

Once the end-effector is disturbed it will follow some trajectory, which is limited by the constraints imposed by the cables (assuming the cables do not break). These constraints form *constraint surfaces* in the task space of the manipulator. For

[12]Note that we will not be considering impulsive wrenches that act against the constraint of the cables, because the magnitude of an impulse is theoretically infinite, and thus would always cause a cable to break.

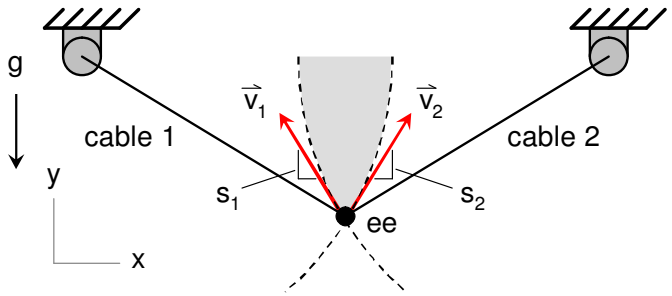

Figure 19: Example of constraint surfaces.

example, consider the cable robot with a point-mass end-effector shown in Figure 19. The end-effector (labeled *ee*) is suspended from two cables. Each of the cables has a fixed length and thus imposes a constraint on the position of the end-effector. In this case the constraint surfaces are represented by the dashed arcs, where the end-effector must be inside the circle bounded by each dashed arc. Thus the shaded area is the set of all positions that the end-effector could be located without violating the cable constraints.

Given that the end-effector will be disturbed, we wish for the end-effector to return to its original pose as quickly as possible. However, determining the complete trajectory of the end-effector is very complex and will depend on many factors not included in the idealized model, including contact of cables with the end-effector, contact of cables with each other, damping due to the environment, friction, spring rates of the cables, mass of the cables, losses in the cables, etc. In particular, if a manipulator is given a significantly large disturbance, the manipulator will "bounce around" the constraint surfaces as the end-effector moves until a cable is taut and then springs back. Such a system is highly unpredictable and extremely difficult to analyze. Large displacements of the end-effector also require complete knowledge of the constraint surfaces, which are quite complicated. Rather than trying to determine the trajectory and corresponding settling time for a disturbed end-effector, this analysis will focus on determining the initial acceleration of the end-effector back

toward the original pose assuming small displacements of the end-effector. Examining the initial acceleration of the end-effector provides insight into the response of the manipulator without requiring analysis of unpredictable motion, knowledge of non-ideal system behavior or a complete model of the constraint surfaces.

The approach for this analysis is to determine the possible initial accelerations of the end-effector, specifically the vertical acceleration of the end-effector. We choose to examine the vertical acceleration of the end-effector because it will be shown in Section 4.4.3 that the vertical acceleration is proportional to the magnitude of the acceleration energy of the total (linear and angular) acceleration vector.

The set of possible initial accelerations of the end-effector is determined by the possible initial twists of the end-effector, which are in turn determined by the constraint surfaces. Section 4.4.2 describes the effect of the constraint surfaces by forming the set of all possible initial twists of the end-effector. Section 4.4.3 then shows how the corresponding accelerations of the end-effector can be determined. **Based on this set of accelerations, the *impulsive disturbance robustness measure* is defined in Section 4.4.4 by the smallest (magnitude) acceleration of the end-effector back towards its original pose. Note that since no initial acceleration will have an upward component, the smallest vertical acceleration possible is 0 (the worst case) and the largest possible is $\overline{g}$ (the best case).** Similar to the static disturbance robustness measure, this measure captures the worst-case scenario for the manipulator. Defining impulsive robustness using the lowest acceleration provides a lower bound on the magnitude of the initial acceleration of the end-effector back to its original pose and corresponds (excluding the case of unpredictable "bouncing") to the slowest return of the end-effector to its original pose.

Assumptions

As stated earlier, the analysis will be performed assuming small displacements of

the end-effector in order to reduce the complexity of modeling the constraint surface. A displacement is considered to be "small" if a linear approximation of the constraint surfaces is valid. Note that for simplicity we are considering an impulsive disturbance that acts on the end-effector and then no additional disturbances are present. The lengths of the cables are held constant and the end-effector is in static equilibrium prior to the disturbance.

4.4.2 Unconstrained Twists

Forming the complete constraint surface for a particular pose of an underconstrained cable robot can be very difficult. However, in order to find the initial twists (and corresponding accelerations) of the end-effector it is only necessary to form the constraint surface locally, that is, in an infinitesimal sense. Because the local constraint surface only limits the infinitesimal displacement of the end-effector, it is appropriate to think of the constraint surface as providing a constraint on the instantaneous twists that the end-effector could be given at this pose. Thus the effects of the local constraint surface can be examined by forming the set of all twists that the end-effector can undergo instantaneously without violating the constraints imposed by the cables. This set will be referred to as the set of *unconstrained twists*, U.

The set U can be formed by analysis of the Jacobian matrix of the robot. Recall from Chapter 3 that the Jacobian matrix $\boldsymbol{J}$ defines the linear relationship between the velocities of the cables extending or retracting $(\dot{q}_1 \ ... \ \dot{q}_m)$ and the resulting twist of the end-effector $\$^t = \begin{pmatrix} \overline{v} \\ \overline{\omega} \end{pmatrix}$:

$$\begin{pmatrix} \dot{q}_1 \\ \vdots \\ \dot{q}_p \end{pmatrix} = \boldsymbol{J}\$^t \tag{76}$$

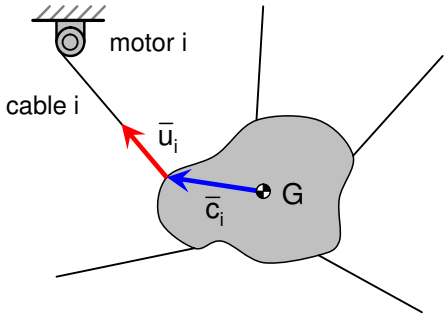

Figure 20: Diagram of kinematic parameters.

where

$$\boldsymbol{J} = \left[\$_1^w \ \ldots \ \$_p^w\right]^T \tag{77}$$

and $\$_i^w$ is the wrench from the i^{th} cable (in ray coordinates):

$$\$_i^w = \begin{pmatrix} \overline{u}_i \\ \\ \overline{c}_i \times \overline{u}_i \end{pmatrix} \tag{78}$$

where $\overline{u}_i$ is the unit vector running along cable i directed away from the end-effector, $\overline{c}_i$ is the vector from G, the center of gravity of the end-effector, to the point on the end-effector where cable i is connected, as illustrated in Figure 20, and there are p cables attached to the end-effector. Note that $\dot{q}_i > 0$ corresponds to the i^{th} cable being reeled in. For this Jacobian relationship to hold all cables must remain in tension.

Based on $\boldsymbol{J}$, the set of unconstrained twists U can be formed. A method is presented first for determining U when the manipulator is not redundant. After the method is presented, it will be discussed briefly how the method must be modified for redundant manipulators.

The set U consists of two subsets of twists, termed *Bi-Directional Unconstrained Twists* and *Uni-Directional Unconstrained Twists*. These subsets can be formed by examining the nullspace of $\boldsymbol{J}$ and the nullspaces of modified $\boldsymbol{J}$'s, respectively.

4.4.2.1 Bi-Directional Unconstrained Twists

In order to find the bi-directional unconstrained twists (also referred to here as simply "bi-directional twists"), it is necessary to determine whether $\boldsymbol{J}$ has a nontrivial nullspace. If it does, that means that there exists a twist that the end-effector can instantaneously undergo without violating any cable constraints or causing any of the cables to go slack. If $p < n$, this will always be the case regardless of the location of the end-effector within the workspace. If, however, $p \geq n$, a nontrivial nullspace of the Jacobian means that the manipulator is in a configuration where the constraints imposed by the cables have degenerated due to the geometry of the pose. Such a situation has been termed a "wrench deficiency" of a cable robot [12], and is very similar to a singularity of a parallel robot.

Regardless, if a nontrivial nullspace of $\boldsymbol{J}$ exists of dimension s, then a set of s linearly independent twists that span the nullspace of $\boldsymbol{J}$ can be formed and labeled $\$^t_{bi,1}$ through $\$^t_{bi,s}$. These twists are bi-directional twists, so named because the end-effector can move in either the positive or negative direction, $\$^t_{bi,j}$ or $-\$^t_{bi,j}$, without violating a cable constraint. The span of these twists forms the complete set of all bi-directional twists.

4.4.2.2 Uni-Directional Unconstrained Twists

The remaining elements of U are uni-directional unconstrained twists (also referred to here as simply "uni-directional twists"), which cause one or more cables to go slack. In order to form the uni-directional twists, sub-matrices of the Jacobian must be formed. First we form the Jacobian matrix, $\boldsymbol{J}_{mod,i}$, that would result if the i^{th} cable were removed by removing the i^{th} row of $\boldsymbol{J}$:

$$\boldsymbol{J}_{mod,i} = \begin{bmatrix} \$^w_1 & \dots & \$^w_{i-1} & \$^w_{i+1} & \dots & \$^w_p \end{bmatrix}^T. \tag{79}$$

The nullspace of this modified matrix $\boldsymbol{J}_{mod,i}$ is one dimension higher than the original nullspace of $\boldsymbol{J}$. A new twist, termed $\$^t_{uni,i}$, can be constructed such that the set of

twists $\left\{\$^t_{uni,i},\ \$^t_{bi,1},\ \ldots,\$^t_{bi,s}\right\}$ spans the nullspace of $\boldsymbol{J}_{mod,i}$ and $\$_i{}^T\$^t_{uni,i} > 0$.

If the end-effector undergoes any twist $\beta\$^t_{uni,i}$, where β is a scalar, then if $\beta > 0$ cable i will go slack, if $\beta < 0$ the constraint imposed by cable i is violated, and if $\beta = 0$ cable i remains taut. This is the source of the name "uni-directional unconstrained twist," because $\beta\$^t_{uni,i}$ is an instantaneously permissible motion only if $\beta \geq 0$ (i.e. the motion along the twist is permitted in only one direction). This can be easily verified by noting that

$$\boldsymbol{J}\left\{\beta\$^t_{uni,i}\right\} = \beta\begin{bmatrix}\$_1{}^T\\ \vdots \\ \$_p{}^T\end{bmatrix}\$^t_{uni,i} = \beta\begin{bmatrix}0\\ \vdots\\ 0\\ \$_i{}^T\$^t_{uni,i}\\ 0\\ \vdots\\ 0\end{bmatrix} = \begin{bmatrix}0\\ \vdots\\ 0\\ \dot{q}_i\\ 0\\ \vdots\\ 0\end{bmatrix} \tag{80}$$

where $\dot{q}_i$ is the velocity at which cable i must be reeled in ($\dot{q}_i > 0$) or out ($\dot{q}_i < 0$) in order to keep the cable taut. Noting that $\dot{q}_i = \beta\$_i{}^T\$^t_{uni,i}$, and $\$_i{}^T\$^t_{uni,i} > 0$, then if all cable lengths are held fixed, $\beta < 0$ would result in the cable needing to be reeled out, thus the cable constraint is being violated. $\beta > 0$ would result in the cable needing to be reeled in, thus the cable will go slack.

This procedure can be repeated for each of the cables, where the nullspace of $\boldsymbol{J}_{mod,i}$ is used to form the twist $\$^t_{uni,i}$, resulting in the set of twists $\left\{\$^t_{uni,1},\ \ldots,\$^t_{uni,p}\right\}$. The set of bi-directional and uni-directional twists $\left\{\$^t_{bi,1},\ \ldots,\$^t_{bi,s},\ \$^t_{uni,1},\ \ldots,\$^t_{uni,p}\right\}$ is referred to here as the set of *principal twists*, denoted by $\mathcal{P}$.

4.4.2.3 Forming U

Theorem **:**

The set of all unconstrained twists U can be described as:

$$\begin{aligned} U \;=\; \{\$^t \mid \$^t = a_1\$^t_{bi,1} + a_2\$^t_{bi,2} + ... + a_s\$^t_{bi,s} \\ + b_1\$^t_{uni,1} + b_2\$^t_{uni,2} + ... + b_p\$^t_{uni,p}, \\ \text{where} \quad a_i \in (-\infty, \infty) \quad \text{and} \quad b_j \in [0, \infty) \,\}. \end{aligned} \tag{81}$$

Proof **:**

First we prove that the twists in $\left\{\$^t_{bi,1} \; ... \; \$^t_{bi,s} \;\; \$^t_{uni,1} \; ... \; \$^t_{uni,p}\right\}$ are linearly independent by contradiction. Assume that these twists are linearly dependent. Then there are coefficients $a_1, ..., a_s, b_1, ..., b_p \in I\!R$, with not all coefficients zero such that:

$$a_1\$^t_{bi,1} + ... + a_s\$^t_{bi,s} + b_1\$^t_{uni,1} + ... + b_p\$^t_{uni,p} = \overline{0} \tag{82}$$

so

$$\boldsymbol{J}\left(a_1\$^t_{bi,1} + ... + a_s\$^t_{bi,s} + b_1\$^t_{uni,1} + ... + b_p\$^t_{uni,p}\right) \;=\; \boldsymbol{J}\overline{0} \;=\; \overline{0} \tag{83}$$

$$a_1\boldsymbol{J}\$^t_{bi,1} + ... + a_s\boldsymbol{J}\$^t_{bi,s} + b_1\boldsymbol{J}\$^t_{uni,1} + ... + b_p\boldsymbol{J}\$^t_{uni,p} \;=\; \overline{0}. \tag{84}$$

Because each $\$^t_{bi,i}$ is in the nullspace of $\boldsymbol{J}$, $\boldsymbol{J}\$^t_{bi,i} = 0$ for $i = 1, ..., s$. Thus

$$b_1\boldsymbol{J}\$^t_{uni,1} + ... + b_p\boldsymbol{J}\$^t_{uni,p} = \overline{0}. \tag{85}$$

Let ${\$_i}^T\$^t_{uni,i} = d_i > 0$. Then using the results of (80) equation (85) becomes:

$$b_1\begin{bmatrix} d_1 \\ 0 \\ \vdots \\ 0 \end{bmatrix} + ... + b_p\begin{bmatrix} 0 \\ \vdots \\ 0 \\ d_p \end{bmatrix} = \begin{bmatrix} b_1d_1 \\ \vdots \\ b_pd_p \end{bmatrix} = \overline{0}. \tag{86}$$

And because each $d_i > 0$, the only way this can be true is if $b_1 = ... = b_p = 0$. Thus equation (82) can only be true if $a_1\$^t_{bi,1} + ... + a_s\$^t_{bi,s} = \overline{0}$. Not all a_i may be zero, thus in order for this to be true, the twists $\$^t_{bi,1}, ..., \$^t_{bi,s}$ must be linearly dependent. However, this set is defined in Section 4.4.2.1 as being linearly independent. This is a contradiction. Thus the assumption cannot be true and the twists in $\left\{\$^t_{bi,1} \; ... \; \$^t_{bi,s} \;\; \$^t_{uni,1} \; ... \; \$^t_{uni,p}\right\}$ are linearly independent.

Because these twists are linearly independent and $s + p = n$ (because the manipulator is not redundant), these twists span the space $I\!R^n$ and thus any arbitrary twist $\$^t_i$ can be expressed as a linear combination of these twists:

$$\$^t_i = a_1\$^t_{bi,1} + ... + a_s\$^t_{bi,s} + b_1\$^t_{uni,1} + ... + b_p\$^t_{uni,p}. \tag{87}$$

Now we investigate the range of values of a_i and b_j that define the unconstrained twists. It can be determined whether or not this twist $\$^t_i$ violates any of the cable constraints by checking the power product of this twist with the wrench along each cable. If the power product with any cable is less than zero, the cable constraint is violated. The power product of the twist with the screw along cable j is:

$$\mathbb{P}_j = \$^T_j\$^t_i. \tag{88}$$

Because $\$^t_i$ can be expressed as a linear combination of the previously defined twists, this becomes:

$$\mathbb{P}_j = \$^T_j \left(a_1\$^t_{bi,1} + ... + a_s\$^t_{bi,s} + b_1\$^t_{uni,1} + ... + b_p\$^t_{uni,p}\right). \tag{89}$$

However, because $\$^T_j$ is a row of $\boldsymbol{J}$ and all twists $\$^t_{bi,1}, ..., \$^t_{bi,s}$ lie in the nullspace of $\boldsymbol{J}$,

$$\mathbb{P}_j = \$^T_j \left(b_1\$^t_{uni,1} + ... + b_p\$^t_{uni,p}\right). \tag{90}$$

Also, because each twist $\$^t_{uni,k}$ lies in the nullspace of $\boldsymbol{J}_{mod,k}$,

$$\$^T_j\$^t_{uni,k} = 0 \quad k \neq j. \tag{91}$$

Thus the power product of the twist with wire j becomes:

$$\mathbb{P}_j = b_j \$_j^T \$_{uni,j}^t. \tag{92}$$

Because $\$_{uni,j}^t$ is constructed such that $\$_j^T \$_{uni,j}^t > 0$, $\mathbb{P}_j$ will be greater than zero iff $b_j > 0$. Thus if any b_j's are less than zero, $\mathbb{P}_j$ will be less than zero and thus a cable constraint will be violated, while if no b_j's are less than zero, all $\mathbb{P}_j$'s will be greater than or equal to zero and no cable constraints are violated and thus the twist is unconstrained. Therefore a twist lies in the set of unconstrained twists U iff $a_i \in (-\infty, \infty)$ and $b_j \in [0, \infty)$. Q.E.D. □

4.4.2.4 Modification for Redundant Manipulators

Note that for non-redundant cable robots $p+s = n$, where s was the dimension of the nullspace of $\boldsymbol{J}$ and n is the dimension of the task space. For a redundant manipulator, the procedure must be modified slightly. If there are p cables and the dimension of the task space is n and $p > n$, then the modified $\boldsymbol{J}$s must be formed by removing $(p - n + 1)$ rows at a time. The corresponding uni-directional twists must then be formed by checking that each $\$_{uni,i,j,...}^t$ has a positive power product with the rows removed from $\boldsymbol{J}$ to form the corresponding $\boldsymbol{J}_{mod,i,j,...}$.

Example:

For example, if a manipulator with a point-mass end-effector ($n = 3$) is suspended from four cables ($p = 4$), 6 modified Jacobian matrices ($\boldsymbol{J}_{mod,1,2}$, $\boldsymbol{J}_{mod,1,3}$, $\boldsymbol{J}_{mod,1,4}$, $\boldsymbol{J}_{mod,2,3}$, $\boldsymbol{J}_{mod,2,4}$, $\boldsymbol{J}_{mod,3,4}$) must be formed, where $\boldsymbol{J}_{mod,i,j}$ is formed by removing rows i and j from $\boldsymbol{J}$. The corresponding uni-directional twists $\$_{uni,i,j}^t$ can then be constructed using these matrices in the same manner as before, where $\$_{uni,i,j}^t$ must satisfy ${\$_i}^T \$_{uni,i,j}^t > 0$ and ${\$_j}^T \$_{uni,i,j}^t > 0$. Note, however that not all twists $\$_{uni,i,j}^t$ can be constructed such that both inequalities are satisfied. If such a twist cannot be constructed it is discarded. In general, $\binom{p}{p-n+1}$ different $\boldsymbol{J}_{mod}$ matrices must be formed, but the maximum number of resulting uni-directional twists is p.

4.4.3 Acceleration

Recall that the end-effector started in a static-equilibrium pose and an impulsive disturbance was applied to the end-effector, resulting in an initial twist. We now wish to find the possible initial accelerations of the end-effector (after the impulse is done acting on the end-effector) and then define the disturbance robustness of the pose of the manipulator by the lowest acceleration.

For general motion, the equations of motion of the end-effector are:

$$\begin{pmatrix} \overline{F} \\ \overline{M} \end{pmatrix} = \boldsymbol{M} \begin{pmatrix} \overline{a} \\ \overline{\alpha} \end{pmatrix} + \begin{pmatrix} \overline{0} \\ \overline{\omega} \times ([\boldsymbol{In}]\,\overline{\omega}) \end{pmatrix} \tag{93}$$

where $\boldsymbol{M}$ is the 6×6 inertia matrix and $[\boldsymbol{In}]$ is the 3×3 rotational inertia (mass moment of inertia) matrix.

Because a linear approximation of the constraint surface is being used locally (they are modeled as planar), this approximation is only valid if the displacements of the end-effector are small. If the impulse is large (i.e. it imparts a large amount of kinetic energy to the end-effector) then the resulting twist will be large, causing the end-effector to have a large displacement. Thus in order to use the linear approximation of the constraint surfaces the analysis here is restricted to situations where the impulse is small. As such, it is also assumed that the initial angular velocity is small enough that the term $\overline{\omega} \times ([\boldsymbol{In}]\,\overline{\omega})$ can be neglected. In other words, it is assumed that $\| \overline{\omega} \times ([\boldsymbol{In}]\,\overline{\omega}) \| \ll \| [\boldsymbol{In}]\,\overline{\alpha} \|$. Then the equations of motion are approximately:

$$\begin{pmatrix} \overline{F} \\ \overline{M} \end{pmatrix} \approx \boldsymbol{M} \begin{pmatrix} \overline{a} \\ \overline{\alpha} \end{pmatrix}. \tag{94}$$

Recall that $\$^a = \begin{pmatrix} \overline{a} \\ \overline{\alpha} \end{pmatrix}$, so since $\boldsymbol{M} = m\boldsymbol{A}^2$ and $\boldsymbol{B} = \boldsymbol{A}^{-1}$

$$\$^w \approx \boldsymbol{M}\$^a \tag{95}$$

$$\$^w \approx m\boldsymbol{A}^2\$^a \tag{96}$$

$$\boldsymbol{B}\$^w \approx m\boldsymbol{A}\$^a. \tag{97}$$

Let the mapping of $\$^a$ to the intermediate space (via $\boldsymbol{A}$) be called a generalized acceleration, $\hat{a}$. Then the equations of motion become:

$$\hat{f} = m\hat{a} \tag{98}$$

which is equivalent in form to the dynamics of a point-mass. Thus if the assumption that $\overline{\omega}$ is very small is valid, the dynamics of the end-effector reduce to that of a (generalized) point-mass with pure forces acting on it. In addition, because the constraint surfaces are approximated as planar in the intermediate space, the generalized force reactions due to the constraint surfaces will be perpendicular to these planar surfaces. This allows the acceleration of the end-effector to be found relatively easily.

The initial acceleration of the end-effector depends upon the direction of the initial twist, because the effect of the constraint surfaces on the initial acceleration will differ depending on the initial motion. Several cases must now be considered in order to find the case that corresponds to the smallest magnitude vertical acceleration. The disturbance can cause the initial twist to be 1) along a bi-directional twist (0 cables go slack), 2) along a uni-directional twist (1 cable goes slack[13]), 3) along a constraint surface (but not a principal twist - more than 1 cable goes slack), and 4) not along a constraint surface (all cables go slack).

[13]One cable goes slack for motion along a uni-directional twist for a non-redundant manipulator. In the case of redundancy ($p > n$), then $p - n + 1$ cables go slack for motion along a uni-directional twist.

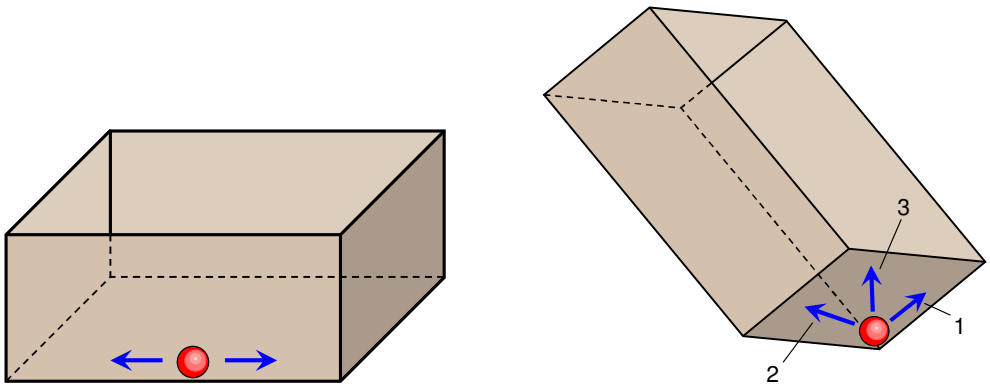

(a) Marble rolling along a horizontal edge.

(b) Marble 1) rolling along an edge, 2) rolling along a side and 3) moving up into the air.

Figure 21: Analogy of a marble rolling inside a box.

As a simple illustration of these cases, consider Figure 21. The movement of the end-effector along the constraint surfaces in the intermediate space can be thought of as a marble moving in a box. The marble begins in static equilibrium and is then disturbed by an impulse, resulting in a small initial velocity. We wish to then find the initial acceleration of the marble due to gravity back towards is equilibrium position. Figure 21(a) shows a case where the sides of the box are such that the marble can roll horizontally to the right or left. Given a horizontal disturbance the marble can roll in either direction. This is analogous to motion of the end-effector along a bi-directional twist. Figure 21(b) shows the case where the box is angled such that the marble rests in one of the corners of the box. If the marble is disturbed it can 1) roll along one of the edges of the box (analogous to motion along a uni-directional twist), 2) roll along one of the sides of the box (analogous to motion along a constraint surface) or 3) move up into the air, not contacting the box (analogous to motion not along a constraint surface).

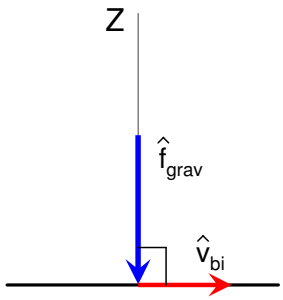

Figure 22: Acceleration along a bi-directional twist in the intermediate space.

4.4.3.1 Acceleration Along Bi-Directional Twists

The first case is when the disturbance causes the initial twist to be along a bi-directional twist. For any bi-directional twist $\$^t_{bi,i}$, the end-effector can undergo $\$^t_{bi,i}$ and $-\$^t_{bi,i}$ without violating any cable constraints. Let these twists be mapped to $\hat{v}_{bi,i}$ and $-\hat{v}_{bi,i}$ and let the gravitational wrench $m\overline{g}$ be mapped to $\hat{f}_{grav}$. Because the end-effector begins at a static equilibrium pose, $\hat{v}_{bi,i}$ and $-\hat{v}_{bi,i}$ must both be perpendicular to $\hat{f}_{grav}$. That is because if $\hat{v}_{bi,i}$ or $-\hat{v}_{bi,i}$ were not perpendicular to $\hat{f}_{grav}$, the power product between the twists and gravity would be nonzero, and thus gravity would push the end-effector "downhill." Thus in the intermediate space $\hat{v}_{bi,i}$ and $-\hat{v}_{bi,i}$ are horizontal (with respect to gravity). Because the constraint surface along this twist is horizontal, the reaction from the constraint surface will be vertical and equal and opposite to $\hat{f}_{grav}$ as shown in Figure 22. Thus the sum of the generalized forces on the end-effector are zero and the acceleration of the end-effector is zero. As a result, if any pose of a manipulator has any bi-directional twists associated with it, the initial acceleration of the end-effector back towards its original pose will be zero. This is the lowest possible initial acceleration of the end-effector ($\hat{a}_{vert} = 0$). Because of this, the following three cases will only consider situations where the pose has no bi-directional twists associated with it.

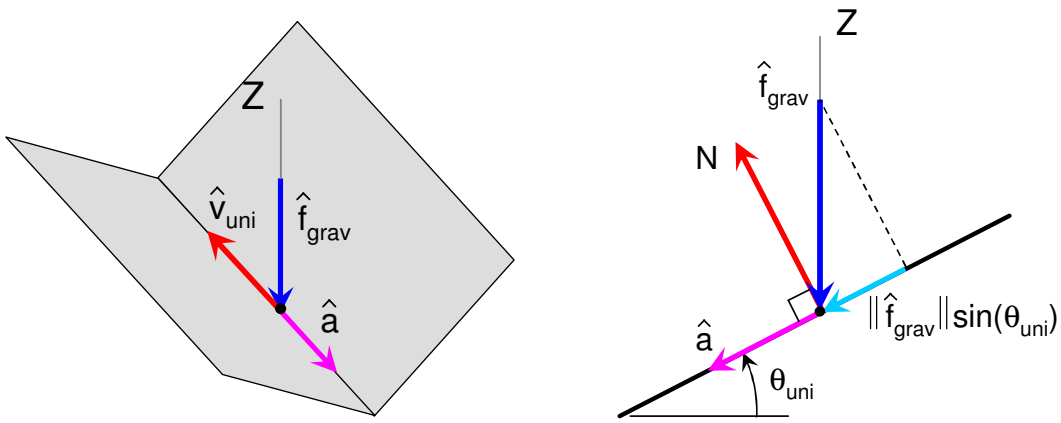

(a) Uni-directional twist along the intersection of two constraint surfaces.

(b) Side view of vertical plane that contains $\hat{v}_{uni,i}$ and $\hat{f}_{grav}$.

Figure 23: Acceleration along a uni-directional twist in the intermediate space.

4.4.3.2 Acceleration Along Uni-Directional Twists

The second possibility is that the initial twist is along a uni-directional twist. Let uni-directional twist $\$^t_{uni,i}$ be mapped to a uni-directional generalized velocity $\hat{v}_{uni,i}$. As illustrated in Figure 23(a), a uni-directional twist runs along the intersection of two constraint surfaces. These constraint surfaces will cause the end-effector to remain along this uni-directional twist while it accelerates or decelerates, much like a point-mass would slide along the slide along the "valley" between two planar surfaces.

Thus in order to determine the acceleration of the end-effector it is only necessary to consider the vertical plane in the intermediate space that contains $\hat{v}_{uni,i}$ and $\hat{f}_{grav}$, shown in Figure 23(b), as all other generalized forces acting on the end-effector act to keep the end-effector along the generalized uni-directional velocity and thus cancel out to zero. Because the end-effector cannot accelerate into the constraint surface, the component of $\hat{f}_{grav}$ perpendicular to the constraint surface will be exactly canceled by the generalized reaction force. Thus the magnitude of the reaction force is $\| \hat{f}_{grav} \| \cos\theta_{uni}$, where θ_{uni} is defined as the angle of the generalized uni-directional velocity (which is along the constraint surface in this plane) with respect to horizontal.

Since the generalized reaction force cancels out the component of $\hat{f}_{grav}$ perpendicular to the constraint surface, the net generalized force on the end-effector has magnitude $\| \hat{f}_{net} \| = \| \overline{f}_{grav} \| \sin\theta_{uni}$ and is directed along the constraint surface back towards the original pose. Thus the generalized acceleration is $\hat{a} = -\frac{\| \hat{f}_{grav} \|}{m} \sin\theta_{uni} \frac{\hat{v}_{uni,i}}{\| \hat{v}_{uni,i} \|}$. Because the vertical component of $\hat{v}_{uni,i}$ is $\| \hat{v}_{uni,i} \| \sin\theta_{uni}$, the vertical acceleration of the end-effector reduces to:

$$\hat{a}_{vert} = -\frac{\| \hat{f}_{grav} \|}{m} \sin\theta_{uni} \frac{\| \hat{v}_{uni,i} \| \sin\theta_{uni}}{\| \hat{v}_{uni,i} \|} \tag{99}$$

$$\hat{a}_{vert} = -g \sin^2\theta_{uni}. \tag{100}$$

By mapping the result back to the task space we get:

$$\overline{a}_{vert} = -g \sin^2\theta_{uni}. \tag{101}$$

The angle of the generalized uni-directional velocity with respect to horizontal, θ_{uni}, can be calculated by decomposing the generalized velocity into a vertical component and a horizontal component. The vertical component of $\hat{v}_i$ can be found by projecting $\hat{v}_i$ onto $\hat{f}_{grav}$:

$$\hat{v}_{i,vert} = \frac{\hat{f}_{grav}}{\| \hat{f}_{grav} \|^2} \hat{f}_{grav} \cdot \hat{v}_i \tag{102}$$

then

$$\sin\theta_{uni} = \frac{\| \hat{v}_{i,vert} \|}{\| \hat{v}_i \|}. \tag{103}$$

Thus the vertical acceleration becomes:

$$\overline{a}_{vert} = -g \frac{\| \hat{v}_{i,vert} \|^2}{\| \hat{v}_i \|^2}. \tag{104}$$

Applying the relationship between the magnitude of a generalized velocity and the kinetic energy of the associated twist then results in:

$$\overline{a}_{vert} = -g \frac{KE(\$^t_{i,vert})}{KE(\$^t_i)}. \tag{105}$$

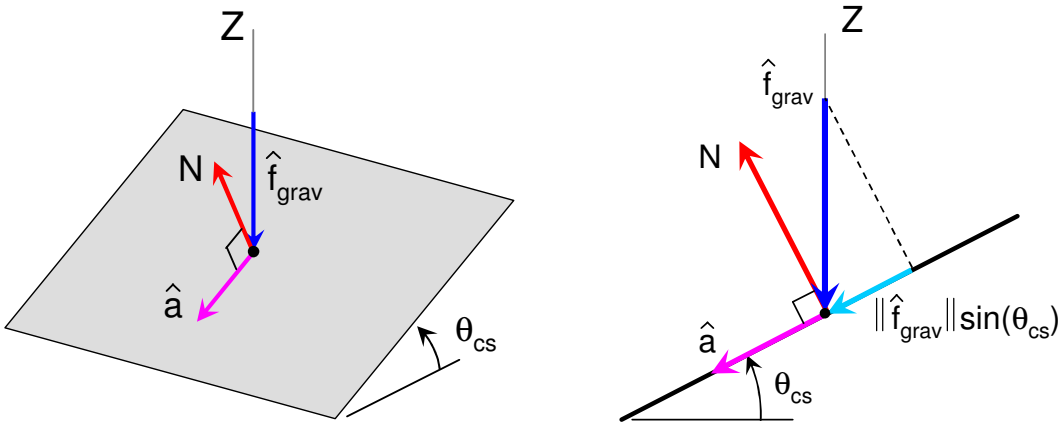

(a) Acceleration along a constraint surface.

(b) Side view of vertical plane that contains $\hat{f}_{grav}$ and the normal to the constraint surface.

Figure 24: Acceleration along a constraint surface in the intermediate space.

4.4.3.3 Acceleration Along Constraint Surfaces

Thirdly, the initial twist can be along a constraint surface (not along a bi- or uni-directional twist), as shown in Figure 24(a). If the end-effector moves along the constraint surface, the reaction force will be normal to the constraint surface. Thus if we now consider the plane that contains $\hat{f}_{grav}$ and the normal to the constraint surface, all the generalized forces are in this plane as shown in Figure 24(b), and thus the resulting acceleration of the end-effector must be in this plane.

In the same manner as was done for acceleration along a uni-directional twist, the generalized gravitational force can be decomposed into a component normal to the constraint surface and tangent to the constraint surface. The generalized reaction force must be equal and opposite to the component of the generalized gravitational force normal to the constraint surface. Thus the magnitude of the reaction force is $\| \hat{f}_{grav} \| \cos\theta_{cs}$, where θ_{cs} is defined as the angle of the constraint surface with respect to horizontal[14]. Since the generalized reaction force cancels out the component of

[14]Note that θ_{cs} is also the angle between the surface normal and vertical.

$\hat{f}_{grav}$ perpendicular to the constraint surface, the remaining generalized force on the end-effector has magnitude $\| \hat{f}_{grav} \| \sin\theta_{cs}$ and is directed along the constraint surface in the most "downhill" direction. Because this is in the same form as the result for acceleration along a principal twist, we can apply the same procedure, which results in:

$$\overline{a}_{vert} = -g \sin^2 \theta_{cs}. \tag{106}$$

4.4.3.4 Acceleration if Not Along a Constraint Surface

The last possibility is that the initial twist is not be along a constraint surface. In this case there are no reaction forces from the constraint surfaces as the motion of the end-effector causes every cable to go slack. Thus the only force on the end-effector is gravity and the acceleration of the end-effector is $\overline{a} = \overline{g}$ (and thus $\overline{a}_{vert} = -g$).

4.4.4 Impulsive Disturbance Robustness Measure

Now that the possible initial acceleration of the end-effector has been determined for all the different possible cases, it is necessary to determine which of these cases results in the smallest (magnitude) vertical acceleration. Note that at the end of this section the smallest total acceleration will be determined as well, using acceleration energy as the norm.

Examining the different cases, it is clear that the smallest possible acceleration is 0, corresponding to the case where there are bi-directional unconstrained twists. However, many manipulators do not have bi-directional unconstrained twists (because the associated Jacobian matrix is full rank) and thus we must consider the other cases. In the case of motion not along a constraint surface the magnitude of the vertical acceleration is g, while in the cases of motion along a uni-directional twist and motion along a constraint surface the magnitude of the associated vertical accelerations are $g \sin^2 \theta_{uni}$ and $g \sin^2 \theta_{cs}$, respectively. Because $0 \leq \sin^2 \theta \leq 1$, the smallest vertical acceleration results from motion along a uni-directional twist or motion along a

constraint surface. It is shown here that for these two types of motion, the smallest vertical acceleration results from motion along a uni-directional twist. Thus because the smallest vertical acceleration of the end-effector is along one of the uni-directional twist, it is only necessary to calculate the acceleration along the p different uni-directional twists.

Theorem **:**

Given two uni-directional twists that positively span a constraint surface. Then the magnitude of the acceleration of the end-effector due to gravity while moving along one of the uni-directional twists will be less than or equal to the magnitude of the acceleration of the end-effector due to gravity while moving along the constraint surface.

Proof **:**

Included in Appendix A.

There are now only two cases to consider: if the manipulator has bi-directional twists and if it does not. If the manipulator has bi-directional twists (which have a corresponding $\sin\theta = 0$ in the intermediate space) the smallest initial vertical (and total) acceleration of the end-effector is zero, while if the manipulator has no bi-directional twists the smallest initial vertical acceleration is $-g\sin^2\theta_{uni}$. Recall that $\mathcal{P}$ is the set of principal twists (the bi-directional twists and uni-directional twists), then these two situations can be combined as follows:

$$a_{vert,min} = \min_{\$^t \in \mathcal{P}} -g\sin^2\left(\theta(\$^t)\right) \tag{107}$$

where $\theta(\$^t)$ is now shown as a function of $\$^t$ to emphasize that each θ is found by mapping the twist to a generalized velocity in the intermediate space and determining the angle of the generalized velocity from horizontal.

Total Acceleration

Let us now also consider the *total* acceleration of the end-effector. Recall that the net generalized force for motion along a principal twist has magnitude:

$$\| \hat{f}_{net} \| = mg \sin\theta \tag{108}$$

and is parallel to the principal twist and directed towards the original pose. The resulting total generalized acceleration is

$$\hat{a} = \frac{1}{m} \hat{f}_{net}. \tag{109}$$

This is the total acceleration of the end-effector, mapped to the intermediate space. Recall the definition of acceleration energy given in (45), which can be used to relate the magnitude of the total acceleration in the intermediate space to the acceleration energy of the corresponding acceleration screw $\$^a$:

$$AE(\$^a) = \frac{1}{2} \$^{aT} \boldsymbol{M} \$^a = \frac{m}{2} \$^{aT} \boldsymbol{A}^2 \$^a = \frac{m}{2} \| \hat{a} \|^2 . \tag{110}$$

The acceleration energy of the net wrench $\$^w_{net} = \boldsymbol{A}^{-1} \hat{f}_{net}$ is then

$$AE(\$^w_{net}) = \frac{1}{2m} \| \hat{f}_{net} \|^2 = \frac{1}{2m} \| mg \sin\theta \|^2 = \frac{m}{2} \| g \sin\theta \|^2 = AE(\$^a). \tag{111}$$

Thus because the magnitude of a generalized acceleration in the intermediate space is tied to the acceleration energy of the corresponding acceleration screw, the magnitude of the total acceleration of the end-effector will be defined as the magnitude of the total generalized acceleration vector in the intermediate space. That is,

$$\| \$^a \|_a := \| \hat{a} \| = \sqrt{\frac{2}{m} AE(\$^a)}. \tag{112}$$

Thus the magnitude of the smallest total acceleration of the end-effector is:

$$\| \$^a \|_{a,min} = \min_{\$^t \in \mathcal{P}} g \sin\left(\theta(\$^t)\right). \tag{113}$$

Because of the common term of $\sin(\theta(\$^t))$ in the vertical acceleration and total acceleration of the end-effector, the proposed impulsive disturbance robustness measure is defined as follows:

Definition: The *impulsive disturbance robustness*, $\mathcal{R}_i$ is defined as

$$\boxed{\mathcal{R}_i = \min_{\$^t \in \mathcal{P}} \sin\left(\theta(\$^t)\right)}. \tag{114}$$

Then if an impulsive disturbance is applied to the manipulator **the smallest possible initial vertical acceleration of the end-effector is** $a_{vert,min} = -g\mathcal{R}_i^2$ **and the smallest possible initial total acceleration of the end-effector is** $\| \$^a \|_{a,min} = g\mathcal{R}_i$**.**

Thus it is clear that the possible initial accelerations of the end-effector are determined by the lowest "slope" twists in $\mathcal{P}$[15]. This measure can have values between 0 and 1, with 1 corresponding to a manipulator with the highest impulsive disturbance robustness (where the initial vertical acceleration is $\overline{g}$) and 0 corresponding to the lowest impulsive disturbance robustness (where the initial acceleration is 0). Like the static disturbance robustness measure, $\mathcal{R}_i$ is pose-dependent. The calculation of this measure is also relatively easy, as demonstrated in the following example.

Example

Consider the planar 3-DOF 3-cable manipulator shown in Figure 25. Note that this is the same manipulator used in the example in 4.3.6.2. The end-effector is a 2 m $\times$ 4 m rectangle with a mass of 100 kg and rotational inertia of $\frac{500}{3}\text{kg} \cdot \text{m}^2$ ($\rho_z = \sqrt{\frac{5}{3}}\,\text{m}$). In the given pose the bottom edge has a slope of $-\frac{1}{2}$ with respect to gravity (i.e. $\tan\theta = \frac{1}{2}$), cable 1 is collinear with G, cable 2 is vertical and cable 3 is aligned with the right edge of the end-effector. The origin of the x-y coordinate frame is placed at G, with the axes parallel to the edges of the end-effector. While

[15]Note that if the gyroscopic effect were included in this analysis, the initial acceleration would depend not only on the slopes of the constraint surfaces but also on the magnitude of the initial twist.

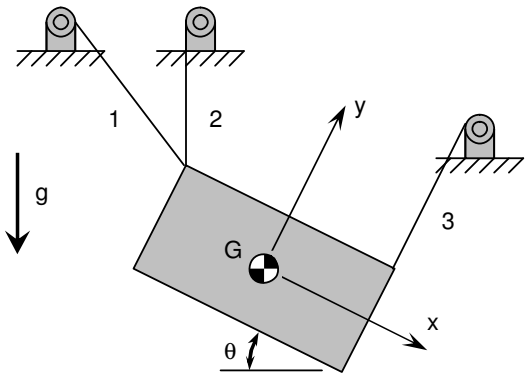

Figure 25: Impulsive robustness calculation example.

in a planar problem it would be possible to simply align the y-axis with gravity, the coordinate frame is aligned with the geometry of the end-effector to illustrate how the coordinate frame would align with the principal axes of a spatial end-effector.

Forming $\boldsymbol{J}$ results in:

$$\boldsymbol{J} = \begin{bmatrix} \frac{-2}{\sqrt{5}} & \frac{1}{\sqrt{5}} & 0 \\ \frac{-1}{\sqrt{5}} & \frac{2}{\sqrt{5}} & \frac{-3}{\sqrt{5}}\,\mathrm{m} \\ 0 & 1 & 2\,\mathrm{m} \end{bmatrix}.$$

Calculation of the gravitational wrench and U results in:

$$\$^{w}_{grav} = \begin{pmatrix} \frac{1}{\sqrt{5}} \\ \frac{-2}{\sqrt{5}} \\ 0 \end{pmatrix} 980\,\mathrm{N} \qquad \$^{t}_{uni,1} = \begin{pmatrix} -7\,\mathrm{m} \\ -2\,\mathrm{m} \\ 1 \end{pmatrix} \frac{1}{\mathrm{s}}$$

$$\$^{t}_{uni,2} = \begin{pmatrix} 1\,\mathrm{m} \\ 2\,\mathrm{m} \\ -1 \end{pmatrix} \frac{1}{\mathrm{s}} \qquad \$^{t}_{uni,3} = \begin{pmatrix} 1\,\mathrm{m} \\ 2\,\mathrm{m} \\ 1 \end{pmatrix} \frac{1}{\mathrm{s}}$$

where $U = \left\{ \$^{t} \mid \$^{t} = c_1 \$^{t}_{uni,1} + c_2 \$^{t}_{uni,2} + c_3 \$^{t}_{uni,3} \right\}$. $\boldsymbol{A}$ is:

$$\boldsymbol{A} = \begin{bmatrix} 1 & 0 & 0 \\ 0 & 1 & 0 \\ 0 & 0 & \sqrt{\frac{5}{3}}\,\mathrm{m} \end{bmatrix}$$

and $\boldsymbol{B} = \boldsymbol{A}^{-1}$.

Mapping the gravitational wrench and uni-directional twists to the intermediate space results in:

$$\hat{f}_{grav} = \begin{pmatrix} \frac{1}{\sqrt{5}} \\ \frac{-2}{\sqrt{5}} \\ 0 \end{pmatrix} 980\,\mathrm{N} \qquad \hat{v}_{uni,1} = \begin{pmatrix} -7 \\ -2 \\ \sqrt{\frac{5}{3}} \end{pmatrix} \frac{\mathrm{m}}{\mathrm{s}}$$

$$\hat{v}_{uni,2} = \begin{pmatrix} 1 \\ 2 \\ -\sqrt{\frac{5}{3}} \end{pmatrix} \frac{\mathrm{m}}{\mathrm{s}} \qquad \hat{v}_{uni,3} = \begin{pmatrix} 1 \\ 2 \\ \sqrt{\frac{5}{3}} \end{pmatrix} \frac{\mathrm{m}}{\mathrm{s}}.$$

By applying (102) the vertical components of the generalized velocities can be formed. Here the twists were chosen such that the generalized velocities all have the same vertical components:

$$\hat{v}_{uni,1,vert} = \hat{v}_{uni,2,vert} = \hat{v}_{uni,3,vert} = \frac{3}{5} \begin{pmatrix} -1 \\ 2 \\ 0 \end{pmatrix} \frac{\mathrm{m}}{\mathrm{s}}$$

thus

$$\| \hat{v}_{uni,1,vert} \| = \| \hat{v}_{uni,2,vert} \| = \| \hat{v}_{uni,3,vert} \| = \frac{3\sqrt{5}}{5} \frac{\mathrm{m}}{\mathrm{s}}.$$

Equation (103) can now be applied to find $\sin\theta$ for each generalized principal velocity:

$$\sin\theta_1 = \frac{\|\hat{v}_{uni,1,vert}\|}{\|\hat{v}_{uni,1}\|} = \frac{\left(\frac{3\sqrt{5}}{5}\frac{\mathrm{m}}{\mathrm{s}}\right)}{\left(\sqrt{\frac{164}{3}}\frac{\mathrm{m}}{\mathrm{s}}\right)} = 0.1815$$

$$\sin\theta_2 = \frac{\|\hat{v}_{uni,2,vert}\|}{\|\hat{v}_{uni,2}\|} = \frac{\left(\frac{3\sqrt{5}}{5}\frac{\mathrm{m}}{\mathrm{s}}\right)}{\left(\sqrt{\frac{20}{3}}\frac{\mathrm{m}}{\mathrm{s}}\right)} = 0.5196$$

$$\sin\theta_3 = \frac{\|\hat{v}_{uni,3,vert}\|}{\|\hat{v}_{uni,3}\|} = \frac{\left(\frac{3\sqrt{5}}{5}\frac{\mathrm{m}}{\mathrm{s}}\right)}{\left(\sqrt{\frac{20}{3}}\frac{\mathrm{m}}{\mathrm{s}}\right)} = 0.5196.$$

Because $\sin\theta_1$ is the smallest, $\mathcal{R}_i = \sin\theta_1 = 0.1815$ and the smallest initial acceleration of the end-effector will occur for motion along $\$^t_{uni,1}$.

Interpretation

Thus if the end-effector is disturbed by an impulsive disturbance, the smallest possible initial vertical acceleration of the end-effector will be $a_{vert} = -g\mathcal{R}_i^2 = -\left(9.81\frac{\text{m}}{\text{s}^2}\right)0.1815^2 = -0.323\frac{\text{m}}{\text{s}^2}$, and the smallest possible initial total acceleration of the end-effector (using the acceleration energy norm) will be $\| \$^a \|_a = g\mathcal{R}_i = \left(9.81\frac{\text{m}}{\text{s}^2}\right)0.1815 = 1.78\frac{\text{m}}{\text{s}^2}$.

4.5 Robustness Measure

Now that there are two robustness measures, $\mathcal{R}_s$ and $\mathcal{R}_i$, it is of interest to see how these measures relate to each other. This relationship can be found by examining the geometry of NW_{avail} in the intermediate space.

Figure 26(a) shows an example NW_{avail}. For this example the manipulator has three cables and is planar (and thus the task space is three-dimensional). However, the analysis and results of this example apply to a manipulator with any number of cables and a task space of any dimension. Recall that in Section 4.3.6 it was shown that the smallest static disturbance wrench is found by examining C, the set of critical wrenches, that cause a cable to go slack. This set was mapped to $\hat{C}$ in the intermediate space and the smallest static disturbance wrench was the one that corresponded to the smallest generalized force in $\hat{C}$. Note that C is the set of upper boundaries of $-NW_{avail}$, so $-C$ is the set of lower boundaries of NW_{avail}. Thus if we find the smallest wrench in the lower boundaries of NW_{avail}, this wrench is the smallest wrench in $-C$ and thus will be equal and opposite to the smallest disturbance wrench in C. Let us thus consider one of the lower boundaries of NW_{avail}, labeled in Figure 26(a) as side S. Note that $S \in -C$.

Let us map the wrenches in S to the intermediate space, resulting in the set $\hat{S}$. An edge-view close-up of $\hat{S}$ is shown in Figure 26(b). Because S is spanned by $\$_2$ and $\$_3$, the smallest generalized force in $\hat{S}$ is equal and opposite to the smallest

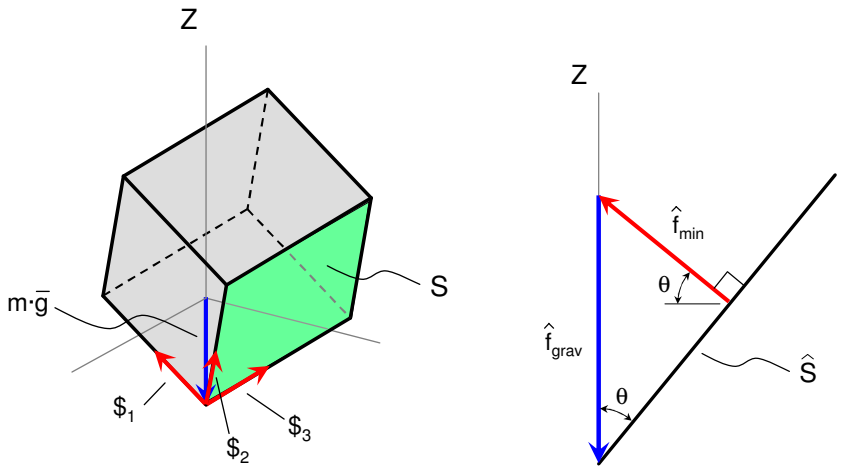

(a) Example Available Net Wrench Set, NW_{avail}.

(b) Edge-view of side $\hat{S}$.

Figure 26: Robustness measure example.

generalized force that causes cable 1 to go slack. Because $\hat{S}$ is planar, the vector to the smallest generalized force in $\hat{S}$ is perpendicular to this plane. Figure 26(b) shows the generalized force $\hat{f}_{min}$. This generalized force is perpendicular to $\hat{S}$ and is equal and opposite to the smallest generalized force in $\hat{S}$. Thus $\hat{f}_{min}$ is the smallest generalized force that causes cable 1 to go slack. We know from Section 4.3.6 that this generalized force has a magnitude of $mg\mathcal{R}_s$. Because $\hat{f}_{min}$ is perpendicular to $\hat{S}$, if the angle of $\hat{f}_{min}$ with respect to horizontal is θ, then the angle between $\hat{S}$ and vertical is also θ. Then $\| \hat{f}_{min} \| = \| \hat{f}_{grav} \| \sin\theta$, and because $\| \hat{f}_{grav} \| = mg$ we can conclude that $\| \hat{f}_{min} \| = mg \sin\theta$. However, we also know that the principal twist $\$^t_{uni,1}$ is reciprocal to $\$_2$ and $\$_3$ (the columns of $\boldsymbol{J}_{mod,1}$). Consequently the generalized principal twist vector $\hat{v}_{uni,1}$ is perpendicular to $\hat{S}$ and must therefore be parallel to $\hat{f}_{min}$. Thus the angle of $\hat{v}_{uni,1}$ with respect to horizontal must also be θ.

This procedure can be repeated for each of the lower sides of NW_{avail} to determine the θ for each side. Let the angle θ for side i be denoted θ_i. Then because $\mathcal{R}_s$ is defined

as

$$\mathcal{R}_s = \frac{1}{mg} \min_{\hat{f} \in \hat{C}} \| \hat{f} \| \tag{115}$$

then

$$\mathcal{R}_s = \min_{i=1,2,3} \sin \theta_i. \tag{116}$$

Similarly, because $\mathcal{R}_i$ is defined as

$$\mathcal{R}_i = \min_{\$^t \in \mathcal{P}} \sin \left(\theta(\$^t) \right) \tag{117}$$

then

$$\mathcal{R}_i = \min_{i=1,2,3} \sin \theta_i. \tag{118}$$

Noting again that this procedure can be repeated for any number of cables and a task space of any dimension with the same result, it is clear that $\mathcal{R}_s = \mathcal{R}_i$. Let us therefore combine these two measures and define the Disturbance Robustness Measure:

Definition: The *Disturbance Robustness Measure*, $\mathcal{R}$ is defined as:

$$\boxed{\mathcal{R} = \mathcal{R}_s = \mathcal{R}_i}. \tag{119}$$

Thus this single measure describes both the static and impulsive disturbance robustness of the manipulator. In addition, there are several equivalent ways to calculate this measure:

$$\begin{aligned}
\mathcal{R} &= \min_{\$^t \in \mathcal{P}} \sin \left(\theta(\$^t) \right) && (120) \\
&= \min_{\$^t \in \mathcal{P}} \sqrt{\frac{KE(\$^t_{vert})}{KE(\$^t)}} && (121) \\
&= \min_{\$^a \in A} \frac{1}{g} \| \$^a \|_a && (122) \\
&= \min_{\overline{a} \in A_{vert}} \sqrt{\frac{1}{g} \| \overline{a} \|}. && (123)
\end{aligned}$$

where A is the set of all possible acceleration screws of the end-effector after it is disturbed and A_{vert} is the set of all possible vertical accelerations of the center of

gravity of the end-effector after it is disturbed. This is very advantageous, because it allows calculation of $\mathcal{R}$ in whatever method is easiest.

4.5.1 Discussion

The fact that this measure captures both the static and impulsive disturbance robustness is very significant. In both cases the measure describes the worst-case scenario for the manipulator: the smallest static disturbance wrench ($\| \$^w_{min} \|_a = mg\mathcal{R}$) and the lowest acceleration of an impulsively disturbed end-effector back to its original pose ($\| \$^a_{min} \|_a = g\mathcal{R},\ a_{vert,min} = -g\mathcal{R}^2$). Because the robustness measure is equivalent to $\mathcal{R}_s$ and $\mathcal{R}_i$, it has the same properties of scale- and frame-invariance. In addition, it is not difficult to adapt this measure to allow robustness to be computed in the presence of any constant external wrench, not just gravity. This can be accomplished by simply replacing $\$^w_{grav}$ in all calculations with the net external wrench due to gravity and additional constant external wrenches.

The robustness measure does have some limitations. First, the inertial properties of the end-effector must be known completely. This information may not be available if the end-effector picks up objects with unknown masses and dimensions.

Second, the measure only describes the robustness of a single pose of a manipulator, but does not provide an overall measure of robustness for a manipulator. This is addressed in Section 4.5.2.

Additionally, poses with very high robustness may sometimes require very high cable tensions to counteract the gravitational wrench. Thus it is important to ensure that cable tension limits are not exceeded.

Lastly, it is not obvious what an acceptable minimum value is for $\mathcal{R}$. This will typically be application-dependent and experimentation and practical considerations may need to be taken into account to determine what constitutes an appropriate minimum necessary value of $\mathcal{R}$ for a given manipulator. However, given such a value,

it is possible to construct a *Specified Robustness Workspace*, the set of all poses of a manipulator where $\mathcal{R}$ meets or exceeds the a specified robustness value. This workspace is discussed in more detail in Section 5.6. Consideration of upper tension limits can also be incorporated into this workspace, allowing avoidance of the high cable tension condition mentioned earlier.

The following section discusses the application of the robustness measure to the problem of determining the overall robustness of a manipulator. Section 4.6 then shows how the robustness measure can be extended to the case of cable robots with multi-body end-effectors.

4.5.2 Applications

The question remains as to how a manipulator can be described as robust or not robust to disturbances considering that the robustness of the poses of the manipulator can differ greatly from one pose to another. One approach involves examining the robustness of poses of the robot within its desired workspace (the positional and rotational space that the robot can reach statically and in which the robot is required to operate). The desired task space, D, can be discretized into a finite number of poses, P, and the robustness measure can be applied to each one of these poses, resulting in a scalar field of manipulator robustness over the desired workspace. There are many possible ways to use this information to define the robustness of the robot, but only three will be described here.

- *Average Robustness Over Desired Workspace* - Defined as:

$$\mathcal{R}_{ave} = \frac{\int\limits_{D} \mathcal{R}(P)\,\mathrm{d}P}{\int\limits_{D} \mathrm{d}P}. \tag{124}$$

  This measure determines the robustness of a manipulator based on the average robustness of each pose in the desired workspace. While this provides a good overall indication of the robustness of the manipulator, it does not factor in how

widely the robustness may vary over the workspace. The best possible value of R_{ave} is 1 and the worst possible value is 0.

- *Minimum Robustness Over Desired Workspace* - Defined as:

$$\mathcal{R}_{min} = \min_{P \in D} \mathcal{R}(P). \tag{125}$$

This measure characterizes the manipulator by its lowest robustness value in D, essentially providing the worst-case scenario for using the manipulator in this workspace. The best possible value of R_{min} is 1 and the worst possible value is 0.

- *Weighted Average Robustness Over Desired workspace* - Defined as:

$$\mathcal{R}_{w.a.} = \frac{\int_D w(P)\mathcal{R}(P)\,\mathrm{d}P}{\int_D w(P)\mathrm{d}P}. \tag{126}$$

This measure is very similar to R_{ave} but now the function $w(P)$ is added as a weighting function. This allows more emphasis to be placed on regions of the workspace that are used more frequently or possibly in regions where more external disturbances are expected. The best possible value of $R_{w.a.}$ is 1 and the worst possible value is 0.

Using this kind of measure to describe the overall disturbance robustness of a cable robot, it is possible to now use that information to optimize the robot by choosing optimal cable-mount locations or end-effector geometry. Additionally, it would make sense to use these measures in conjunction with each other. For example, a manipulator could be optimized to maximize $\mathcal{R}_{w.a.}$ but must also meet a certain standard for $\mathcal{R}_{min}$. Note, however, that calculating the overall robustness of a manipulator using one of these methods may be computationally time-consuming as the task space must be discretized and the robustness measure applied at each of these poses.

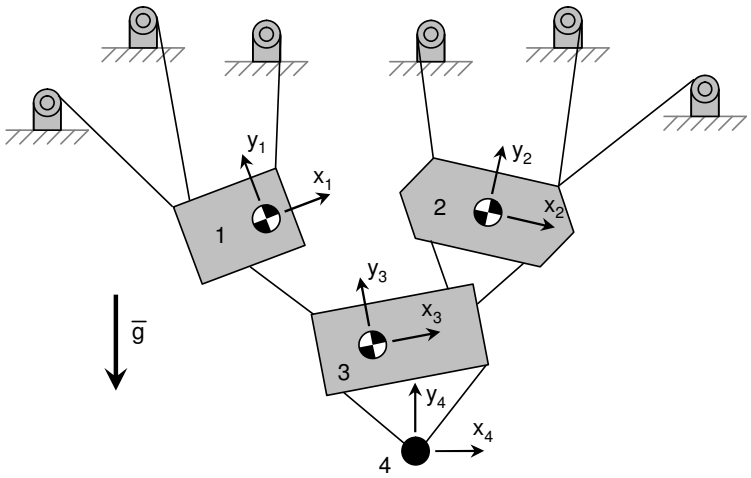

Figure 27: Example manipulator with a four-body end-effector.

4.6 Disturbance Robustness of Cable Robots with Multi-Body End-Effectors

The development of the disturbance robustness measure assumed an end-effector comprised of a single rigid body. However, the analysis developed for single-bodies can be extended to include the case of multiple suspended bodies. The approach here is to develop a similar mapping to the intermediate space and to develop the robustness measure based on geometric properties within this space.

4.6.1 Mapping to the Intermediate Space

Let us assume that there are b rigid bodies suspended from p cables. The bodies may be connected to each other by additional cables and/or by passive joints[16]. For each body let a coordinate frame be defined with the origin located at the center of gravity of the body and axes aligned with the principal axes of the body as illustrated for a manipulator with a 4-body end-effector in Figure 27.

Let the twist $\$_i^t$ of body i be expressed in terms of the coordinate frame associated

[16]Note that if two bodies are joined by an actuated joint, the actuator is assumed locked and the two bodies can be treated as a single rigid body.

with body i. Let the *collective twist*, $\$^t_{coll}$ of the system of bodies be defined as:

$$\$^t_{coll} = \begin{pmatrix} \$^t_1 \\ \$^t_2 \\ \vdots \\ \$^t_b \end{pmatrix}. \tag{127}$$

Note that the collective twist is not technically a twist, but rather a vector containing b different twists. Similarly, let $\$^w_i$ be the wrench acting on body i in terms of the coordinate frame associated with body i. Then the *collective wrench*, $\$^w_{coll}$ acting on the system of bodies is defined as:

$$\$^w_{coll} = \begin{pmatrix} \$^w_1 \\ \$^w_2 \\ \vdots \\ \$^w_b \end{pmatrix}. \tag{128}$$

We now wish to define a mapping to the intermediate space that is consistent with the mapping defined for single bodies. Let the mass of body i be m_i and the total mass of the bodies be $m_{tot} = m_1 + m_2 + ... + m_b$. Also, let us define the normalized mass of body i, μ_i, as $\mu_i = \frac{m_i}{m_{tot}}$. The mapping of a collective twist to a generalized collective velocity in the intermediate space is now defined as:

$$\hat{v}_{coll} = \boldsymbol{A}\$^t_{coll} \tag{129}$$

where

$$\boldsymbol{A} = \begin{bmatrix} \sqrt{\mu_1}\boldsymbol{A}_1 & 0 & \cdots & 0 \\ 0 & \sqrt{\mu_2}\boldsymbol{A}_2 & \cdots & 0 \\ \vdots & \vdots & \ddots & \vdots \\ 0 & 0 & \cdots & \sqrt{\mu_b}\boldsymbol{A}_b \end{bmatrix} \tag{130}$$

and where $\boldsymbol{A}_i$ is the mapping matrix for body i defined in (17), such that $\boldsymbol{M}_i = m_i \boldsymbol{A}_i^2$. Note that the total system inertia matrix, $\boldsymbol{M}$, is defined as $\boldsymbol{M} = m_{tot}\boldsymbol{A}^2$:

$$\boldsymbol{M} = m_{tot}\boldsymbol{A}^2 = m_{tot}\begin{bmatrix} \mu_1\boldsymbol{A}_1^2 & 0 & \cdots & 0 \\ 0 & \mu_2\boldsymbol{A}_2^2 & \cdots & 0 \\ \vdots & \vdots & \ddots & \vdots \\ 0 & 0 & \cdots & \mu_b\boldsymbol{A}_b^2 \end{bmatrix} =$$

$$= \begin{bmatrix} m_1\boldsymbol{A}_1^2 & 0 & \cdots & 0 \\ 0 & m_2\boldsymbol{A}_2^2 & \cdots & 0 \\ \vdots & \vdots & \ddots & \vdots \\ 0 & 0 & \cdots & m_b\boldsymbol{A}_b^2 \end{bmatrix} = \begin{bmatrix} \boldsymbol{M}_1 & 0 & \cdots & 0 \\ 0 & \boldsymbol{M}_2 & \cdots & 0 \\ \vdots & \vdots & \ddots & \vdots \\ 0 & 0 & \cdots & \boldsymbol{M}_b \end{bmatrix}. \tag{131}$$

Similarly, the mapping of a collective wrench to a generalized collective wrench in the intermediate space is defined as:

$$\hat{f}_{coll} = \boldsymbol{B}\$^w_{coll} \tag{132}$$

where

$$\boldsymbol{B} = \boldsymbol{A}^{-1} = \begin{bmatrix} \frac{1}{\sqrt{\mu_1}}\boldsymbol{B}_1 & 0 & \cdots & 0 \\ 0 & \frac{1}{\sqrt{\mu_2}}\boldsymbol{B}_2 & \cdots & 0 \\ \vdots & \vdots & \ddots & \vdots \\ 0 & 0 & \cdots & \frac{1}{\sqrt{\mu_b}}\boldsymbol{B}_b \end{bmatrix}. \tag{133}$$

The mapping matrices $\boldsymbol{A}$ and $\boldsymbol{B}$ are defined this way such that all of the properties of the intermediate space described in Section 4.2.2 still hold. For example, the total kinetic energy of the system undergoing collective twist $\$^t_{coll}$ is:

$$KE(\$^t_{coll}) = \frac{1}{2}\$^t_{coll}{}^T\boldsymbol{M}\$^t_{coll} = \frac{m_{tot}}{2}\$^t_{coll}{}^T\boldsymbol{A}^2\$^t_{coll} = \frac{m_{tot}}{2}\parallel \hat{v}_{coll} \parallel^2. \tag{134}$$

4.6.2 Principal Collective Twists

As in the single-body case, the fixed lengths of the cables impose constraints on the poses of the bodies. In this case, however, there may also be constraints due to the

passive joints. As in the case of the single-body end-effector, these constraints limit the possible initial twists of the bodies. Thus in order to define these constraint surfaces locally it is necessary to form the set of all possible initial collective twists that the system of bodies can undergo without violating any constraints. While it was possible to use the Jacobian matrix to find this set for a single body, it is very complex to form the possible velocities of a collection of bodies coupled by joints and cables. In fact, for many traditional manipulators (those without cables) mobility analysis can be very complicated, particularly for closed-chain linkages. Thus it is beyond the scope of this research to formulate the set of all possible instantaneous motions for a general set of bodies joined by cables and joints. Instead, in order to continue this analysis it will be assumed that this set of motions can be formed and is termed the set of *unconstrained collective twists*. Note that for simple systems it is still fairly easy to form this set of twists, as is illustrated in Section 4.6.5.

While the set U is not known in general, we know that it is possible to positively span the set U with a set of *principal collective twists* because the constraint surfaces are locally linear. Thus if there are κ different principal collective twists, $\$^t_{princ,i}$, then for any collective twist $\$^t_{coll}$ in U

$$\$^t_{coll} = b_1\$^t_{princ,1} + ... + b_\kappa\$^t_{princ,\kappa}. \tag{135}$$

Let the set of principal collective twists $\{\$^t_{princ,1}, ..., \$^t_{p,\kappa}\}$ be again denoted by $\mathcal{P}$.

We now wish to analyze this set of twists in the same way as for a single-body end-effector. That is, given an impulsive disturbance we wish to find the smallest acceleration of the bodies back toward their original pose. Because the constraint surfaces are again modeled locally as linear constraints, the same method for finding this acceleration can be used. Thus the lowest acceleration will be determined by the principal collective twist with the lowest slope in the intermediate space.

4.6.3 Definition of Vertical Direction

Before the principal collective twist with the lowest slope can be calculated, we first need to define the vertical direction in the intermediate space for the collection of bodies. This is not trivial, as each of the bodies has a unique coordinate frame in the task space in which the vertical direction is defined. We wish for this definition of the vertical direction to be consistent with the single-body case. That is, if a single body is treated as a collection of particles, the result for the multi-body case ought to be consistent with the results already determined for the single-body case.

In the single-body case, the vertical direction in the intermediate space is parallel to the generalized gravitational force. Let the gravitational wrench on body i be denoted $\$^w_{grav,i}$. Let $\hat{f}_{grav,i} = \boldsymbol{B}_i \$^w_{grav,i}$. Combining the gravitational wrenches of all of the bodies into the collective gravitational wrench, $\$^w_{coll,grav}$, and mapping it to the generalized collective gravitational force, $\hat{f}_{coll,grav}$, results in:

$$\hat{f}_{coll,grav} = \boldsymbol{B}\$^w_{coll,grav} = \boldsymbol{B}\begin{pmatrix} \$^w_{grav,1} \\ \$^w_{grav,2} \\ \vdots \\ \$^w_{grav,b} \end{pmatrix} = \begin{pmatrix} \frac{1}{\sqrt{\mu_1}}\boldsymbol{B}_1\$^w_{grav,1} \\ \frac{1}{\sqrt{\mu_2}}\boldsymbol{B}_2\$^w_{grav,2} \\ \vdots \\ \frac{1}{\sqrt{\mu_b}}\boldsymbol{B}_b\$^w_{grav,b} \end{pmatrix} = \begin{pmatrix} \frac{1}{\sqrt{\mu_1}}\hat{f}_{grav,1} \\ \frac{1}{\sqrt{\mu_2}}\hat{f}_{grav,2} \\ \vdots \\ \frac{1}{\sqrt{\mu_b}}\hat{f}_{grav,b} \end{pmatrix}. \quad (136)$$

Let us now construct the vertical unit vector $\hat{u}_{vert}$ by normalizing $\hat{f}_{coll,grav}$. Noting that $\| \hat{f}_{grav,i} \| = m_i g$ and $\mu_1 + \mu_2 + ... + \mu_b = 1$, we get

$$\hat{u}_{vert} = -\frac{\hat{f}_{coll,grav}}{\| \hat{f}_{coll,grav} \|} = \frac{1}{\| \hat{f}_{coll,grav} \|} \begin{pmatrix} -\frac{1}{\sqrt{\mu_1}} \hat{f}_{grav,1} \\ -\frac{1}{\sqrt{\mu_2}} \hat{f}_{grav,2} \\ \vdots \\ -\frac{1}{\sqrt{\mu_b}} \hat{f}_{grav,b} \end{pmatrix}$$

$$= \frac{1}{\| \hat{f}_{coll,grav} \|} \begin{pmatrix} -\frac{1}{\sqrt{\mu_1}} (\mu_1 m_{tot} g) \frac{\hat{f}_{grav,1}}{\|\hat{f}_{grav,1}\|} \\ -\frac{1}{\sqrt{\mu_2}} (\mu_2 m_{tot} g) \frac{\hat{f}_{grav,2}}{\|\hat{f}_{grav,2}\|} \\ \vdots \\ -\frac{1}{\sqrt{\mu_b}} (\mu_b m_{tot} g) \frac{\hat{f}_{grav,b}}{\|\hat{f}_{grav,b}\|} \end{pmatrix}$$

$$= \frac{1}{\| \hat{f}_{coll,grav} \|} \begin{pmatrix} -\sqrt{\mu_1} (m_{tot} g) \frac{\hat{f}_{grav,1}}{\|\hat{f}_{grav,1}\|} \\ -\sqrt{\mu_2} (m_{tot} g) \frac{\hat{f}_{grav,2}}{\|\hat{f}_{grav,2}\|} \\ \vdots \\ -\sqrt{\mu_b} (m_{tot} g) \frac{\hat{f}_{grav,b}}{\|\hat{f}_{grav,b}\|} \end{pmatrix}. \tag{137}$$

Then using the fact that $\| \hat{f}_{coll,grav} \| = m_{tot} g$, we get

$$\hat{u}_{vert} = \begin{pmatrix} -\sqrt{\mu_1} \frac{\hat{f}_{grav,1}}{\|\hat{f}_{grav,1}\|} \\ -\sqrt{\mu_2} \frac{\hat{f}_{grav,2}}{\|\hat{f}_{grav,2}\|} \\ \vdots \\ -\sqrt{\mu_b} \frac{\hat{f}_{grav,3}}{\|\hat{f}_{grav,3}\|} \end{pmatrix}. \tag{138}$$

Note that $-\frac{\hat{f}_{coll,grav}}{\|\hat{f}_{coll,grav}\|}$ is used rather than $\frac{\hat{f}_{coll,grav}}{\|\hat{f}_{coll,grav}\|}$ so that $\hat{u}_{vert}$ is pointed upward.

This vector can now be used to calculate the vertical component of a generalized collective velocity or a generalized collective force. The vertical component of a generalized collective velocity $\hat{v}_{coll}$ is:

$$\hat{v}_{coll,vert} = (\hat{v}_{coll} \cdot \hat{u}_{vert}) \hat{u}_{vert}. \tag{139}$$

Similarly, the vertical component of a generalized collective force $\hat{f}_{coll}$ is:

$$\hat{f}_{coll,vert} = (\hat{f}_{coll} \cdot \hat{u}_{vert}) \hat{u}_{vert}. \tag{140}$$

Note that if we calculate the vertical component of $\hat{f}_{coll,grav}$, the gravitational wrench, the gravitational wrench is returned ($\hat{f}_{coll,grav,vert} = \hat{f}_{coll,grav}$).

Theorem **:**

If the vertical component of a generalized collective velocity is calculated, the magnitude of the result is equal to the vertical velocity of the center of mass of the system of b bodies.

Proof **:**

Calculating the vertical component of a generalized collective velocity results in:

$$\begin{aligned} \hat{v}_{coll,vert} &= (\hat{v}_{coll} \cdot \hat{u}_{vert})\hat{u}_{vert} \\ &= \begin{pmatrix} \sqrt{\mu_1}\boldsymbol{A}_1\$_1^t \\ \sqrt{\mu_2}\boldsymbol{A}_2\$_2^t \\ \vdots \\ \sqrt{\mu_b}\boldsymbol{A}_b\$_b^t \end{pmatrix}^T \begin{pmatrix} -\sqrt{\mu_1}\frac{\hat{f}_{grav,1}}{\|\hat{f}_{grav,1}\|} \\ -\sqrt{\mu_2}\frac{\hat{f}_{grav,2}}{\|\hat{f}_{grav,2}\|} \\ \vdots \\ -\sqrt{\mu_b}\frac{\hat{f}_{grav,3}}{\|\hat{f}_{grav,3}\|} \end{pmatrix} \hat{u}_{vert}. \end{aligned} \tag{141}$$

Let $\boldsymbol{A}_i\$_i^t = \hat{v}_i$. Then

$$\hat{v}_{coll,vert} = \left(\mu_1\hat{v}_1 \cdot \frac{-\hat{f}_{grav,1}}{\| \hat{f}_{grav,1} \|} + \mu_2\hat{v}_2 \cdot \frac{-\hat{f}_{grav,2}}{\| \hat{f}_{grav,2} \|} + ... + \mu_b\hat{v}_b \cdot \frac{-\hat{f}_{grav,b}}{\| \hat{f}_{grav,b} \|} \right) \hat{u}_{vert}. \tag{142}$$

Now it can be seen that $\hat{v}_i \cdot \frac{-\hat{f}_{grav,i}}{\|\hat{f}_{grav,i}\|}$ produces the vertical component of the generalized velocity of the center of gravity of body i in the associated coordinate frame. That is:

$$\hat{v}_i \cdot \frac{\hat{f}_{grav,i}}{\| \hat{f}_{grav,i} \|} = \hat{v}_{i,vert}. \tag{143}$$

Let the linear velocity portion of twist $\$_i^t$ be denoted as $\$_{i,lin}^t$ and the corresponding linear portion of the generalized velocity denoted as $\hat{v}_{i,lin}$. Also let the vertical component of $\$_{i,lin}^t$ be denoted as $\$_{i,vert}^t$ and the corresponding component of the generalized velocity denoted as $\hat{v}_{i,vert}$. Then because the portion of $\boldsymbol{A}_i$ that maps the

linear velocity terms is the identity matrix (the upper left quadrant),

$$\$^t_{i,lin} = \boldsymbol{A}_i^{-1}\hat{v}_{i,lin} = \hat{v}_{i,lin}. \tag{144}$$

Thus

$$\$^t_{i,vert} = \hat{v}_{i,vert} \tag{145}$$

so

$$\hat{v}_{coll,vert} = \left(\mu_1\$^t_{1,vert} + \mu_2\$^t_{2,vert} + ... + \mu_b\$^t_{b,vert}\right)\hat{u}_{vert}. \tag{146}$$

Since $\hat{u}_{vert}$ is a unit vector,

$$\| \hat{v}_{coll,vert} \| = \mu_1\$^t_{1,vert} + \mu_2\$^t_{2,vert} + ... + \mu_b\$^t_{b,vert}. \tag{147}$$

Now we can use the fact that for a collection of b bodies, if the center of gravity of each body i is located at point $\overline{r}_i = (x_i, y_i, z_i)$ in a fixed global coordinate frame, then the center of gravity, G_{coll}, of the collection of b bodies is given by:

$$G_{coll} = \frac{m_1}{m_{tot}}\overline{r}_1 + \frac{m_2}{m_{tot}}\overline{r}_2 + ... + \frac{m_b}{m_{tot}}\overline{r}_b. \tag{148}$$

Taking the vertical component of these vectors and differentiating them produces the vertical velocity $\$^t_{G,vert}$ of the center of gravity of the system of bodies and b vertical velocities $\$^t_{i,vert}$ of the bodies:

$$\$^t_{G,vert} = \mu_1\$^t_{1,vert} + \mu_2\$^t_{2,vert} + ... + \mu_b\$^t_{b,vert}. \tag{149}$$

By comparing this result with (147) we see that

$$\| \hat{v}_{coll,vert} \| = \| \$^t_{G,vert} \| . \tag{150}$$

Q.E.D. □

In summary, if we map a collective twist to the intermediate space, find the vertical component, and map the vertical component back to the task space, the magnitude of the result is equal to the vertical velocity

of the center of gravity of the system of bodies. This is consistent with the single-body case. That is, if we treat a single body as a collection of smaller bodies, the vertical component of the collective twist of the smaller bodies is equal to the vertical component of the twist of the original body.

4.6.4 Multi-Body Robustness Measure

Because of the form that has been chosen for the mapping to the intermediate space and the manner in which the vertical direction in this space has been constructed the analysis of this space is identical to that performed for the single-body case.

Definition: The robustness measure for manipulators with multi-body end-effectors is defined as:

$$\boxed{\mathcal{R} = \min_{\$^t_{coll} \in \mathcal{P}} \sin\theta(\$^t_{coll})} \tag{151}$$

where

$$\sin\theta(\$^t_{coll}) = \frac{KE(\$^t_{coll,vert})}{KE(\$^t_{coll})} = \frac{\| \hat{v}_{coll,vert} \|}{\| \hat{v}_{coll} \|} \tag{152}$$

and where $\$^t_{coll,vert}$ is found via (139). **Like the single-body case, this measure describes the magnitude of the smallest static disturbance wrench ($\| \$^w_{min} \|_a = m_{tot} g \mathcal{R}$) and the lowest acceleration of an impulsively disturbed end-effector back to its original pose ($\| \$^a_{min} \|_a = g\mathcal{R}$, $a_{vert,min} = -g\mathcal{R}^2$).** Because this measure is also energy based it has the same properties of scale- and frame-invariance.

4.6.5 Example

As an example, consider the cable robot in Figure 28. The manipulator has a two-body end-effector, which can also be thought of as a single-body end-effector (end-effector is body 1) with a suspended point-mass payload (body 2). The mass of body 1 is $m_1 = 3\text{kg}$ with a radius of gyration of $\rho_1 = 1.5\,\text{m}$ and the mass of body 2 is $m_2 = 1\,\text{kg}$. Thus $m_{tot} = 4\,\text{kg}$, $\mu_1 = \frac{3}{4}$ and $\mu_1 = \frac{1}{4}$. A coordinate frame has

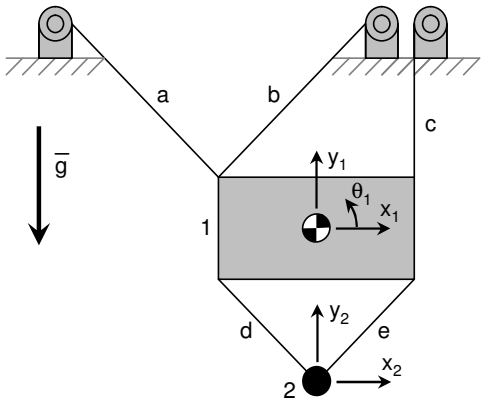

Figure 28: Example manipulator with a two-body end-effector.

been attached to each body, with each origin placed at the center of gravity of the respective body and the y axes aligned with gravity for simplicity. The collective twist of the bodies has the following form:

$$\$^t_{coll} = \begin{pmatrix} \$^t_1 \\ \$^t_2 \end{pmatrix} = \begin{pmatrix} \dot{x}_1 \\ \dot{y}_1 \\ \dot{\theta}_1 \\ \dot{x}_2 \\ \dot{y}_2 \end{pmatrix}.$$

The set of principal collective twists, P, can be found fairly simply for this manipulator. Each principal twist can be found by keeping four of the cables taut while the twist causes the fifth cable to go slack. The cables are labeled a through e. The principal collective twists are:

$$\begin{aligned}
\$^t_{princ,1} &= \begin{pmatrix} -5 & 2 & -1\frac{1}{\mathrm{m}} & -8 & 2 \end{pmatrix}^T \frac{\mathrm{m}}{\mathrm{s}} \\
\$^t_{princ,2} &= \begin{pmatrix} 3 & 2 & -1\frac{1}{\mathrm{m}} & 0 & 2 \end{pmatrix}^T \frac{\mathrm{m}}{\mathrm{s}} \\
\$^t_{princ,3} &= \begin{pmatrix} 1 & 2 & 1\frac{1}{\mathrm{m}} & 4 & 2 \end{pmatrix}^T \frac{\mathrm{m}}{\mathrm{s}} \\
\$^t_{princ,4} &= \begin{pmatrix} 0 & 0 & 0 & -1 & 1 \end{pmatrix}^T \frac{\mathrm{m}}{\mathrm{s}} \\
\$^t_{princ,5} &= \begin{pmatrix} 0 & 0 & 0 & 1 & 1 \end{pmatrix}^T \frac{\mathrm{m}}{\mathrm{s}}
\end{aligned}$$

where $\$^t_{p,1}$ causes cable a to go slack, $\$^t_{p,2}$ causes cable b to go slack, etc.

The matrices $\boldsymbol{A}_1$ and $\boldsymbol{A}_2$ are found by (17):

$$\begin{aligned}\boldsymbol{A}_1 &= \begin{bmatrix} 1 & 0 & 0 \\ 0 & 1 & 0 \\ 0 & 0 & 1.5\,\mathrm{m} \end{bmatrix} \\ \boldsymbol{A}_2 &= \begin{bmatrix} 1 & 0 \\ 0 & 1 \end{bmatrix}.\end{aligned}$$

The matrix $\boldsymbol{A}$ is then found by (130):

$$\boldsymbol{A} = \begin{bmatrix} \frac{\sqrt{3}}{2} & 0 & 0 & 0 & 0 \\ 0 & \frac{\sqrt{3}}{2} & 0 & 0 & 0 \\ 0 & 0 & \frac{3\sqrt{3}}{4}\mathrm{m} & 0 & 0 \\ 0 & 0 & 0 & \frac{1}{2} & 0 \\ 0 & 0 & 0 & 0 & \frac{1}{2} \end{bmatrix}.$$

This can now be used to map each of the principal collective twists to the corresponding principal collective generalized velocities:

$$\begin{aligned}\hat{v}_{princ,1} = \boldsymbol{A}\$^t_{princ,1} &= \begin{pmatrix} \frac{-5\sqrt{3}}{2} & \sqrt{3} & \frac{-3\sqrt{3}}{4} & -4 & 1 \end{pmatrix}^T \frac{\mathrm{m}}{\mathrm{s}} \\ \hat{v}_{princ,2} = \boldsymbol{A}\$^t_{princ,2} &= \begin{pmatrix} \frac{3\sqrt{3}}{2} & \sqrt{3} & \frac{-3\sqrt{3}}{4} & 0 & 1 \end{pmatrix}^T \frac{\mathrm{m}}{\mathrm{s}} \\ \hat{v}_{princ,3} = \boldsymbol{A}\$^t_{princ,3} &= \begin{pmatrix} \frac{\sqrt{3}}{2} & \sqrt{3} & \frac{3\sqrt{3}}{4} & 2 & 1 \end{pmatrix}^T \frac{\mathrm{m}}{\mathrm{s}} \\ \hat{v}_{princ,4} = \boldsymbol{A}\$^t_{princ,4} &= \begin{pmatrix} 0 & 0 & 0 & \frac{-1}{2} & \frac{1}{2} \end{pmatrix}^T \frac{\mathrm{m}}{\mathrm{s}} \\ \hat{v}_{princ,5} = \boldsymbol{A}\$^t_{princ,5} &= \begin{pmatrix} 0 & 0 & 0 & \frac{1}{2} & \frac{1}{2} \end{pmatrix}^T \frac{\mathrm{m}}{\mathrm{s}}.\end{aligned}$$

The vertical unit vector $\hat{u}_{vert}$ is formed according to (138):

$$\begin{aligned}-\frac{\hat{f}_{grav,1}}{\| \hat{f}_{grav,1} \|} &= \begin{pmatrix} 0 & 1 & 0 \end{pmatrix}^T \\ -\frac{\hat{f}_{grav,2}}{\| \hat{f}_{grav,2} \|} &= \begin{pmatrix} 0 & 1 \end{pmatrix}^T\end{aligned}$$

then

$$\hat{u}_{vert} = \begin{pmatrix} -\sqrt{\mu_1}\frac{\hat{f}_{grav,1}}{\|\hat{f}_{grav,1}\|} \\ -\sqrt{\mu_2}\frac{\hat{f}_{grav,2}}{\|\hat{f}_{grav,2}\|} \end{pmatrix} = \begin{pmatrix} 0 \\ \frac{\sqrt{3}}{2} \\ 0 \\ 0 \\ \frac{1}{2} \end{pmatrix}.$$

The vertical component of each principal collective generalized velocity is found via (139):

$$\begin{aligned}
\hat{v}_{princ,1,vert} &= \left(2\frac{\mathrm{m}}{\mathrm{s}}\right)\hat{u}_{vert} \\
\hat{v}_{princ,2,vert} &= \left(2\frac{\mathrm{m}}{\mathrm{s}}\right)\hat{u}_{vert} \\
\hat{v}_{princ,3,vert} &= \left(2\frac{\mathrm{m}}{\mathrm{s}}\right)\hat{u}_{vert} \\
\hat{v}_{princ,4,vert} &= \left(\frac{1}{4}\frac{\mathrm{m}}{\mathrm{s}}\right)\hat{u}_{vert} \\
\hat{v}_{princ,5,vert} &= \left(\frac{1}{4}\frac{\mathrm{m}}{\mathrm{s}}\right)\hat{u}_{vert}.
\end{aligned}$$

Calculating the magnitude of each principal collective generalized velocity results in:

$$\begin{aligned}
\| \hat{v}_{princ,1} \| &= \frac{\sqrt{647}}{4}\frac{\mathrm{m}}{\mathrm{s}} \\
\| \hat{v}_{princ,2} \| &= \frac{\sqrt{199}}{4}\frac{\mathrm{m}}{\mathrm{s}} \\
\| \hat{v}_{princ,3} \| &= \frac{\sqrt{167}}{4}\frac{\mathrm{m}}{\mathrm{s}} \\
\| \hat{v}_{princ,4} \| &= \frac{\sqrt{2}}{2}\frac{\mathrm{m}}{\mathrm{s}} \\
\| \hat{v}_{princ,5} \| &= \frac{\sqrt{2}}{2}\frac{\mathrm{m}}{\mathrm{s}}.
\end{aligned}$$

And for each principal collective generalized velocity $\sin\theta_i = \frac{\|\hat{v}_{princ,i,vert}\|}{\|\hat{v}_{princ,i}\|}$, thus:

$$\begin{aligned}
\sin\theta_1 &= \frac{8}{\sqrt{647}} = 0.315 \\
\sin\theta_2 &= \frac{8}{\sqrt{199}} = 0.567 \\
\sin\theta_3 &= \frac{8}{\sqrt{167}} = 0.619 \\
\sin\theta_4 &= \frac{\sqrt{2}}{4} = 0.354 \\
\sin\theta_5 &= \frac{\sqrt{2}}{4} = 0.354.
\end{aligned}$$

Applying the definition of the robustness measure given in (151) results in $\mathcal{R} = 0.315$. Thus the magnitude of the smallest static disturbance wrench that causes a cable to go slack is $\| \$^w_{min} \|_a = m_{tot} g\mathcal{R} = (4\text{kg})(9.81\frac{\text{m}}{\text{s}^2})(0.315) = 12.36\frac{\text{kg}\cdot\text{m}}{\text{s}^2}$. The lowest acceleration of an impulsively disturbed end-effector back to its original pose has magnitude $\| \$^a_{min} \|_a = g\mathcal{R} = (9.81\frac{\text{m}}{\text{s}^2})(0.315) = 3.09\frac{\text{m}}{\text{s}^2}$ with a vertical component of acceleration of $a_{vert,min} = -g\mathcal{R}^2 = (9.81\frac{\text{m}}{\text{s}^2})(0.315)^2 = 0.973\frac{\text{m}}{\text{s}^2}$.

4.7 Summary and Conclusion

In conclusion, the disturbance robustness measure, $\mathcal{R}$, presented here is an energy-based measure of the robustness of an underconstrained cable robot to static and impulsive disturbances at a particular pose. In order to facilitate the analysis, the intermediate space was introduced. Vector operations within this space carry physical meaning and allow simplified computation of the twist "parallel" to gravity.

The analysis of robustness to static disturbances used the Available Net Wrench Set to find the set of all static disturbance wrenches that cause a cable to begin to go slack. Out of this set, the smallest wrench was found, using acceleration energy to form the wrench norm. The magnitude of this smallest wrench is $mg\mathcal{R}_s$.

The analysis of robustness to impulsive disturbances began with the calculation of the unconstrained twists, U, which is the set of all twists that the end-effector can

instantaneously undergo without violating cable constraints. This set is spanned by the principal twists. If an impulsive disturbance is applied to the end-effector, the resulting initial acceleration (after the impulse has ended) of the end-effector back towards the original pose was found. The smallest acceleration was found to be along a principal twist and has vertical acceleration of $-g\mathcal{R}_i^2$ and a total acceleration of magnitude $g\mathcal{R}_i$ (using an acceleration energy norm).

It was then proven that $\mathcal{R}_s = \mathcal{R}_i$ and thus the robustness measure $\mathcal{R}$ was chosen to be $\mathcal{R} = \mathcal{R}_s = \mathcal{R}_i$. Several measures of overall cable robot robustness were presented. Each of these measures was based on evaluating the robustness measure at all poses within the desired task space. While these measures may be computationally time-consuming to compute, they provide a way of evaluating the overall robustness of the robot and can be used to optimize cable robot designs for robustness.

Lastly, the robustness measure was extended to apply to cable robots with multi-body end-effectors. The mapping to the intermediate space and the definition of the vertical direction in this space was chosen such that it was consistent with the single-body case. As such, the analysis of the manipulator in this space was analogous to that performed in the single-body case, resulting in a nearly identical form for the resulting robustness measure.

4.8 Future Work

There are several areas where future work on disturbance robustness could lead. First, the analysis presented here has been based on linear approximations of the constraint surfaces and small displacements of the end-effector. To refine the analysis, more work is necessary in order to factor in the curvature of the constraint surfaces. Because curvature of constraint surfaces is used in some work in grasp stability, it may be possible to leverage the work that has already been done in this area. However, determining the behavior of the end-effector as it goes through finite displacements

is expected to be very challenging.

The analysis of finite end-effector motion could also lead into an investigation of disturbances that cause the static equilibrium pose to change. Because there are sometimes multiple static-equilibrium poses that the end-effector can take for a given set of cable lengths, it is possible for a disturbance to be large enough that it causes the end-effector to transition into a different static equilibrium pose, and thus never return to the desired pose. The robustness of the end-effector to this type of pose-transition could possibly be measured by the "transition energy" of the pose – the smallest amount of potential energy that must be added to the end-effector in order to move it to a different equilibrium pose.

Because of the similarity between cable-robots and grasping (due to the uni-directional constraints), the disturbance robustness measure could also possibly be extended to an equivalent measure for underconstrained grasped objects.

For some manipulators the effects of cable sag and stretch are too great to be ignored. Thus it is of interest to include cable sag and stretch in the disturbance robustness analysis. A brief initial study on these effects is included in Appendix B.

Lastly, it would also be of interest to see if it is possible to actively cause the manipulator to return to its original pose. That is, to use a control strategy that recognizes when the end-effector has been disturbed and reacts accordingly to bring the end-effector back to its original pose as quickly as possible, preferably with as little residual vibration in the cables as possible.

CHAPTER 5

WRENCH-FEASIBLE WORKSPACE GENERATION

5.1 Introduction

One of the most important issues in robotics is that of manipulator workspace. A *workspace* is defined in a general sense as the set of all poses that the end-effector can reach[1] and operate at effectively. The various types of workspaces are then derived from the many possible ways to define what it means to "operate effectively." While many researchers refer to the "workspace" of a manipulator as simply the set of all reachable poses, not all reachable poses are necessarily useful. For cable robots only a subset of reachable poses are statically stable, and if the manipulator is expected to perform certain operations requiring wrench exertion, not all of the statically stable poses are useful.

Many cable robot applications require the end-effector to operate in regions where it can exert certain wrenches. The *Wrench-Feasible Workspace* is defined as the set of poses where the manipulator can exert a specified set of wrenches. That is, if a given set of wrenches must be exerted by the end-effector on its surroundings in order to accomplish a task, the manipulator can exert these required wrenches at any pose in the Wrench-Feasible Workspace. This region therefore constitutes the workspace which is "usable" by the robot for a particular application. While this workspace has been described in general terms by previous researchers, no tools exist to date for analytically calculating the Wrench-Feasible Workspace.

[1]Note that the workspace is defined as a subset of the task space.

As was stated in Chapter 1, one of the primary advantages of cable robots is that they can have very large workspaces, limited mostly by cable lengths, interference with surroundings, and wrench exertion requirements. This is a significant advantage over traditional manipulators, which typically have relatively small workspaces. In order to fully take advantage of this attribute of cable robots it is important to fully understand the workspace of these manipulators. However, relatively little prior work exists in the area of cable robot workspaces, as was described in Chapter 2. Additionally, most of this work does not provide much insight into the characteristics of cable robot workspaces because the workspace generation was done numerically via "brute force" methods, where the entire taskspace is discretized and exhaustively searched to find the statically reachable poses.

This chapter aims to address this deficiency in cable robot workspace generation. A method is presented here for forming the Wrench-Feasible Workspace (abbreviated WFW) of cable robots. This method applies to both underconstrained and fully-constrained cable robots and is also analytically based, thus the resulting description of the workspace provides insight into the workspace geometry that cannot be obtained through numerical approaches alone.

Organization

The organization of this chapter is as follows. Section 5.2 builds on the wrench analysis presented in Chapter 3 to develop a geometric interpretation of wrench-feasibility. Using this geometric understanding of wrench-feasibility, Section 5.3 shows how geometric methods can be applied to generate the Wrench-Feasible Workspace by defining its boundaries analytically. Section 5.4 discusses the WFW boundary equations and resulting workspace properties for point-mass cable robots[2]. Section

[2]Note that this work was performed by Andrew Riechel in [60]. That work was based on the workspace generation approach presented in this thesis and thus the relevant results of that work are summarized here.

5.5 then applies the workspace generation approach to general planar and spatial cable robots. The concepts developed in Chapter 4 and Section 5.3 are combined in Section 5.6 to create the Specified Robustness Workspace. This workspace consists of the set of all manipulator poses that meet or exceed a specified robustness value. Section 5.7 includes a discussion of several other applications of the available net wrench set and the workspace generation method. Lastly, Section 5.8 discusses and summarizes these results and Section 5.8 presents areas of future work.

Note that in the analysis presented here it is assumed that the cables have negligible mass and do not stretch or sag, the end-effector is a single rigid body with known cable attachment points on the end-effector relative to the center of gravity, the locations of the attachments of the cables to the motors are known and each motor controls exactly one cable. Cable lengths, the direction of gravity and the resulting pose of the mechanism are also assumed to be known.

5.2 Wrench-Feasibility

In many applications, the requirements for a task or set of tasks can be characterized by a required set of wrenches that the end-effector must apply to its surroundings. Given this requirement, the Wrench-Feasible Workspace is defined in [18] as the set of all poses that are *Wrench-Feasible*, i.e. where the manipulator can apply the required set of wrenches. Let this set of required wrenches be called NW_{req}, the *Required Net Wrench Set*.

Recall from Chapter 3 that NW_{avail} is the set of wrenches that can be exerted by the manipulator[3]. Thus the Wrench-Feasible Workspace can then be described as the set of all poses P of the end-effector where:

$$NW_{req}(P) \subseteq NW_{avail}(P). \tag{153}$$

[3]Also recall that the geometry of NW_{avail} is pose-dependent.

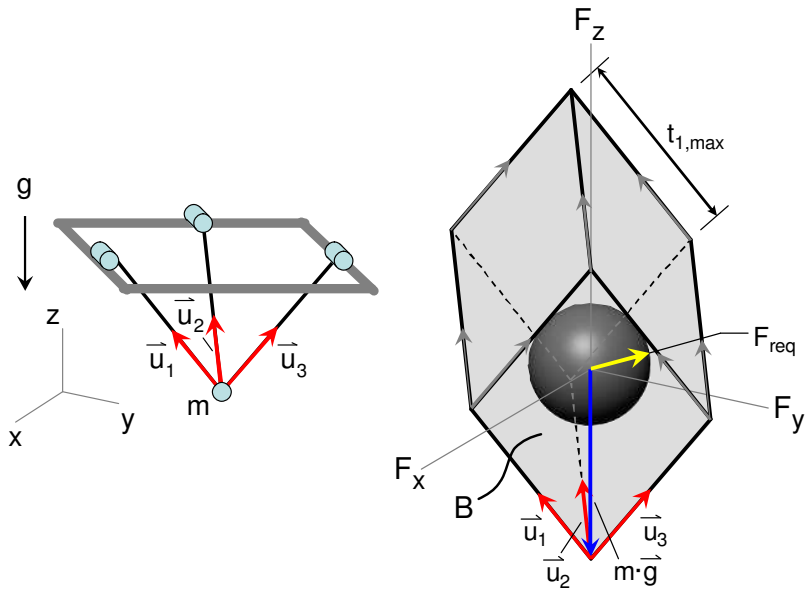

(a) Example manipulator.

(b) Available Net Wrench Set with Required Net Wrench Set.

Figure 29: A point-mass 3-cable manipulator and its Available Net Wrench Set containing its Required Net Wrench Set.

Although NW_{req} can be chosen arbitrarily, it is typically chosen to be a geometrically simple set of wrenches that is independent of P.

For example, consider the point-mass 3-cable manipulator shown in Figure 29(a). Assume that the manipulator's task requires it to exert a minimum required force F_{req} in any direction. The corresponding choice for NW_{req} would then be the set of all forces $\overline{F}$ such that $\| \overline{F} \| \leq F_{req}$. Graphically this set NW_{req} is simply a sphere centered at the origin with radius F_{req}. Figure 29 illustrates an example manipulator (29(a)) and its spherical Required Net Wrench Set NW_{req} and parallelepiped Available Net Wrench Set NW_{avail} (29(b)) at that pose. Note that in Figure 29, NW_{req} is completely contained within NW_{avail}; thus this end-effector pose is wrench-feasible and is therefore contained within the Wrench-Feasible Workspace of this manipulator.

This geometric construction of NW_{req} not only allows wrench-feasibility to be visualized, but also allows wrench-feasibility to be determined by simple geometric

calculation. In this example, determining analytically if the pose is wrench-feasible reduces to simply testing whether the distances between the planes that define the boundaries of NW_{avail} and the origin are greater than or equal to F_{req}.

While visualization of these sets may break down for cases where the dimension of the taskspace is higher than three, the geometric conditions for wrench-feasibility do not. Thus for higher-dimensional task spaces the wrench-feasibility of a pose can be calculated from the distance between the hyperplanes that bound NW_{avail} and the hyper-object (such as a hyper-sphere) that represents NW_{req}.

In general, it is very likely that the geometry of NW_{req} will be simple, resulting in simple geometric conditions for $NW_{req} \subseteq NW_{avail}$. In the case that NW_{req} is more complex, an approximation of this set can be made by choosing a simpler geometry that contains NW_{req}. Using this approximate set will give a conservative estimate of whether or not the pose is wrench-feasible.

5.3 Constructing the Wrench-Feasible Workspace

While it is very advantageous to now be able to check whether or not a pose is wrench-feasible by simple geometric conditions, it is still necessary to construct the entire Wrench-Feasible Workspace. A simple method to accomplish this would be to discretize the task space and evaluate each discrete pose of the manipulator, thus constructing a discretized Wrench-Feasible Workspace as the set of discrete poses that are wrench-feasible. Such a method, while relatively simple, would be time-consuming, computationally expensive and would not produce a complete description of the continuous Wrench-Feasible Workspace. Moreover, such a method would not provide any insight into the nature of the Wrench-Feasible Workspace.

Instead, the Wrench-Feasible Workspace can be constructed by generating the boundaries of the workspace analytically. Consider a pose of a manipulator where NW_{req} is contained in NW_{avail} and is contacting one of the sides of NW_{avail}. A small

change in the pose of the manipulator can cause the pose to remain wrench-feasible (if NW_{req} remains inside NW_{avail}) or to become not wrench-feasible (if part of NW_{req} is now outside of NW_{avail}). Thus this pose of the manipulator must be on the boundary of the WFW because it it is a point of transition between being wrench-feasible and no longer being wrench-feasible. **Thus the boundaries of the WFW consist of the set of all poses of the manipulator such that $NW_{req} \subseteq NW_{avail}$ and one or more of the planes bounding NW_{avail} contact NW_{req}.**

The conditions for this to occur can be represented as geometric conditions on the geometry of the pose. Each plane defining a boundary of NW_{avail} can be expressed as a function of the cable wrenches $\$_1^w$ through $\$_p^w$, which are functions of the pose P. The condition of contact between one of these planes and NW_{req} results in a relationship between the screws $\$_1$ through $\$_p$ that causes contact to occur. This relationship can then be used to construct the geometric conditions that result in the pose being on the boundary of the workspace. Thus these geometric relationships represent an analytical definition of a boundary of the Wrench-Feasible Workspace. Repeating this process for each of the planes that bounds NW_{avail} results in a set of analytical expressions that define the Wrench Feasible Workspace boundaries. Note that because there are $2\binom{p}{q-1}$ sides that bound NW_{avail}, at least $2\binom{p}{q-1}$ workspace boundaries must be formulated.

Sections 5.4 and 5.5 now formulate the boundaries of the WFW for two cases: point-mass cable robots and general cable robots, respectively. Section 5.4 assumes a spherical NW_{req}, as was the case for the example manipulator in Figure 29. Section 5.5 assumes a polyhedral NW_{req} for general cable robots.

5.4 Point-Mass Cable Robots

Based on the approach presented in 5.3, a detailed investigation of forming the WFW for point-mass cable robots was performed by Andrew Riechel in [60] and

[61]. Because that work was based on the workspace generation approach presented in this thesis, the relevant results of that work will be summarized in this section.

5.4.1 Forming the Wrench-Feasible Workspace Boundaries

Point-mass cable robots can only exert forces on their surroundings (and no moments), thus for point-mass cable robots NW_{req} is a set of pure forces. Common geometries of NW_{req} for point-mass cable robots are circles or rectangles for the planar case and spheres or cylinders for the spatial case. Without specific knowledge about the task requirements for the manipulator, it is reasonable to assume the manipulator needs to be able to exert a minimum required force F_{req} in any direction. The corresponding choice for NW_{req} would then be the set of all forces $\overline{F}$ such that $\| \overline{F} \| \leq F_{req}$. Graphically this set NW_{req} is simply a sphere centered at the origin with radius F_{req}, as was shown in Figure 29(b). Because this choice of NW_{req} is fairly general and also simplifies geometric calculations of wrench-feasibility, a spherical NW_{req} is used here.

Given a 3-D point-mass cable robot with three cables ($p = 3$)[4] in a particular end-effector pose, the Available Net Wrench Set is known to be a parallelepiped described by $NW_{avail} = \{\$^w : \$^w = a_1 t_{1,max} \overline{u}_1 + a_2 t_{2,max} \overline{u}_2 + a_3 t_{3,max} \overline{u}_3 + m\overline{g};\ 0 < a_i \leq 1\}$, as shown in Figure 30(b). The Required Net Wrench Set, NW_{req}, is assumed to be a sphere with radius F_{req}.

Based on the conclusions made in Section 5.3, at every pose on the boundary of the Wrench-Feasible Workspace at least one side of NW_{avail} is tangent to the spherical NW_{req}. A set of six vectors can be defined, where each vector is the shortest vector from the origin to one of the six sides of NW_{avail} (orthogonal distance vectors) as illustrated in Figure 30(b). For each of the lower three sides of NW_{avail} the vector $\overline{d}_{ij}$ is directed towards the lower side spanned by $\overline{u}_i$ and $\overline{u}_j$. For each of the three upper

[4]Note that this procedure can be extended to a point-mass cable robot with any number of cables.

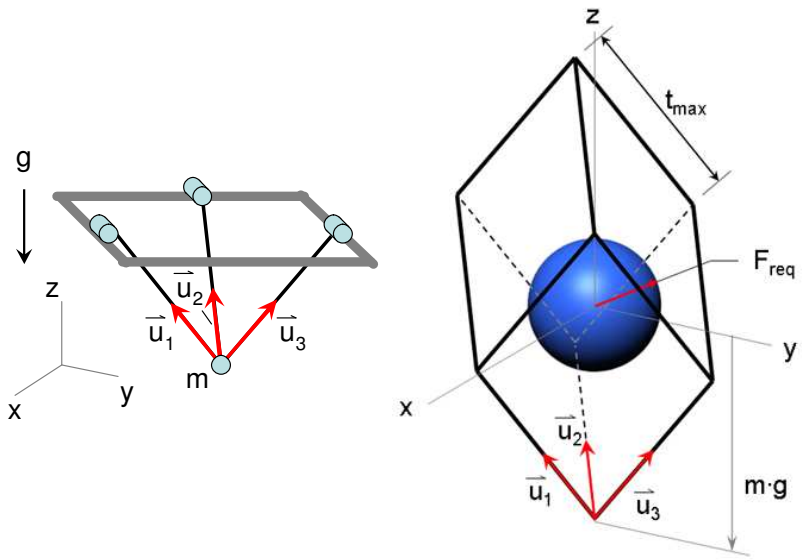

(a) Example manipulator.

(b) Available Net Wrench Set with Required Net Wrench Set.

Figure 30: A point-mass 3-cable manipulator and its Available Net Wrench Set containing its Required Net Wrench Set.

sides of NW_{avail} the vector $\overline{d}'_{ij}$ is directed towards the upper side spanned by $\overline{u}_i$ and $\overline{u}_j$.

Because NW_{req} is a sphere of radius F_{req}, an intersection with the boundary of NW_{avail} will occur whenever $\| \overline{d}_{ij} \| \leq F_{req}$ or $\| \overline{d}'_{ij} \| \leq F_{req}$. Thus an end-effector position is included in the Wrench-Feasible Workspace if and only if it satisfies the following inequalities:

$$\| \overline{d}_{ij} \| \geq F_{req} \qquad \text{and} \qquad \| \overline{d}'_{ij} \| \geq F_{req}, \tag{154}$$

$$\text{for } \{i,j\} \in \{\{1,2\},\{2,3\},\{3,1\}\}\,.$$

By forming a series of vector loop equations involving known vectors the magnitudes $\| \overline{d}_{ij} \|$ and $\| \overline{d}'_{ij} \|$ can be calculated. For brevity the details of the derivation are not included here but can be found in [60]. If $\overline{u}_i = (x_i, y_i, z_i)$, motor mount location i is $\overline{M}_i = (M_x, M_y, M_z)$ and the end-effector location is

$\overline{ee} = (ee_x, ee_y, ee_z)$, then solving the vector loop equations for each d_{ij} and d'_{ij} results in:

$$\| \overline{d}_{ij} \| = \frac{mg(x_j y_i - x_i y_j)}{\sqrt{(y_i z_j - y_j z_i)^2 + (x_j z_i - x_i z_j)^2 + (x_i y_j - x_j y_i)^2}} \tag{155}$$

$$\| \overline{d}'_{ij} \| = t_{k,max} \sin\left[\cos^{-1}(\overline{u}_j \cdot \overline{u}_k)\right] \sin\left[\cos^{-1}(\overline{u}_k \cdot \overline{u}_i)\right] - d_{ij} \tag{156}$$

$$\text{for } \{i, j, k\} \in \{\{1, 2, 3\}, \{2, 3, 1\}, \{3, 1, 2\}\}$$

where

$$x_\ell = \frac{M_{\ell x} - ee_x}{\sqrt{(M_{\ell x} - ee_x)^2 + (M_{\ell y} - ee_y)^2 + (M_{\ell z} - ee_z)^2}} \tag{157}$$

$$y_\ell = \frac{M_{\ell y} - ee_y}{\sqrt{(M_{\ell x} - ee_x)^2 + (M_{\ell y} - ee_y)^2 + (M_{\ell z} - ee_z)^2}} \tag{158}$$

$$z_\ell = \frac{M_{\ell y} - ee_y}{\sqrt{(M_{\ell x} - ee_x)^2 + (M_{\ell y} - ee_y)^2 + (M_{\ell z} - ee_z)^2}} \tag{159}$$

$$\text{for } \ell = 1, 2, 3.$$

Note that $\cos^{-1}$ is assumed to yield a result between 0 and π.

The boundaries of the Wrench-Feasible Workspace can now be expressed analytically. By substituting identities (157) through (159) into Equations (155) and (156) and setting each distance $\| \overline{d}_{ij} \|$ and $\| \overline{d}'_{ij} \|$ equal to F_{req}, Equations (155) and (156) represent six implicit expressions of the six boundaries of the Wrench-Feasible Workspace. The Wrench-Feasible Workspace can alternatively be constructed by substituting $\| \overline{d}_{ij} \|, \| \overline{d}'_{ij} \| \geq F_{req}$ into Equations (155) and (156) and determining the intersection of the six resulting regions.

5.4.2 Results of Workspace Derivation

From the equations for the WFW boundaries in the previous section, several workspace properties and trends can be observed. These will be listed briefly here,

but full derivations of the properties and workspace trends are included in [60] and [61]. In addition, details of the workspace derivation for a 2-cable planar point-mass cable robot are also included in [60] and [61].

Based on the expressions for the boundaries of the WFW for a point-mass cable robot with spherical NW_{req} the following properties can be observed. The properties of the 2-D case (a planar point-mass cable robot with circular NW_{req}) are included in parentheses.

Property 1: Lower workspace boundaries, i.e. those defined by Equation (155), are always planes. (For the 2-D case the lower boundaries are lines.)

Property 2: All lower workspace boundaries have the same relative angle from vertical. (For the 2-D case the lower boundaries are lines with the same relative angle from vertical.)

Property 3: Each workspace boundary must pass through exactly two motor mount locations.

As an illustration of these properties, consider the WFW shown in Figure 31 for a 2-cable point-mass 2-D cable robot. Here NW_{req} is a circle. The four curves are the four workspace boundaries found using the 2-D versions of (155) and (156) and the shaded region is the resulting WFW. The lower two boundaries (the straight lines) come from the 2-D version of (155), which correspond to the condition of contact between NW_{req} and the lower sides of NW_{avail}. Similarly, the upper two boundaries (the curved lines) come from the 2-D version of (156), which correspond to the condition of contact between NW_{req} and the upper sides of NW_{avail}.

As an example of what a 3-D version of the WFW looks like for a point-mass cable robot, consider Figure 32, which shows a discretized 3-D workspace with the edges of the planar lower boundaries highlighted. Note that the workspace can be found analytically, but is plotted in a discretized manner in order to make visualization

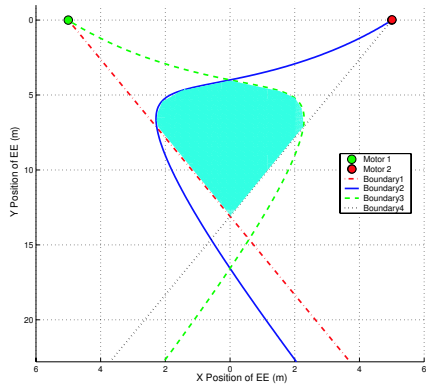

Figure 31: Example of 2-D Wrench-Feasible Workspace for a 2-cable point mass cable robot.

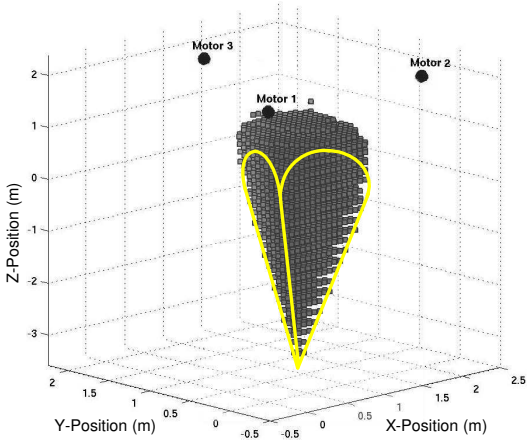

Figure 32: Example of discretized 3-D Wrench-Feasible Workspace for a 3-cable point mass cable robot.

easier.

Given the analytical expressions for the workspace boundaries, it is possible to vary different design parameters and see how they affect the geometry of the Wrench-Feasible Workspace. When designing a point-mass cable robot these trends can be used to adjust the manipulator design appropriately to achieve the desired workspace geometry. The specific trends are not included here, but [60] and [61] examine the effects of 1) varying maximum cable tensions, 2) varying end-effector mass, 3) varying the radius of NW_{req} and 4) varying motor mount locations.

5.5 General Cable Robots

5.5.1 Polyhedral Required Net Wrench Set

Because point-mass cable robots only exert forces, the selection of an appropriate geometry for NW_{req} is relatively simple. However, for general cable robots the wrench-exertion requirements may vary greatly from task to task. For example, one task may primarily require large moments to be exerted with very small associated forces, while another task may primarily require large forces to be exerted with very small associated moments. Thus it is not easy to choose a single geometry of NW_{req} that is representative of the various possible task requirements.

Therefore, rather than selecting a single geometry of NW_{req} and formulating the WFW boundary equations for that geometry, NW_{req} will be assumed to be defined by an arbitrary polyhedron (or collection of polyhedra) with a finite number of vertices[5]. This allows a great deal of flexibility when specifying NW_{req}, as nearly any arbitrary object can be closely approximated by a collection of polyhedra.

Given such a geometry for NW_{req}, the question now is how to test if a pose is wrench-feasible. It is shown in the following theorem that in order to test if $NW_{req} \subseteq NW_{avail}$ we only need to check that V, the set of vertices of NW_{req}, is inside NW_{avail}.

Theorem **:**

If NW_{req} is a collection of a finite number of bounded polyhedra[6], each of which has a finite number of vertices, and if the set of vertices for the polyhedra is V, then

$$NW_{req} \subseteq NW_{avail} \quad \Leftrightarrow \quad V \subseteq NW_{avail}. \tag{160}$$

[5] A polyhedron is defined as a body bounded by planes [15] or equivalently as the intersection of a finite number of half-spaces [80]. It is assumed that none of the vertices of the polyhedra are located at infinity, and thus NW_{req} is actually assumed to be a set of *polytopes*, or bounded polyhedra [80].

[6] Note that for this proof and for the generation of the WFW a collection of polyhedra can be equivalently replaced with the convex hull of the vertices of the polyhedra.

***Proof* :**

This proof contains two directions, the first of which is trivial:

Proof of $NW_{req} \subseteq NW_{avail} \Rightarrow V \subseteq NW_{avail}$:

$V \subseteq NW_{req}$, so from $NW_{req} \subseteq NW_{avail}$ it follows that $V \subseteq NW_{avail}$.

Proof of $NW_{req} \subseteq NW_{avail} \Leftarrow V \subseteq NW_{avail}$:

First we must prove that NW_{avail} is convex. A set S is said to be convex if $\mu x + (1-\mu)y \in S$ for all $x, y \in S$ and $0 \leq \mu \leq 1$ [79]. Recall that $NW_{avail} = \{\$^w : \$^w = a_1 t_{1,max} \$_1^w + ... + a_p t_{p,max} \$_p^w + m\overline{g};\ 0 \leq a_i \leq 1\}$, where $t_{i,max}$ is the maximum allowable tension in cable i and $\$_i^w$ is the i^{th} column of $\boldsymbol{J}^T$. Then given two wrenches, $\$_\alpha^w$, $\$_\beta^w \in NW_{avail}$:

$$\$_\alpha^w = a_{\alpha,1} t_{1,max} \$_1^w + ... + a_{\alpha,p} t_{p,max} \$_p^w + m\overline{g} \qquad 0 \leq a_{\alpha,i} \leq 1$$

$$\$_\beta^w = a_{\beta,1} t_{1,max} \$_1^w + ... + a_{\beta,p} t_{p,max} \$_p^w + m\overline{g} \qquad 0 \leq a_{\beta,i} \leq 1.$$

Let $0 \leq \mu \leq 1$. Then let $\$_\gamma^w$ be a convex combination of $\$_\alpha^w$ and $\$_\beta^w$:

$$\begin{aligned}
\$_\gamma^w &= \mu \$_\alpha^w + (1-\mu)\$_\beta^w \\
&= \mu a_{\alpha,1} t_{1,max} \$_1^w + ... + \mu a_{\alpha,p} t_{p,max} \$_p^w + \mu m\overline{g} + ... \\
&\quad + (1-\mu) a_{\beta,1} t_{1,max} \$_1^w + ... + (1-\mu) a_{\beta,p} t_{p,max} \$_p^w + (1-\mu) m\overline{g} \\
&= (\mu a_{\alpha,1} + (1-\mu) a_{\beta,1})\, t_{1,max} \$_1^w + ... + (\mu a_{\alpha,p} + (1-\mu) a_{\beta,p})\, t_{p,max} \$_p^w + m\overline{g}.
\end{aligned}$$

Because $0 \leq a_{\alpha,i} \leq 1$ and $0 \leq a_{\beta,i} \leq 1$,

$$0 \leq (\mu a_{\alpha,i} + (1-\mu) a_{\beta,i}) \leq 1.$$

If we define a new set of coefficients $a_{\gamma,i}$ as:

$$a_{\gamma,i} = (\mu a_{\alpha,i} + (1-\mu) a_{\beta,i}) \qquad i = 1, ..., p$$

then

$$\$_\gamma^w = a_{\gamma,1} t_{1,max} \$_1^w + ... + a_{\gamma,p} t_{p,max} \$_p^w + m\overline{g} \qquad 0 \leq a_{\gamma,i} \leq 1.$$

Thus $\$_\gamma^w \in NW_{avail}$. Therefore we conclude that NW_{avail} is convex.

Because NW_{avail} is convex, if the set of vertices V is contained in NW_{avail}, then $conv(V)$, the convex hull of V, is contained in NW_{avail}. Because NW_{req} is a set of polyhedra, $NW_{req} \subseteq conv(V)$. Thus because $conv(V) \subseteq NW_{avail}$, $NW_{req} \subseteq NW_{avail}$. Therefore $NW_{req} \subseteq NW_{avail} \Leftarrow V \subseteq NW_{avail}$. Q.E.D. $\square$

Recall that the WFW boundaries are the set of all poses of the manipulator such that $NW_{req} \subseteq NW_{avail}$ and one or more of the planes bounding NW_{avail} contact NW_{req}. Because NW_{avail} is convex, if a plane bounding NW_{avail} contacts NW_{req}, it must contact it at at least one vertex. **Thus the set of boundary equations is simply the set of all expressions for contact between a vertex of NW_{req} and a side of NW_{avail}.**

Consider Figure 33(a), which illustrates an example of a polyhedral NW_{req} (in this case a cube) contained inside a NW_{avail}. In order to form the WFW boundaries it is necessary to form the set of equations that describe the condition of contact between a vertex of NW_{req} and a side of NW_{avail}.

The boundary equations can be formulated in determinant form. Consider the illustration in Figure 33(b) of contact between a lower side of NW_{avail} and vertex v_1. The vertex contacts the lower side if the vector $(\overline{v}_1 - m\overline{g})$ is a linear combination of $\$_2^w$ and $\$_3^w$. This condition can be formulated as:

$$\det \begin{bmatrix} \$_2^w & \$_3^w & (\overline{v}_1 - m\overline{g}) \end{bmatrix} = 0. \tag{161}$$

Similarly, Figure 33(c) illustrates contact between an upper side of NW_{avail} and vertex v_2. The vertex contacts the lower side if the vector $(\overline{v}_2 - m\overline{g} - t_{3,max}\$_3^w)$ is a linear combination of $\$_1^w$ and $\$_2^w$. This condition can be formulated as:

$$\det \begin{bmatrix} \$_1^w & \$_2^w & (\overline{v}_2 - m\overline{g} - t_{3,max}\$_3^w) \end{bmatrix} = 0. \tag{162}$$

In general, for an n-dimensional task space a side S of NW_{avail} is spanned by $(n-1)$ wrenches. Let E be the set of wrenches along the edges of NW_{avail} that must

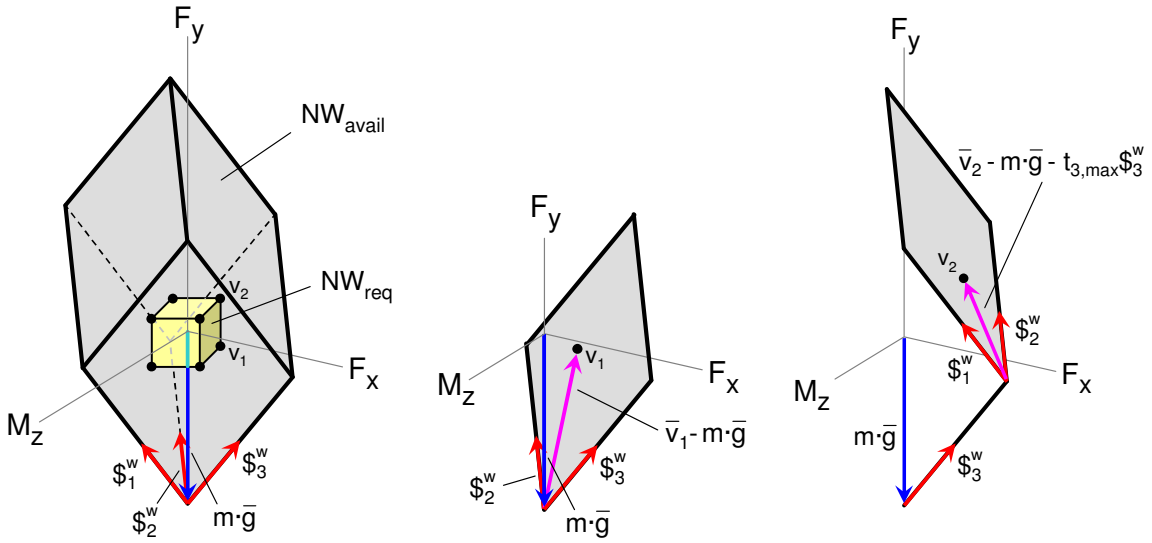

(a) Example polyhedral NW_{req} contained in NW_{avail}.

(b) Contact between a lower side of NW_{avail} and vertex v_1.

(c) Contact between an upper side of NW_{avail} and vertex v_2.

Figure 33: An example Available Net Wrench Set containing its polyhedral Required Net Wrench Set.

be traced to get from the bottom of NW_{avail} (which is $m\overline{g}$) to the bottom of side S and let SP be the set of $(n-1)$ wrenches that positively span S. Then S can be expressed as $S = \{\$^w : \$^w = \sum_{\$_e^w \in E} t_{e,max}\$_e^w + \sum_{\$_j^w \in SP} a_j t_{j,max}\$_j^w;\ 0 \leq a_j \leq 1\}$. As an example, again consider Figure 33. In the case of Figure 33(b), $\$_2^w$ and $\$_3^w$ span the side we are interested in, and the bottom of the side is the same as the bottom of NW_{avail}. Thus $E = \{\emptyset\}$ and $SP = \{\$_2^w, \$_3^w\}$. In the case shown in Figure 33(c), $\$_1^w$ and $\$_2^w$ span the side we are interested in, and in order to get from the bottom of NW_{avail} to the bottom of the side, we must traverse the edge that is along $\$_3^w$. Thus $E = \{\$_3^w\}$ and $SP = \{\$_1^w, \$_2^w\}$. Thus the boundary equation corresponding to contact between any vertex $\overline{v}$ and a side of NW_{avail} is of the form

$$\det \left[\begin{array}{cccc} \$_a^w & \$_b^w & \cdots & \$_i^w \end{array} \left(\overline{v} - m\overline{g} - \sum_{\$_j^w \in E} t_{j,max}\$_j^w \right) \right] = 0 \qquad (163)$$

where $\{\$_a^w, \$_b^w, \ldots, \$_i^w\} = SP$.

Note that this must be done for *every* vertex $\overline{v}$ of NW_{req} contacting *each*

of the sides of NW_{avail}. Thus if there are w different vertices of NW_{req}, then $2w\binom{p}{q-1}$ boundary equations must be formed. In the example shown in Figure 33, NW_{avail} has 6 sides and NW_{req} has 8 vertices, thus 48 boundary equations must be formed. Clearly, the number of boundaries that must be formed is relatively large, even for simple geometries of NW_{req}. Thus if NW_{req} is complicated, a simplified approximation of NW_{req} with fewer vertices will make the computations more manageable. In addition, for underconstrained robots if the upper tension limits of the manipulator are high, the geometry of the WFW is dominated by the boundaries corresponding to contact between the vertices of NW_{req} and the lower boundaries of NW_{avail} (i.e. those that correspond to a cable having zero tension). Thus in some cases it may only be necessary to form a few of the workspace boundaries in order to determine the majority of the geometry of the workspace.

5.5.2 Wrench-Feasible Workspace of Planar Cable Robots

This section examines in more detail the form of the WFW boundaries for planar cable robots. The complete expression for the lower WFW boundaries (those that correspond to contact between a vertex of NW_{req} and a lower side of NW_{avail}) are derived in Section 5.5.2.1 and applied to an example manipulator in Section 5.5.2.3. Section 5.5.2.2 discusses the approach for formulation of the upper WFW boundaries (those that correspond to contact between a vertex of NW_{req} and an upper side of NW_{avail}).

5.5.2.1 Analytically Determined Lower WFW Boundaries

Consider a general planar cable robot where the wrench-exertion requirements of a task are defined by a polyhedral NW_{req}. Let the set of all vertices of NW_{req} be V. As shown in Figure 34, the pose of the end-effector is defined as (x, y, θ), where (x, y) is the position of the center of gravity of the end-effector in the fixed global coordinate frame X-Y and θ is the rotation of the end-effector, defined as the relative

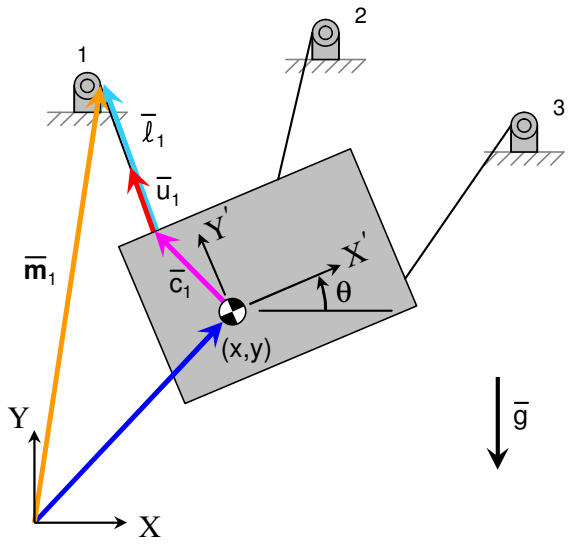

Figure 34: Kinematic parameters for a planar cable robot.

angle between the moving coordinate frame X'-Y' attached to the end-effector and the global coordinate frame X-Y. Without loss of generality, the fixed coordinate frame can be chosen such that the Y axis is vertical (aligned with gravity), the X axis points to the right and counterclockwise rotations (and moments) are considered positive.

The location of motor i (or location of the pulley through which the cable is routed) with respect to the fixed global frame is $\overline{\mathbf{m}}_i$ and the vectors from (x, y) to the attachment point of the cable i is $\overline{c}_i$. The notation used for these vectors is as follows:

$$\overline{\mathbf{m}}_i = \begin{pmatrix} \mathbf{m}_{i,x} \\ \mathbf{m}_{i,y} \end{pmatrix} \qquad \overline{c}_i = \begin{pmatrix} c_{i,x} \\ c_{i,y} \end{pmatrix}.$$

Note that the vector $\overline{\mathbf{m}}_i$ is defined in the fixed global coordinate frame, while $\overline{c}_i$ is defined in the moving coordinate frame attached to the end-effector. Thus both vectors are constant vectors (i.e. they do not change in their respective frames as the end-effector moves).

Let us define the cable length vector $\overline{\ell}_i$ in the global coordinate frame as the vector along cable i directed from the cable attachment points to the corresponding motor

locations:

$$\overline{\ell}_i = \overline{\mathbf{m}}_i - \left[\begin{pmatrix} x \\ y \end{pmatrix} + \boldsymbol{R}(\theta)\overline{c}_i \right] \tag{164}$$

where

$$\boldsymbol{R}(\theta) = \begin{bmatrix} \cos(\theta) & -\sin(\theta) \\ \sin(\theta) & \cos(\theta) \end{bmatrix}. \tag{165}$$

Note that the length of cable i is $\| \overline{\ell}_i \|$.

The unit vector $\overline{u}_i$ along cable i directed away from the end-effector is then defined as:

$$\overline{u}_i = \frac{\overline{\ell}_i}{\| \overline{\ell}_i \|}. \tag{166}$$

When $\| \overline{\ell}_i \| = 0$, the corresponding unit vector is undefined and is chosen to be $\overline{0}$. However, such a condition only results when the end-effector comes in contact with the motor mount and should therefore be avoided in order to avoid interference. Thus such a pose will not be considered to be part of the WFW.

Using (163), the equation for any one of the lower boundaries is of the form

$$\det \begin{bmatrix} \$_i^w & \$_j^w & (\overline{v} - m\overline{g}) \end{bmatrix} = 0. \tag{167}$$

Let the wrench corresponding to vertex $\overline{v}$ be expressed as $\overline{v} = (F_x, F_y, M)$. Then using (10) and noting that here $m\overline{g} = (0, -mg, 0)^T$, (167) becomes:

$$det \begin{bmatrix} u_{i,x} & u_{j,x} & F_x \\ u_{i,y} & u_{j,y} & F_y + mg \\ (\boldsymbol{R}(\theta)\overline{c}_i) \times \overline{u}_i & (\boldsymbol{R}(\theta)\overline{c}_j) \times \overline{u}_j & M \end{bmatrix} = 0. \tag{168}$$

Note that while the cross-product operation is only strictly defined for three-dimensional vectors, it is used here on two-dimensional vectors in order to retain the same form of the boundary equations as that obtained for the general case. In two dimensions the operation $\overline{a} \times \overline{b}$ is defined as $\overline{a} \times \overline{b} = det \left[\overline{a} \ \overline{b} \right]$.

Evaluation of (168) results in the following:

$$u_{i,x}u_{j,y}M \;+\; u_{jx}(F_y+mg)((\boldsymbol{R}(\theta)\overline{c}_i)\times\overline{u}_i) \;+\; F_x u_{i,y}((\boldsymbol{R}(\theta)\overline{c}_j)\times\overline{u}_j) \;-$$
$$-\; u_{i,x}(F_y+mg)((\boldsymbol{R}(\theta)\overline{c}_j)\times\overline{u}_j) \;-\; u_{j,x}u_{i,y}M \;-\; F_x u_{j,y}((\boldsymbol{R}(\theta)\overline{c}_i)\times\overline{u}_i)=0. \quad (169)$$

Substituting for $\overline{u}_i$ and $\overline{u}_j$ in terms of $\overline{\ell}_i$ and $\overline{\ell}_j$ as defined in (166) results in each term having a common factor of $\frac{1}{\|\overline{\ell}_i\|\cdot\|\overline{\ell}_j\|}$. Thus multiplying both sides of (169) by $\| \overline{\ell}_i \| \cdot \| \overline{\ell}_j \|$ results in:

$$\ell_{i,x}\ell_{j,y}M \;+\; \ell_{jx}(F_y+mg)((\boldsymbol{R}(\theta)\overline{c}_i)\times\overline{\ell}_i) \;+\; F_x \ell_{i,y}((\boldsymbol{R}(\theta)\overline{c}_j)\times\overline{\ell}_j) \;-$$
$$-\; \ell_{i,x}(F_y+mg)((\boldsymbol{R}(\theta)\overline{c}_j)\times\overline{\ell}_j) \;-\; \ell_{j,x}\ell_{i,y}M \;-\; F_x\ell_{j,y}((\boldsymbol{R}(\theta)\overline{c}_i)\times\overline{\ell}_i)=0. \quad (170)$$

which eliminates the complexity of the square-root and quadratic terms in $\| \overline{\ell}_i \|$ and $\| \overline{\ell}_j \|$. Each of the terms in (170) can now be expressed in terms of known constants ($\overline{\mathbf{m}}_i$, $\overline{\mathbf{m}}_j$, $\overline{c}_i$, $\overline{c}_j$, mg, F_x, F_y and M) and the variables of interest (x,y and θ):

$$\begin{aligned}
\ell_{i,x}\ell_{j,y}M &= (\mathbf{m}_{i,x}-x-\cos(\theta)c_{i,x}+\sin(\theta)c_{i,y})(\mathbf{m}_{j,y}-y-\sin(\theta)c_{j,x}-\cos(\theta)c_{j,y})M && (171)\\
\ell_{jx}(F_y+mg)((\boldsymbol{R}(\theta)\overline{c}_i)\times\overline{\ell}_i) &= (\mathbf{m}_{j,x}-x-\cos(\theta)c_{j,x}+\sin(\theta)c_{j,y})(F_y+mg)\cdot ... \\
&\quad ...\cdot\Big[(\cos(\theta)c_{i,x}-\sin(\theta)c_{i,y})(\mathbf{m}_{i,y}-y-\sin(\theta)c_{i,x}-\cos(\theta)c_{i,y})-... \\
&\quad ...-(\sin(\theta)c_{i,x}+\cos(\theta)c_{i,y})(\mathbf{m}_{i,x}-x-\cos(\theta)c_{i,x}+\sin(\theta)c_{i,y})\Big] && (172)\\
F_x\ell_{i,y}((\boldsymbol{R}(\theta)\overline{c}_j)\times\overline{\ell}_j) &= (\mathbf{m}_{i,y}-y-\sin(\theta)c_{i,x}-\cos(\theta)c_{i,y})F_x\cdot ... \\
&\quad ...\cdot\Big[(\cos(\theta)c_{j,x}-\sin(\theta)c_{j,y})(\mathbf{m}_{j,y}-y-\sin(\theta)c_{j,x}-\cos(\theta)c_{j,y})-... \\
&\quad ...-(\sin(\theta)c_{j,x}+\cos(\theta)c_{j,y})(\mathbf{m}_{j,x}-x-\cos(\theta)c_{j,x}+\sin(\theta)c_{j,y})\Big] && (173)\\
\ell_{i,x}(F_y+mg)((\boldsymbol{R}(\theta)\overline{c}_j)\times\overline{\ell}_j) &= (\mathbf{m}_{i,x}-x-\cos(\theta)c_{i,x}+\sin(\theta)c_{i,y})(F_y+mg)\cdot ... \\
&\quad ...\cdot\Big[(\cos(\theta)c_{j,x}-\sin(\theta)c_{j,y})(\mathbf{m}_{j,y}-y-\sin(\theta)c_{j,x}-\cos(\theta)c_{j,y})-... \\
&\quad ...-(\sin(\theta)c_{j,x}+\cos(\theta)c_{j,y})(\mathbf{m}_{j,x}-x-\cos(\theta)c_{j,x}+sin(\theta)c_{j,y})\Big] && (174)\\
\ell_{j,x}\ell_{i,y}M &= (\mathbf{m}_{i,y}-y-\sin(\theta)c_{i,x}-\cos(\theta)c_{i,y})(\mathbf{m}_{j,x}-x-\cos(\theta)c_{j,x}+\sin(\theta)c_{j,y})M && (175)\\
F_x\ell_{j,y}((\boldsymbol{R}(\theta)\overline{c}_i)\times\overline{\ell}_i) &= (\mathbf{m}_{j,y}-y-\sin(\theta)c_{j,x}-\cos(\theta)c_{j,y})(F_x)\cdot ... \\
&\quad ...\cdot\Big[(\cos(\theta)c_{i,x}-\sin(\theta)c_{i,y})(\mathbf{m}_{i,y}-y-\sin(\theta)c_{i,x}-\cos(\theta)c_{i,y})-... \\
&\quad ...-(\sin(\theta)c_{i,x}+\cos(\theta)c_{i,y})(\mathbf{m}_{i,x}-x-\cos(\theta)c_{i,x}+\sin(\theta)c_{i,y})\Big]. && (176)
\end{aligned}$$

Collecting terms results in a boundary equation of the form:

$$a_1x^2+a_2x+a_3xy+a_4y+a_5y^2+a_6=0 \quad (177)$$

where each a_i is a function of θ and known constants:

$$a_1 = (F_y + mg)(\sin(\theta)(c_{j,x} - c_{i,x}) + \cos(\theta)(c_{j,y} - c_{i,y})) \tag{178}$$

$$\begin{aligned} a_2 = &\Big[(\mathbf{m}_{i,y} - \mathbf{m}_{j,y}) - \sin(\theta)(c_{i,x} - c_{j,x}) - \cos(\theta)(c_{i,y} - c_{j,y})\Big] M - ... \\ &... - (F_y + mg)\Big[\cos(\theta)(c_{i,x}\mathbf{m}_{i,y} - c_{j,x}\mathbf{m}_{j,y} - c_{i,y}\mathbf{m}_{i,x} + c_{j,y}\mathbf{m}_{j,x}) - ... \\ &... - \sin(\theta)(c_{i,y}\mathbf{m}_{i,y} - c_{j,y}\mathbf{m}_{j,y} + c_{i,x}\mathbf{m}_{i,x} - c_{j,x}\mathbf{m}_{j,x})\Big] + ... \\ &...+\Big[F_x(\mathbf{m}_{i,y} - \sin(\theta)c_{i,x} - \cos(\theta)c_{i,y}) - (F_y + mg)(\mathbf{m}_{i,x} - \cos(\theta)c_{i,x} + \sin(\theta)c_{i,y})\Big](\sin(\theta)c_{j,x} + \cos(\theta)c_{j,y}) + ... \\ &...+\Big[(F_y + mg)(\mathbf{m}_{j,x} - \cos(\theta)c_{j,x} + \sin(\theta)c_{j,y}) - F_x(\mathbf{m}_{j,y} - \sin(\theta)c_{j,x} - \cos(\theta)c_{j,y})\Big](\sin(\theta)c_{i,x} + \cos(\theta)c_{i,y}) \end{aligned} \tag{179}$$

$$a_3 = (F_y + mg)\Big[(\cos(\theta)(c_{i,x} - c_{j,x}) - \sin(\theta)(c_{i,y} - c_{j,y})\Big] + F_x\Big[(\sin(\theta)(c_{i,x} - c_{j,x}) + \cos(\theta)(c_{i,y} - c_{j,y})\Big] \tag{180}$$

$$\begin{aligned} a_4 = &\Big[(\mathbf{m}_{j,x} - \mathbf{m}_{i,x}) - \cos(\theta)(c_{j,x} - c_{i,x}) + \sin(\theta)(c_{j,y} - c_{i,y})\Big] M + ... \\ &... + F_x\Big[\cos(\theta)(c_{i,x}\mathbf{m}_{i,y} - c_{j,x}\mathbf{m}_{j,y} - c_{i,y}\mathbf{m}_{i,x} + c_{j,y}\mathbf{m}_{j,x}) - ... \\ &... - \sin(\theta)(c_{i,y}\mathbf{m}_{i,y} - c_{j,y}\mathbf{m}_{j,y} + c_{i,x}\mathbf{m}_{i,x} - c_{j,x}\mathbf{m}_{j,x})\Big] - ... \\ &...-\Big[F_x(\mathbf{m}_{i,y} - \sin(\theta)c_{i,x} - \cos(\theta)c_{i,y}) - (F_y + mg)(\mathbf{m}_{i,x} - \cos(\theta)c_{i,x} + \sin(\theta)c_{i,y})\Big](\cos(\theta)c_{j,x} - \sin(\theta)c_{j,y}) - ... \\ &...-\Big[(F_y + mg)(\mathbf{m}_{j,x} - \cos(\theta)c_{j,x} + \sin(\theta)c_{j,y}) - F_x(\mathbf{m}_{j,y} - \sin(\theta)c_{j,x} - \cos(\theta)c_{j,y})\Big](\cos(\theta)c_{i,x} - \sin(\theta)c_{i,y}) \end{aligned} \tag{181}$$

$$a_5 = F_x(\cos(\theta)(c_{j,x} - c_{i,x}) - \sin(\theta)(c_{j,y} - c_{i,y})) \tag{182}$$

$$\begin{aligned} a_6 = &(\mathbf{m}_{i,x} - \cos(\theta)c_{i,x} + \sin(\theta)c_{i,y})(\mathbf{m}_{j,y} - \sin(\theta)c_{j,x} - \cos(\theta)c_{j,y})M - ... \\ &... - (\mathbf{m}_{i,y} - \sin(\theta)c_{i,x} - \cos(\theta)c_{i,y})(\mathbf{m}_{j,x} - \cos(\theta)c_{j,x} + \sin(\theta)c_{j,y})M + ... \\ &... + \Big[F_x(\mathbf{m}_{i,y} - \sin(\theta)c_{i,x} - \cos(\theta)c_{i,y}) - (F_y + mg)(\mathbf{m}_{i,x} - \cos(\theta)c_{i,x} + \sin(\theta)c_{i,y})\Big] \cdot ... \\ &... \cdot \Big[\cos(\theta)(c_{j,x}\mathbf{m}_{j,y} - c_{j,y}\mathbf{m}_{j,x}) - \sin(\theta)(c_{j,y}\mathbf{m}_{j,y} + c_{j,x}\mathbf{m}_{j,x})\Big] - ... \\ &... - \Big[F_x(\mathbf{m}_{j,y} - \sin(\theta)c_{j,x} - \cos(\theta)c_{j,y}) - (F_y + mg)(\mathbf{m}_{j,x} - \cos(\theta)c_{j,x} + \sin(\theta)c_{j,y})\Big] \cdot ... \\ &... \cdot \Big[\cos(\theta)(c_{i,x}\mathbf{m}_{i,y} - c_{i,y}\mathbf{m}_{i,x}) - \sin(\theta)(c_{i,y}\mathbf{m}_{i,y} + c_{i,x}\mathbf{m}_{i,x})\Big]. \end{aligned} \tag{183}$$

Because these coefficients are fairly complicated it is not trivial to plot this workspace boundary. However, if the manipulator is considered at a known constant orientation, each a_i becomes a constant and the boundary equation reduces to a relatively simple polynomial in x and y. Thus it is possible to get a good representation of the workspace boundary by plotting multiple constant orientation boundary curves, essentially viewing the workspace boundary one "slice" at a time. This will be demonstrated using the example in Section 5.5.2.3.

Special Case:

If instead we would like to generate the static equilibrium workspace ($NW_{req} = (F_x,\, F_y,\, M)^T = (0,\, 0,\, 0)^T$), the expression for the workspace boundary becomes even simpler:

$$a_1 = \sin(\theta)(c_{j,x} - c_{i,x}) + \cos(\theta)(c_{j,y} - c_{i,y}) \tag{184}$$

$$\begin{aligned} a_2 = &\Big[\sin(\theta)(c_{i,y}\mathbf{m}_{i,y} - c_{j,y}\mathbf{m}_{j,y} + c_{i,x}\mathbf{m}_{i,x} - c_{j,x}\mathbf{m}_{j,x}) - \cos(\theta)(c_{i,x}\mathbf{m}_{i,y} - c_{j,x}\mathbf{m}_{j,y} - c_{i,y}\mathbf{m}_{i,x} + c_{j,y}\mathbf{m}_{j,x})\Big] - ... \\ &... - (\mathbf{m}_{i,x} - \cos(\theta)c_{i,x} + \sin(\theta)c_{i,y})(\sin(\theta)c_{j,x} + \cos(\theta)c_{j,y}) + ... \\ &... + (\mathbf{m}_{j,x} - \cos(\theta)c_{j,x} + \sin(\theta)c_{j,y})(\sin(\theta)c_{i,x} + \cos(\theta)c_{i,y}) \end{aligned} \tag{185}$$

$$a_3 = \Big[(\cos(\theta)(c_{i,x} - c_{j,x}) - \sin(\theta)(c_{i,y} - c_{j,y})\Big] \tag{186}$$

$$\begin{aligned} a_4 = &(\mathbf{m}_{i,x} - \cos(\theta)c_{i,x} + \sin(\theta)c_{i,y})(\cos(\theta)c_{j,x} - \sin(\theta)c_{j,y}) - ... \\ &... - (\mathbf{m}_{j,x} - \cos(\theta)c_{j,x} + \sin(\theta)c_{j,y})(\cos(\theta)c_{i,x} - \sin(\theta)c_{i,y}) \end{aligned} \tag{187}$$

$$a_5 = 0 \tag{188}$$

$$\begin{aligned} a_6 = &-(\mathbf{m}_{i,x} - \cos(\theta)c_{i,x} + \sin(\theta)c_{i,y})\Big[\cos(\theta)(c_{j,x}\mathbf{m}_{j,y} - c_{j,y}\mathbf{m}_{j,x}) - \sin(\theta)(c_{j,y}\mathbf{m}_{j,y} + c_{j,x}\mathbf{m}_{j,x})\Big] + ... \\ &... + (\mathbf{m}_{j,x} - \cos(\theta)c_{j,x} + \sin(\theta)c_{j,y})\Big[\cos(\theta)(c_{i,x}\mathbf{m}_{i,y} - c_{i,y}\mathbf{m}_{i,x}) - \sin(\theta)(c_{i,y}\mathbf{m}_{i,y} + c_{i,x}\mathbf{m}_{i,x})\Big]. \end{aligned} \tag{189}$$

Thus for the static equilibrium workspace the workspace boundary equation can be put in the form $y = g(x, \theta)$, where

$$y = g(x, \theta) = -\frac{a_1 x^2 + a_2 x + a_6}{a_3 x + a_4}. \tag{190}$$

Again if we consider a constant orientation of the end-effector each a_i becomes a constant and the constant-orientation boundary has a polynomial form. Thus the lower boundaries of the static equilibrium workspace can be plotted quite easily for constant orientation of a planar cable robot.

5.5.2.2 Upper WFW Boundaries

Using (163), an upper boundary of a planar cable robot has the form:

$$\det\left[\begin{array}{cc} \$_i^w & \$_j^w \end{array} \quad \left(\overline{v} - m\overline{g} - \sum_{\$_k^w \in E} t_{k,max}\$_k^w\right)\right] = 0. \tag{191}$$

Note that this is the same form as the lower boundaries, but for the lower boundaries $E = \{\emptyset\}$, while in this case $E \neq \{\emptyset\}$. Let $SP = \{\$_\alpha^w, \$_\beta^w, ...\}$. Then using the previously defined notation the boundary equation becomes:

$$det\begin{bmatrix} u_{i,x} & u_{j,x} & F_x + t_{\alpha,max}u_{\alpha,x} + t_{\beta,max}u_{\beta,x} + ... \\ u_{i,y} & u_{j,y} & F_y + mg + t_{\alpha,max}u_{\alpha,y} + t_{\beta,max}u_{\beta,y} + ... \\ (\boldsymbol{R}(\theta)\overline{c}_i) \times \overline{u}_i & (\boldsymbol{R}(\theta)\overline{c}_j) \times \overline{u}_j & M + t_{\alpha,max}\left(\boldsymbol{R}(\theta)\overline{c}_\alpha\right) \times \overline{u}_\alpha + t_{\beta,max}\left(\boldsymbol{R}(\theta)\overline{c}_\beta\right) \times \overline{u}_\beta + ... \end{bmatrix} = 0. \tag{192}$$

Evaluation of (192) results in an expression similar in form to (169), and substitutions can be made for $\overline{u}_i$, $\overline{u}_j$, $\overline{u}_\alpha$, $\overline{u}_\beta$, etc. in terms of $\overline{\ell}_i$, $\overline{\ell}_j$, $\overline{\ell}_\alpha$, $\overline{\ell}_\beta$, etc.. However, unlike (169), the factor of $\frac{1}{\|\overline{\ell}_i\|\cdot\|\overline{\ell}_j\|\cdot\|\overline{\ell}_\alpha\|\cdot\|\overline{\ell}_\beta\|\cdot\ldots}$ is not common to all terms and therefore cannot be canceled. Thus the resulting boundary equation will no longer have polynomial form and will include many square-root terms.

Because of this amount of complexity, it does not appear useful to fully detail the analytical form of the upper WFW boundaries, as the resulting equations will not provide much insight into the geometry of the boundaries and will likely need to be plotted using numerical techniques. However, for both underconstrained and fully-constrained manipulators, if the upper tension limits are relatively high then the lower WFW boundaries determine the majority of the geometry of the WFW. Thus the lower workspace boundaries found previously are the key boundaries to consider.

5.5.2.3 Example

As an example, let us examine the Wrench-Feasible Workspace of the manipulator shown in Figure 35. The pose of the manipulator is $(x, y, \theta)^T$, where the pose of the manipulator as shown in Figure 35 is $(0, 0, 0)^T$. Motor 1 is located at $(-1.5\,\mathrm{m}, 2\,\mathrm{m})^T$, motor 2 is located at $(0, 2\,\mathrm{m})^T$ and motor 3 is located at $(1.5\,\mathrm{m}, 2\,\mathrm{m})^T$. The vectors from the center of gravity to the cable attachment points are $\overline{c}_1 = (-0.3\,\mathrm{m}, 0)^T$, $\overline{c}_2 = (0, 0.05\,\mathrm{m})^T$ and $\overline{c}_3 = (0.3\,\mathrm{m}, 0)^T$. The weight of the end-effector is 20 N and the cables are assumed to have very high upper tension limits. We will now generate the WFW numerically for several choices of NW_{req} and compare the results to the analytically determined WFW boundaries.

Using MATLAB, the WFW is first calculated for $NW_{req} = (0, 0, 0)^T$ (i.e. the static equilibrium workspace) using a numerical approach, where the taskspace is discretized and searched exhaustively. The resulting discretized workspace is shown in Figure 36. Note that due to the symmetry of the manipulator the workspace

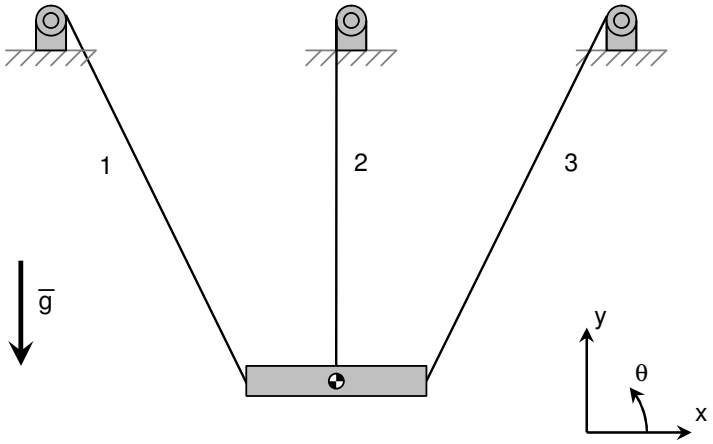

Figure 35: Example manipulator (note: not drawn to scale).

is symmetric. The MATLAB code for generating this workspace and each of the following example workspaces is included in Appendix C.

Now let us change NW_{req} to a polyhedral with two vertices (i.e. a line segment). Let the two vertices be the origin and a pure force of 5 N to the right. Then $NW_{req} = conv\{(0,0,0)^T, (5\,\mathrm{N}, 0, 0)^T\}$. The resulting WFW is shown in Figure 37. Note that because the origin is included in NW_{req} the WFW is a subset of the static equilibrium workspace.

Let us also consider a case where the vertices are the origin and a pure moment of $1\frac{\mathrm{N}}{\mathrm{m}}$. Then $NW_{req} = conv\{(0,0,0)^T, (0,0,1\frac{\mathrm{N}}{\mathrm{m}})^T\}$. The resulting WFW is shown in Figure 38. Note again that because the origin is included in NW_{req} the WFW is a subset of the Static Equilibrium Workspace.

Now let us compare the numerical results with analytical results for the workspace boundaries. In the first case, where $NW_{req} = (0,0,0)^T$, there is only one vertex to consider. Because the upper tension limits of the cables are very high, only the lower workspace boundaries will be considered. For simplicity we will only consider a constant orientation "slice" of the workspace at $\theta = \frac{\pi}{8}$. Using (177) through (183),

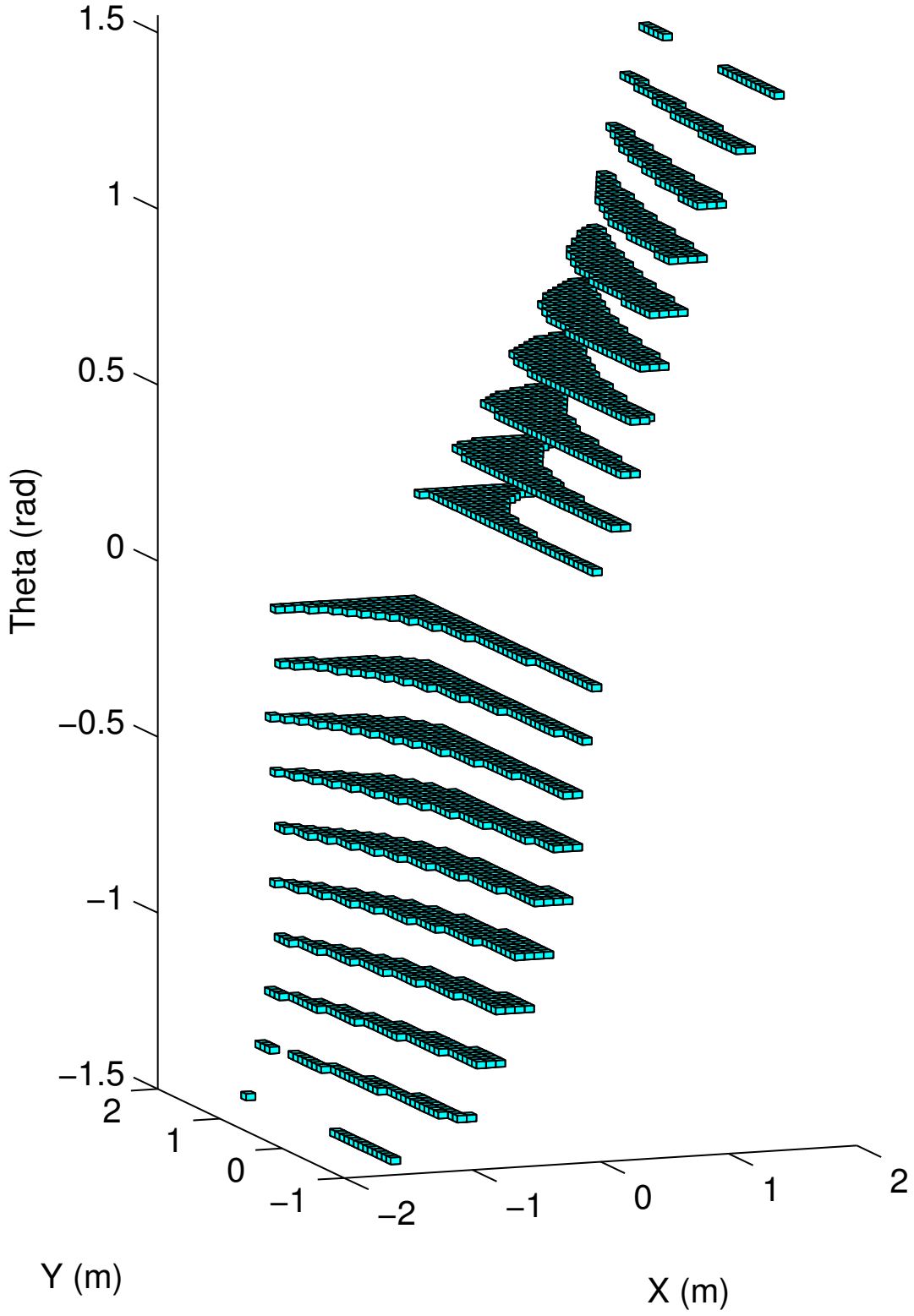

Figure 36: Numerically determined Static Equilibrium Workspace for an example manipulator.

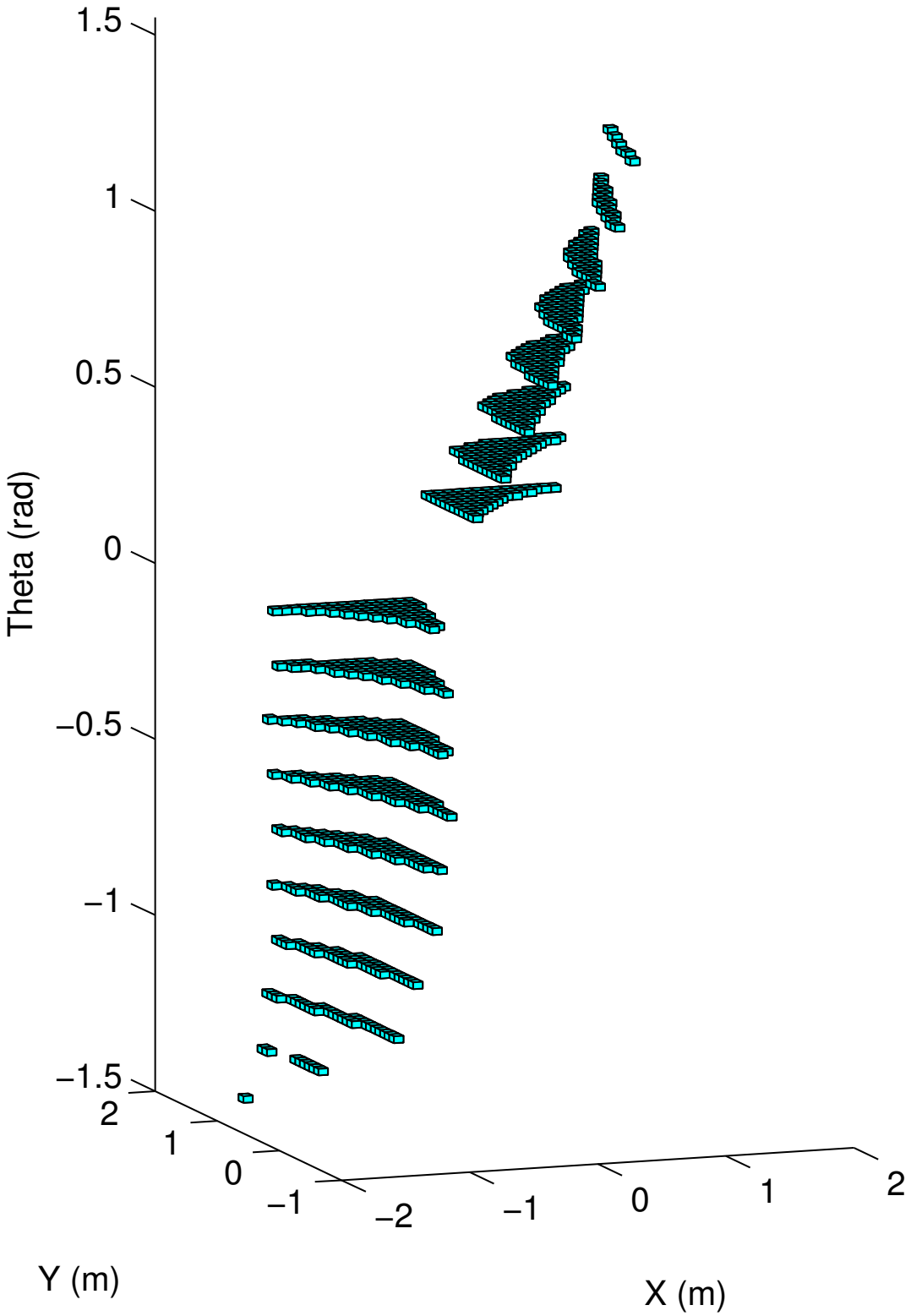

Figure 37: Numerically determined Wrench-Feasible Workspace for an example manipulator - $NW_{req} = conv\{(0,0,0)^T, (5\text{N},0,0)^T\}$.

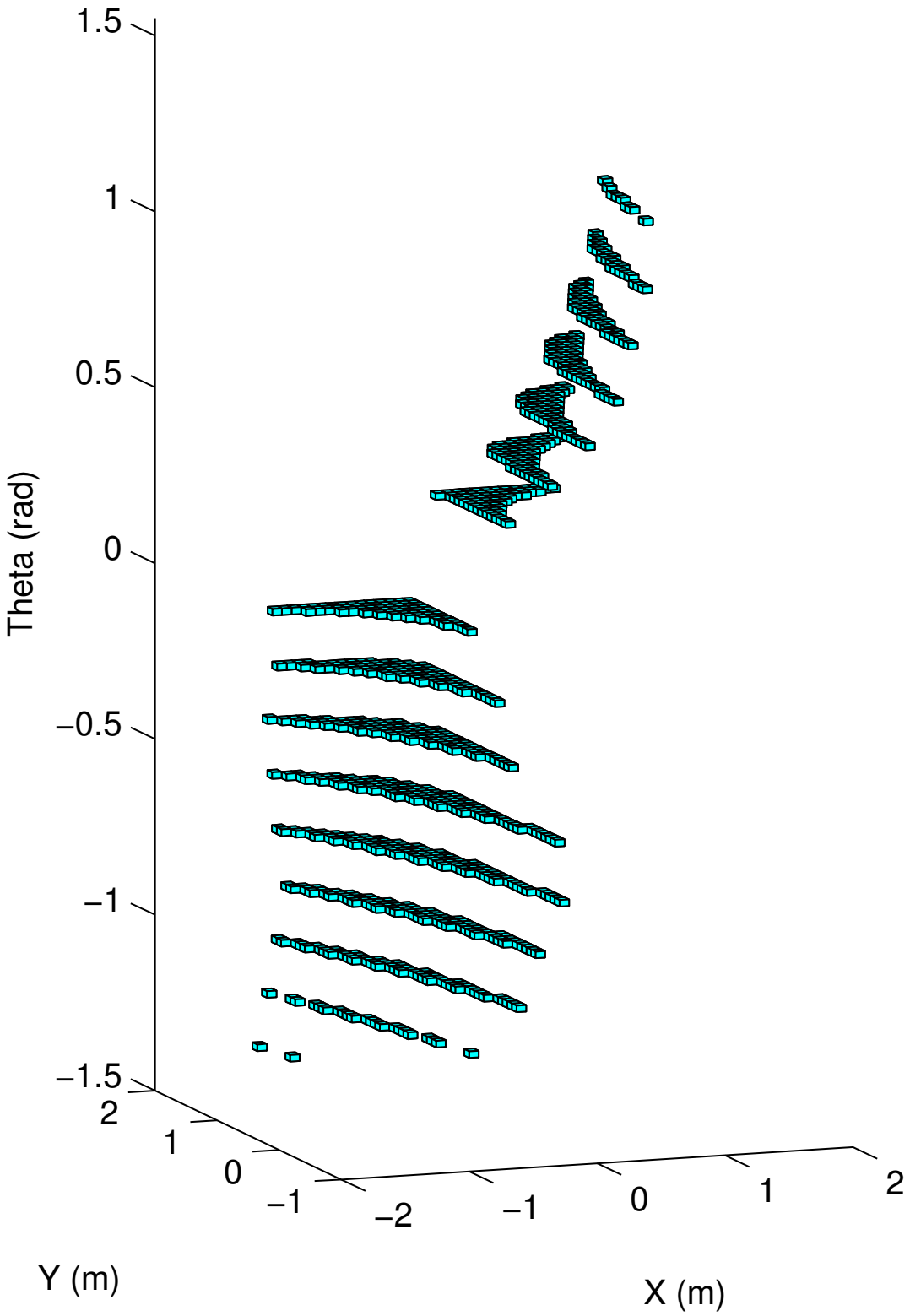

Figure 38: Numerically determined Wrench-Feasible Workspace for an example manipulator - $NW_{req} = conv\{(0,0,0)^T, (0,0,1\frac{\mathrm{N}}{\mathrm{m}})^T\}$.

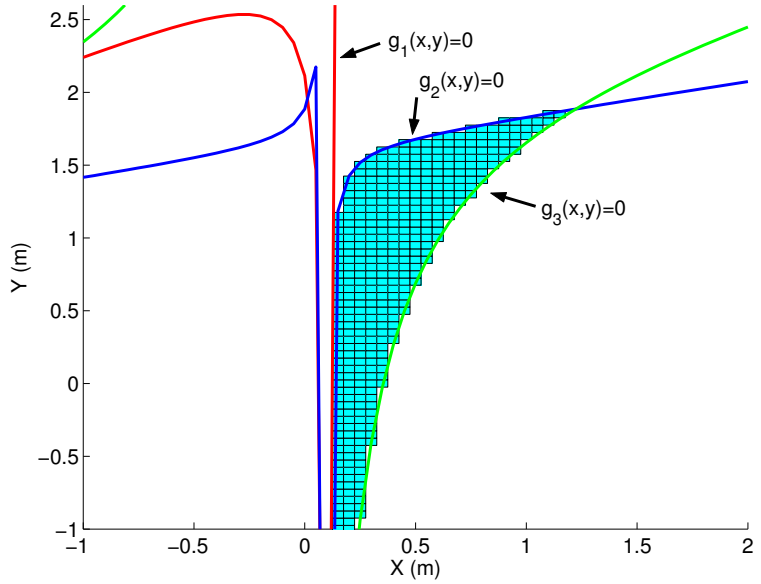

Figure 39: Numerically determined WFW and analytically determined WFW boundaries for an example manipulator at a constant orientation of $\theta = \frac{\pi}{8}$ and $NW_{req} = \{(0,0,0)^T\}$.

the three boundary equations are:

$$\begin{aligned} g_1(x,y) &= 3.22x^2 + 14.851x - 5.161xy + 0.574y - 1.214 = 0 \\ g_2(x,y) &= 1.372x^2 + 9.494x - 5.926xy + 0.574y - 1.082 = 0 \\ g_3(x,y) &= 4.592x^2 + 22.173x - 11.087xy - 8.423 = 0 \end{aligned}$$

where $g_1(x,y) = 0$ is the boundary equation corresponding to contact between NW_{req} and the lower side of NW_{avail} spanned by $\$_1^w$ and $\$_2^w$, $g_2(x,y) = 0$ is the boundary equation corresponding to contact between NW_{req} and the lower side of NW_{avail} spanned by $\$_2^w$ and $\$_3^w$ and $g_3(x,y) = 0$ is the boundary equation corresponding to contact between NW_{req} and the lower side of NW_{avail} spanned by $\$_1^w$ and $\$_3^w$. The boundary equations are plotted with the discretized workspace in Figure 39. Note that the analytically determined boundaries agree exactly with the bounds of the numerically determined workspace.

Let us now consider the second case, where $NW_{req} = conv\{(0,0,0)^T, (5\,\mathrm{N}, 0, 0)^T\}$. In this case there are two vertices to consider, thus we must form six boundary

equations – three for each vertex. Because one of the vertices is the origin, which was the vertex used in the previous case, the first three equations are $g_1(x, y) = 0$, $g_2(x, y) = 0$ and $g_3(x, y) = 0$ as given in the previous case. Using (177) through (183), the three additional boundary equations are:

$$\begin{aligned} g_4(x,y) &= 3.22x^2 + 16.461x - 5.966xy - 5.373y + 1.29y^2 + 5.479 = 0 \\ g_5(x,y) &= 1.372x^2 + 10.18x - 6.269xy - 4.416y + 1.481y^2 + 3.012 = 0 \\ g_6(x,y) &= 4.592x^2 + 24.469x - 12.235xy - 11.087y + 2.772y^2 + 2.466 = 0 \end{aligned}$$

where $g_4(x, y) = 0$ is the boundary equation corresponding to contact between $(5\,\mathrm{N}, 0, 0)^T$ and the lower side of NW_{avail} spanned by $\$_1^w$ and $\$_2^w$, $g_5(x, y) = 0$ is the boundary equation corresponding to contact between $(5\,\mathrm{N}, 0, 0)^T$ and the lower side of NW_{avail} spanned by $\$_2^w$ and $\$_3^w$ and $g_6(x, y) = 0$ is the boundary equation corresponding to contact between $(5\,\mathrm{N}, 0, 0)^T$ and the lower side of NW_{avail} spanned by $\$_1^w$ and $\$_3^w$. The boundary equations are plotted with the discretized workspace in Figure 40. Note that the analytically determined boundaries again agree exactly with the bounds of the numerically determined workspace.

Note that because the third case (where $NW_{req} = conv\{(0, 0, 0)^T, (0, 0, 1\frac{\mathrm{N}}{\mathrm{m}})^T\}$) also has two vertices, six boundary equations are necessary for this case. However, because that case is very similar to the second case ($NW_{req} = conv\{(0, 0, 0)^T, (5\mathrm{m}, 0, 0)^T\}$) the resulting plot of the boundary equations for the third case is very similar to the one shown for the second case and thus is not included here.

5.5.3 Wrench-Feasible Workspace of Spatial Cable Robots

The formulation of the WFW boundaries for spatial cable robots is quite similar to that of planar cable robots. Using (163), each boundary equation is of the form:

$$\det\left[\begin{array}{ccccc} \$_a^w & \$_b^w & \$_c^w & \$_d^w & \$_e^w \end{array} \left(\overline{v} - m\overline{g} - \sum_{\$_j^w \in E} t_{j,max}\$_j^w\right)\right] = 0 \qquad (193)$$

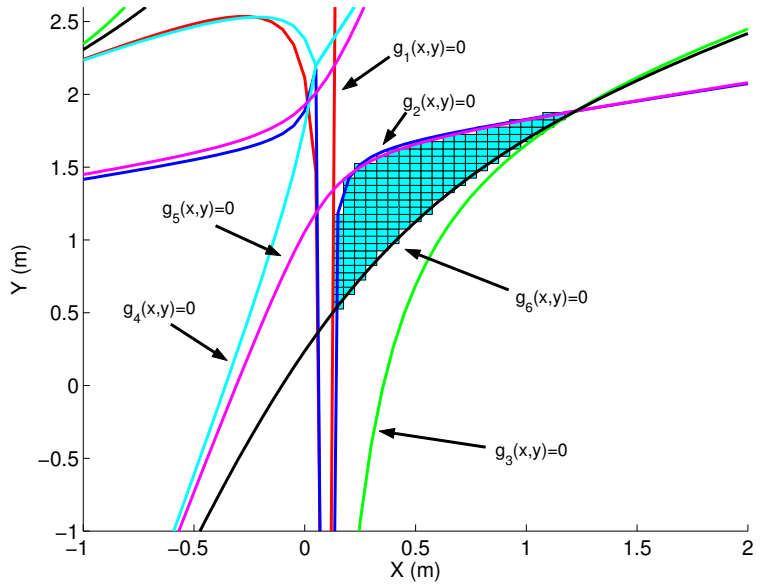

Figure 40: Numerically determined WFW and analytically determined WFW boundaries for an example manipulator at a constant orientation of $\theta = \frac{\pi}{8}$ and $NW_{req} = conv\{(0,0,0)^T, (5\text{m},0,0)^T\}$.

where $\{\$_a^w, \$_b^w, \ldots, \$_e^w\} = SP$. Note that because the manipulator is spatial, this is a 6×6 matrix (i.e. SP always contains 5 wrenches). Also, note that each wrench $\$^w$ is a function of both the position of the end-effector (x, y, z) and of the orientation of the end-effector, expressed here in Euler angles (ψ, θ, ϕ).

It would be desirable to expand (193) in terms of known system parameters and the pose of the manipulator $(x, y, z, \psi, \theta, \phi)$ similar to what was done for (5.5.2.1). However, even in the simpler case of forming lower boundaries, evaluating (193) results in a 5^{th} order polynomial equation in x, y and z, where each of the 56 polynomial coefficients is a function of ψ, θ and ϕ:

$$a_1x^5 + a_2x^4y + a_3x^4z + \ldots + a_{53}xz^4 + a_{54}yz^4 + a_{55}z^5 + a_{56} = 0. \qquad (194)$$

Thus even for the simple case of the lower workspace boundaries the resulting polynomial expressions are very complicated and thus are not detailed here. However, if desired it would be possible to use a symbolic manipulation program to perform the calculation of the coefficients. If that were performed, the easiest method of

representing the boundaries would likely be examining a constant orientation of the end-effector and plotting "slices" of the wokspace by also holding one of the position variables constant and plotting 2-D workspace boundary curves. Keep in mind, however, that if there are p cables and w vertices of NW_{req}, then $(p \cdot w)$ boundary curves must be plotted.

As was the case for planar cable robots, the upper WFW boundaries for spatial cable robots are more complicated, due to the inclusion of $\| \ell_i \|$ terms. As a result it is unlikely that forming these boundaries analytically will be useful. Again, if the upper tension limits of the cables are very high, the geometry of the WFW will be largely determined by the lower workspace boundaries.

5.5.4 Discussion

The Wrench-Feasible Workspace analysis presented here developed a method for forming the WFW boundaries for planar and spatial cable robots using a polyhedral NW_{req}. Because NW_{req} is allowed to be a polyhedron or collection of polyhedra, this allows for a wide variety of geometries to be chosen for NW_{req}. However, it was shown that the number of workspace boundaries that must be calculated increases with the number of vertices of NW_{req}, thus it is advantageous to keep the complexity of NW_{req} lower so as to reduce the number of boundary equations that must be formed.

The method for forming workspace boundaries for a polyhedral NW_{req} can also be extended to the case of point-mass cable robots. Specifically, (167) and (191) can be used to form the lower and upper boundaries of such a WFW. By allowing a polyhedral NW_{req}, this allows the WFW to be calculated for geometries of NW_{req} other than a sphere. Note that even with a polyhedral NW_{req} many of the workspace properties enumerated in Section 5.4.2 and [60] for point-mass cable robot Wrench-Feasible Workspaces will still hold, such as having planar lower workspace boundaries.

For planar cable robots the complete analytical form of the lower WFW

boundaries was calculated. The determinant form of the upper workspace boundaries was given, but because these boundaries are much more complicated their complete analytical form was not calculated. However, if the upper tension limits in the cables is very high the lower boundaries will largely determine the workspace geometry. An example manipulator was considered and the WFW was calculated for a few different choices of NW_{req}. Analytically calculated workspace boundaries were then compared to the numerically determined workspaces and were found to agree exactly with each other.

For spatial cable robots the determinant form of the WFW boundaries is the same as for the planar case. Due to the increased complexity of evaluating the determinant of the 6×6 matrix the analytical form of the workspace boundaries was not calculated. **However, we did find that the form of the lower WFW boundary equations is a 5^{th} order polynomial in x, y and z with coefficients that are functions of the end-effector orientation. Like the planar case, the upper WFW boundaries are much more complicated and thus the analytical expressions for the boundaries are not likely to be useful.** Again, if the upper tension limits in the cables are very high the lower boundaries will largely determine the workspace geometry. If the upper tension limits are not very high in either the planar case or the spatial case, then the most efficient method of forming the WFW will be numerically. However, despite the complexity of the expressions for the WFW boundaries of general cable robots, we now have a much better understanding of the nature of the boundaries and their degree of complexity.

For both the planar and spatial case it is possible to examine the analytical expressions for the lower workspace boundaries and determine how the workspace geometry is affected by the varying of different manipulator parameters, similar to what was done for point-mass manipulators in [60]. This would allow design guidelines to be synthesized for obtaining a WFW of a

desired geometry. Unfortunately, because the workspace boundary equations are so complicated it is not easy to obtain these workspace properties directly from the equations. Instead, it is likely necessary to plot a large number of workspaces for various sets of design parameters and glean the workspace geometry trends from the results. Such an analysis is beyond the scope of this thesis and is therefore left as a topic for future research.

5.6 Specified Robustness Workspace

Given the results of the disturbance robustness analysis, we have a measure $\mathcal{R}$ that describes the robustness of the manipulator to external disturbances *at that pose*. For a given application, the manipulator might be required to maintain a certain required amount of disturbance robustness throughout its motions. Because the robustness of the manipulator is pose-dependent, it is of interest to determine the set of all poses where the manipulator meets or exceeds this specified robustness value.

Definition: The *Specified Robustness Workspace*, or SRW, is defined as the set of all poses where $\mathcal{R}(P)$ is greater than or equal to a required robustness value $\mathcal{R}_{req}$.

Note that $\mathcal{R}$ is written explicitly as a function of the pose P to emphasize that the robustness value is pose-dependent. It is assumed for the remainder of this discussion that $\mathcal{R}_{req}$ is a constant and is thus not pose-dependent.

5.6.1 Equivalent Required Net Wrench Set

The calculation of the SRW can actually be performed analytically using the same approach used for the Wrench-Feasible Workspace. The approach is most easily understood by considering the intermediate space. Consider a single pose of a manipulator. If we then find the value of the robustness measure, $\mathcal{R}$, for this pose then the smallest static disturbance wrench that causes a cable to go slack has magnitude

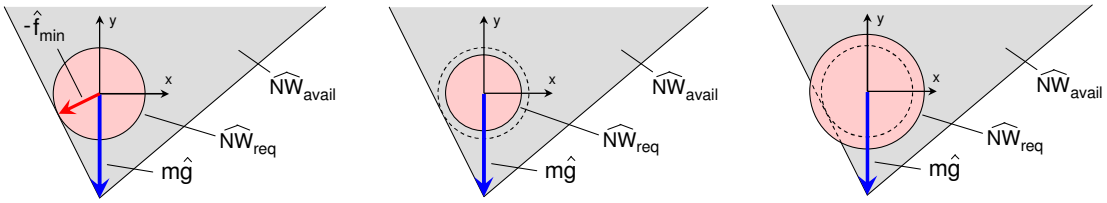

(a) $\mathcal{R} = \mathcal{R}_{req}$. (b) $\mathcal{R} > \mathcal{R}_{req}$. (c) $\mathcal{R} < \mathcal{R}_{req}$.

Figure 41: Three cases of $\widehat{NW}_{req,eq} = \{\hat{f} \mid \| \hat{f} \| \leq mg\mathcal{R}_{req}\}$.

$mg\mathcal{R}$.

Let us map NW_{avail} to the intermediate space, producing $\widehat{NW}_{avail}$. Let us then construct a generalized Required Net Wrench Set (i.e. a Required Net Wrench Set mapped to the intermediate space) as the set of all generalized forces, $\hat{f}$, such that $\| \hat{f} \| \leq mg\mathcal{R}$ (i.e. $\widehat{NW}_{req} = \{\hat{f} \ : \| \hat{f} \| \leq mg\mathcal{R}_{req}\}$)[7]. Then $\widehat{NW}_{req}$ is a circle, sphere or hypersphere (depending on the dimension of the task space) in the intermediate space centered at the origin with radius $mg\mathcal{R}$. Let the smallest static disturbance wrench be $\$^{w}_{min}$ and let this wrench be mapped to $\hat{f}_{min}$ in the intermediate space. Becasue $\| \hat{f}_{min} \| = mg\mathcal{R}$, $\hat{f}_{min} \in \widehat{NW}_{req}$ and $-\hat{f}_{min} \in \widehat{NW}_{req}$. Because $\hat{f}_{min}$ is in $\hat{C}$, the set of critical generalized forces, $-\hat{f}_{min}$ must be on one of the lower sides of NW_{avail}. Thus $\widehat{NW}_{req}$ is tangent to NW_{avail}, as shown in Figure 41(a) for a planar, 2-cable point-mass cable robot.

Now let us instead choose the radius of $\widehat{NW}_{req,eq}$ to be $mg\mathcal{R}_{req}$ (i.e. $\widehat{NW}_{req,eq} = \{\hat{f} \ : \| \hat{f} \| \leq mg\mathcal{R}_{req}\}$). If $\mathcal{R} \geq \mathcal{R}_{req}$ then the pose is wrench-feasible, as shown in Figure 41(b), and the pose is in the SRW (because the robustness of the pose exceeds the required robustness). If $\mathcal{R} < \mathcal{R}_{req}$ then the pose is not wrench-feasible, as shown in Figure 41(c), and the pose is not in the SRW (because the robustness of the pose is less than the required robustness). **Thus for $\widehat{NW}_{req,eq} = \{\hat{f} \ : \| \hat{f} \| \leq mg\mathcal{R}_{req}\}$), a pose**

[7]Note that if NW_{avail} and NW_{req} are mapped to the intermediate space the condition for wrench-feasibility simply becomes $NW_{req} \subseteq NW_{avail}$

is wrench-feasible if and only if the pose meets the specified robustness criteria (and is thus in the SRW).

This NW_{req} is termed the *Equivalent Required Net Wrench Set*, denoted $NW_{req,eq}$. Note that the $NW_{req,eq}$ is a sphere (or hypersphere) only in the intermediate space. In the task space this set is an ellipsoid (or hyper-ellipsoid). In the task space $NW_{req,eq}$ is given by:

$$NW_{req,eq} = \left\{ \$^w = \begin{pmatrix} \overline{F} \\ \overline{M} \end{pmatrix} : F_x^2 + F_y^2 + F_z^2 + \frac{M_x^2}{\rho_x^2} + \frac{M_y^2}{\rho_y^2} + \frac{M_z^2}{\rho_z^2} \leq (mg\mathcal{R}_{req})^2 \right\}. \quad (195)$$

Or more simply, in the intermediate space:

$$\widehat{NW}_{req,eq} = \left\{ \hat{f} \ : \| \hat{f} \| \leq mg\mathcal{R}_{req} \right\}. \quad (196)$$

As a result, the workspace generation techniques developed earlier can be applied to a manipulator using $NW_{req} = NW_{req,eq}$ and no upper tension limits on the cables (i.e. only the "lower" boundaries are needed) to produce the SRW. The procedure is as follows: 1) specify $\mathcal{R}_{req}$, 2) define $NW_{req,eq}$ according to (195), and 3) calculate the WFW for $NW_{req,eq}$. The result is the SRW.

5.6.2 Modification

Alternatively, the upper tension limits can be used in addition to the lower tension limits to generate a secondary workspace. Then the combination of the lower and upper workspace boundaries ensure that the manipulator can resist a static wrench with a specified acceleration energy norm without a cable going slack or a cable being overtensioned.

5.7 Other Applications

The Available Net Wrench Set and the techniques developed for generating the Wrench-Feasible Workspace can be used in several other applications. Sections 5.7.1

and 5.7.2 discuss other applications of the WFW generation techniques and Sections 5.7.3 and 5.7.4 discuss other applications of the Available Net Wrench Set.

5.7.1 Force-Only Wrench-Feasible Workspace

In some cases a planar or spatial manipulator may be required to exert a certain set of forces without consideration for the associated moments. That is, the manipulator must exert the desired force while the corresponding moment it applies does not matter. This kind of situation may occur if a manipulator is used to position an object that has constrained orientation. In this case, the standard approach for generating the WFW cannot be used, as there is no NW_{req} (with forces and moments) corresponding to such task requirements.

Instead, a modification can be made to the workspace generation approach that allows such a workspace to be generated. Recall that NW_{avail} is the set of wrenches that can be exerted by the manipulator: $NW_{avail} = \{\$^w : \$^w = a_1 t_{1,max} \$_1^w + a_2 t_{2,max} \$_2^w + \ ... \ + a_p t_{p,max} \$_p^w + m\overline{g};\ \ 0 \leq a_i \leq 1\}$. Because we are only interested in the forces that can be exerted, define the *Available Force Set*, F_{avail} as $F_{avail} = \{\overline{F} : \overline{F} = a_1 t_{1,max} \overline{u}_1 + a_2 t_{2,max} \overline{u}_2 + \ ... \ + a_p t_{p,max} \overline{u}_p + m\overline{g};\ \ 0 \leq a_i \leq 1\}$. This set is the set of all forces that can be exerted by the manipulator. Note the similarity between this set and NW_{avail} for point-mass cable robots. However, unlike the point-mass case, $\overline{u}_i$ is both a function of the position and orientation of the manipulator:

$$\overline{u}_i = \frac{\overline{\ell}_i}{\| \overline{\ell}_i \|} \tag{197}$$

where

$$\overline{\ell}_i = \overline{\mathbf{m}}_i - \left[\begin{pmatrix} x \\ y \\ z \end{pmatrix} + \boldsymbol{R}(\psi, \theta, \phi) \overline{c}_i \right]. \tag{198}$$

However, if the end-effector is considered at a constant orientation, a new motor

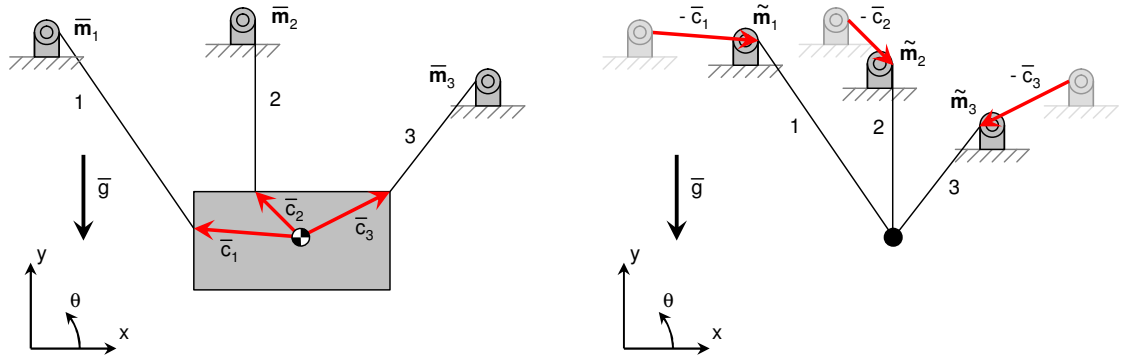

(a) Example planar cable robot.

(b) Equivalent point-mass cable robot.

Figure 42: Force-only WFW example.

mount location $\tilde{\mathbf{m}}_i$ (as shown in Figure 42(b)) can be defined as:

$$\tilde{\mathbf{m}}_i = \overline{\mathbf{m}}_i - \boldsymbol{R}(\psi, \theta, \phi)\overline{c}_i. \tag{199}$$

Then (198) can be rewritten as:

$$\overline{\ell}_i = \tilde{\mathbf{m}}_i - \begin{pmatrix} x \\ y \\ z \end{pmatrix} \tag{200}$$

which is identical to the case of a point mass cable robot with motors located at the new positions given by $\tilde{\mathbf{m}}_i$. Thus for a planar or spatial cable robot, if only the forces generated by the end-effector are of interest, an *equivalent cable robot* can be created, with motor positions given by $\tilde{\mathbf{m}}_i$, such that the Wrench-Feasible Workspace of the equivalent cable robot and the required set of forces for the planar or spatial cable robot (expressed as NW_{req} for the point-mass manipulator) is exactly equal to the Force-Only Wrench-Feasible Workspace of the corresponding planar or spatial cable robot at the considered orientation.

As an example, consider the example planar cable robot in Figure 42(a). If we wish to find the Force-Only Wrench-Feasible Workspace of the manipulator at this orientation, we must construct the equivalent point-mass cable robot. For each motor

we construct a new motor location $\tilde{\mathbf{m}}_i = \overline{\mathbf{m}}_i - \boldsymbol{R}(\theta)\overline{c}_i$. In the pose shown here $\theta = 0$, thus $\boldsymbol{R}(\theta)\overline{c}_i = \overline{c}_i$. The equivalent point-mass cable robot for this orientation is shown in Figure 42(b). Thus the Force-Only Wrench-Feasible Workspace of this manipulator at this orientation can be determined in the same manner that the WFW would be calculated for the point-mass cable robot shown in Figure 42(b).

This approach is very advantageous, because it allows us to utilize the workspace generation approaches developed for point-mass cable robots. In fact, all of the properties and workspace geometry trends found for point-mass cable robots apply to this situation as well. Note that some caution must be taken in using this approach. If wrenches are being applied *to* the manipulator (rather than being applied by the manipulator), a large moment applied to the manipulator could possibly cause cable tension limits to be exceeded even though the associated force applied to the manipulator might be within the limits given by F_{avail}.

5.7.2 Constructing Other Workspaces

One of the additional benefits of the method developed here for generating the WFW is that several previously proposed workspaces can be described using this theoretical framework. The Static Equilibrium Workspace is defined in [2] as the set of all end-effector poses that can be reached statically. As discussed in previous sections, this is actually a special case of the WFW where $NW_{req} = \{\overline{0}\}$. The controllable workspace, defined in [75], is a special case of the WFW where NW_{req} is a single point in the wrench space. Thus the method presented in the previous sections for analytically forming the WFW can be used to analytically form the Static Equilibrium Workspace and controllable workspace.

The dynamic workspace, defined in [8] as the set of all poses of the end-effector where the end-effector can be given a specific acceleration, can also be formed using the method developed for the WFW. Assuming all cables are in tension, for a given

pose and instantaneous velocities and accelerations the dynamic equations of motion are as follows:

$$\boldsymbol{M}\begin{pmatrix} \ddot{\overline{x}} \\ \dot{\overline{\omega}} \end{pmatrix} = \boldsymbol{J}^T\overline{t} + \$_{ext}^w + \overline{B}\left(\dot{\overline{x}}, \overline{\omega}\right) \tag{201}$$

where $\boldsymbol{M}$ is the inertia matrix of the end-effector defined about G, $\$_{ext}^w$ is the external wrench applied at the center of gravity of the end-effector (typically the gravitational wrench), and $\overline{B}$ contains all other dynamic effects (i.e. gyroscopic effects, damping, etc.). Note that it is assumed that the inertial effects of the cables and the motors is very small compared to the inertial effects of the end-effector and thus can be neglected. Using the fact that the set of all possible values of $(\boldsymbol{J}^T\overline{t} + \$_{ext}^w)$ is NW_{avail}, the set of all possible accelerations that the end-effector can be given without violating the tension limits in the cables can then be defined as A_{avail}, the *Available Acceleration Set*, where:

$$A_{avail} = \boldsymbol{M}^{-1}\left[NW_{avail} \oplus \overline{B}\left(\dot{\overline{x}}, \overline{\omega}\right)\right]. \tag{202}$$

The set A_{avail} is simply NW_{avail} shifted by $\overline{B}$ and scaled by $\boldsymbol{M}^{-1}$. Thus A_{avail}, like NW_{avail}, is some form of a parallelogram, parallelepiped or hyper-parallelepiped. If we define the set of accelerations that are required of the end-effector at this pose as A_{req}, the *Required Acceleration Set*, the dynamic workspace of the manipulator can be defined as the set of poses P such that:

$$A_{req} \subseteq A_{avail}(P). \tag{203}$$

Because the geometric properties of A_{avail} are the same as NW_{avail}, the same geometric techniques can be used to form the dynamic workspace analytically. In fact, this construction allows a more general definition of the dynamic workspace. The dynamic workspace as defined by Barrette et al. [8] would be limited to A_{req} consisting of a single acceleration of the end-effector. Here we can extend this definition to allow A_{req} to consist of a *set* of accelerations.

5.7.3 Optimal Control Using Acceleration Limits

The Available Acceleration Set (A_{avail}) may also be incorporated into a control scheme for the cable robot. The set A_{avail} establishes limits on what accelerations the end-effector can be given at pose P. Using A_{avail} to bound the accelerations of the end-effector, the method proposed by Bobrow et al. [10] (often referred to as "bang-bang" control) may be applied to determine the time-optimal trajectory of the manipulator along a desired path. By keeping the acceleration of the end-effector within A_{avail}, it is guaranteed that a trajectory can be followed without wires going slack, wires exceeding their maximum tension, or the end-effector leaving its desired trajectory. In addition, if a payload is suspended from the end-effector it may be desirable to apply input-shaping to the resulting trajectory in order to prevent oscillation of the payload as described in [32].

5.7.4 Payload Specification

Given $NW_{avail}(P)$ and NW_{req}, it is possible to use these sets to specify the maximum payload of a cable robot. If the WFW of the manipulator has been calculated and the manipulator is required to operate in a region T within the task space, where $T \subseteq WFW$, then at any pose in T the maximum payload[8] can be determined by adding mass to the end-effector until NW_{req} is no longer completely contained within NW_{avail}. The highest load at which NW_{req} is still contained within NW_{avail} is $L(P)$, the maximum payload for that pose. The maximum payload for each pose can be found and the payload for the manipulator can be specified as the smallest of these payloads:

$$Payload = \min_{P \in T} L(P). \tag{204}$$

[8]Note that it is assumed that the mass of the payload is added at G.

5.8 Summary and Conclusion

For manipulator tasks that require the end-effector to exert a specific set of wrenches, the Wrench-Feasible Workspace represents the usable workspace of the robot. The Required Net Wrench Set, NW_{req}, was defined to be the set of wrenches that the manipulator must exert. Using the Available Net Wrench Set, NW_{avail}, which was presented in Chapter 3, the condition of wrench feasibility could be represented as $NW_{req} \subseteq NW_{avail}$. The geometric construction of NW_{req} and NW_{avail} not only allowed for wrench-feasibility to be visualized, but also allowed wrench-feasibility to be determined by simple geometric calculations.

The geometric properties of NW_{avail} were then used to form analytical expressions for the WFW boundaries for point-mass, planar and spatial cable robots. The investigation of the point-mass case was performed in [60] and is summarized here. For the investigation performed here, NW_{req} is assumed to be a collection of polyhedra. This allows a great deal of flexibility when specifying NW_{req}, as nearly any arbitrary object can be closely approximated by a collection of polyhedra. However, selecting a very complicated set of polyhedra greatly increases the number of boundaries that must be formed.

The complete analytical expressions of the lower WFW boundaries were detailed for planar cable robots. For the spatial cable robots the analytical expressions were not derived due to the large number of terms, but the approach for generating these terms was presented. In both the planar and spatial case the upper boundaries are too complex to be very useful, and thus were not calculated. However, if the upper tension limits in the cables are relatively high then the lower workspace boundaries largely determine the overall workspace geometry. Example workspaces were then plotted for a planar cable robot to demonstrate agreement between the analytically determined boundaries and numerical results.

The concepts of robustness and workspace generation were then combined to

introduce a new workspace: the Specified Robustness Workspace. This workspace consists of the set of all poses of the manipulator that meet or exceed a specified robustness value. It was shown that the method for generating the WFW could be used to construct this workspace analytically.

It was then shown how to generate the Force-Only Wrench-Feasible Workspace, a special case where only the forces exerted by the manipulator are considered. It was also shown that the method of calculating the WFW could be extended to include calculation of the static equilibrium workspace, controllable workspace and dynamic workspace. In fact, this approach allows generalization of the definition of the dynamic workspace. In addition, it was shown that the Available Net Wrench Set can be used for applications including optimal control and payload specification.

Limitations

There are, however, some difficulties with this approach that need to be addressed. In order to perform this analysis the pose of the end-effector must be known. If only the cable lengths are known it is not trivial to find the resulting pose of the end-effector, particularly for underconstrained cable robots. The analysis would also need to be modified if the end-effector is not a single rigid body. It has also been assumed that stretching or sagging of the cables is negligible. Excessive cable stretch or sag would change the end-effector pose and the sag would also change the direction of the force applied to the end-effector by the cable. Thus this method would need to be modified to accomodate significant cable stretch or sag.

5.9 Future Work

There are several topics for future work that can be done in this area. Because of the complexity of forming the upper WFW boundaries for planar and spatial cable robots, it is not currently feasible to formulate all workspace boundaries analytically. Thus it would be advantageous to develop a more effective method for formulating

the upper workspace boundaries. For example, an efficient numerical method could be developed for approximating the upper boundaries, which could be coupled with the analytically determined lower boundaries to form a more complete representation of the WFW boundaries.

In addition, it may be necessary to incorporate the effects of cable interference. Interference due to cables contacting each other and cables contacting the end-effector reduces the effective workspace. Thus if analytical expressions were formulated for the condition of interference, these would constitute additional workspace boundaries. However, in order to determine if cables contact the end-effector the complete geometry of the end-effector must be known. Additionally, if the geometry of the end-effector is complicated the resulting "interference boundaries" will also be complicated.

Another potential area of future work is to determine workspace properties and workspace geometery trends similar to what was done for point-mass manipulators in [60]. This would allow design guidelines to be synthesized for obtaining a WFW of a desired geometry. As was mentioned previously, the workspace boundary equations are so complicated that it is not easy to obtain these workspace properties directly from the equations. Instead, it is likely necessary to plot a large number of workspaces for various sets of design parameters and glean the workspace geometry trends from the results.

Also, the Available Net Wrench Set can be used as described in Section 5.7.3 to calculate time-optimal sway-free paths and trajectories. Based on the results of such an analysis it would be possible to generate design guidelines for selecting optimal paths and trajectories for certain classes of cable robots.

Lastly, it may be of interest to incorporate the effects of cable sag and stretch. Sagging changes the direction of the cable at the point of contact with the end-effector and thus changes the unit vectors $\overline{u}$ and thus changes the Jacobian matrix

and the resulting NW_{avail}. However, different loading conditions on the end-effector will change the amount of sag in the cables, and so a polyhedral model of NW_{avail} may no longer be appropriate. Incorporating cable sag into this workspace generation approach is expected to be very difficult and may only be suitable for inclusion in numerical calculation of the WFW.

CHAPTER 6

CONCLUSIONS AND FUTURE WORK

6.1 Summary and Conclusions

In summary, this work aimed to expand the existing theoretical framework for cable robots in two key areas: disturbance robustness and Wrench-Feasible Workspace generation. Chapter 3 presented the basics of screw theory and Jacobian relationships and introduced the Available Net Wrench Set, the set of all wrenches that can be exerted by the manipulator on its surroundings.

Using this set, Chapter 4 developed the disturbance robustness measure, $\mathcal{R}$. In order to facilitate the analysis, the intermediate space was introduced. The analysis of robustness to static disturbances used the Available Net Wrench Set to find the set of all static disturbance wrenches that cause a cable to begin to go slack. Out of this set, the smallest wrench was found, using acceleration energy to form the wrench norm. The magnitude of this smallest static disturbance wrench is $mg\mathcal{R}_s$. The analysis of robustness to impulsive disturbances found the initial acceleration (after the impulse has ended) of the end-effector back towards the original pose. The smallest acceleration was found to have a vertical acceleration of $-g\mathcal{R}_i^2$ and a total acceleration of magnitude $g\mathcal{R}_i$. It was then proven that $\mathcal{R}_s = \mathcal{R}_i$ and thus the robustness measure $\mathcal{R}$ was chosen to be $\mathcal{R} = \mathcal{R}_s = \mathcal{R}_i$.

Several measures of overall cable robot robustness over the workspace were presented. The robustness measure was then extended to apply to cable robots with multi-body end-effectors, thus allowing analysis of cable robots with suspended payloads.

The Available Net Wrench Set was also used in Chapter 5 to generate the Wrench-Feasible Workspace for cable robots. For manipulator tasks that require the end-effector to exert a specific set of wrenches, the Wrench-Feasible Workspace represents the usable workspace of the robot. The Required Net Wrench Set, NW_{req}, was defined to be the set of wrenches that the manipulator must exert. Using the Available Net Wrench Set, NW_{avail}, the condition of wrench feasibility could be represented as $NW_{req} \subseteq NW_{avail}$. The geometric construction of NW_{req} and NW_{avail} not only allowed for wrench-feasibility to be visualized, but also allowed wrench-feasibility to be determined by simple geometric calculations.

The geometric properties of NW_{avail} were then used to form analytical expressions for the WFW boundaries for point-mass, planar and spatial cable robots. NW_{req} was assumed to be a collection of polyhedra, which allows a great deal of flexibility when specifying NW_{req}, as nearly any arbitrary object can be closely approximated by a collection of polyhedra. The complete analytical expressions of the lower WFW boundaries were detailed for planar cable robots. For the spatial cable robots the analytical expressions were not derived due to the large number of terms, but the approach for generating these terms was presented. Example workspaces were then plotted for a planar cable robot to demonstrate agreement between the analytically determined boundaries and numerical results.

The concepts of robustness and workspace generation were then combined to introduce a new workspace: the Specified Robustness Workspace. This workspace consists of the set of all poses of the manipulator that meet or exceed a specified robustness value. It was shown that the method for generating the WFW could be used to construct this workspace analytically. It was also shown how to generate the Force-Only Wrench-Feasible Workspace, a special case where only the forces exerted by the manipulator are considered. Lastly, it was shown that this method could be extended to include calculation of the Static Equilibrium Workspace, controllable

workspace and dynamic workspace.

6.2 Contributions of this Work

The major contributions of this work are:

1. **A measure of the robustness of a pose of a general underconstrained cable robot.** This measure allows calculation of the robustness of the end-effector to static and impulsive external disturbances. The measure applies to point-mass, planar and spatial cable robots and was extended to include cable robots with multi-body end-effectors. The measure is easy to calculate, requiring only the Jacobian matrix and the inertial properties of the end-effector. The measure describes both the magnitude of the smallest static wrench that disturbs the manipulator and the magnitude of the initial acceleration of the end-effector back to its original pose if disturbed by an impulsive wrench.

2. **A geometric test for wrench-feasibility of a pose.** This geometrically based calculation allows wrench-feasibility to be tested for entire sets of wrenches. This geometric analysis also enables geometric construction of the Wrench-Feasible Workspace.

3. **A technique for generating the Wrench-Feasible Workspace.** Based on the geometric test for wrench-feasibility, this method allows analytical formulation of the equations that define the boundaries of the Wrench-Feasible Workspace. Generating the Wrench-Feasible Workspace analytically should be much faster and more accurate than generating it numerically. Based on the expressions for the WFW boundaries, it should also be possible to determine workspace properties and workspace geometry trends similar to what was done for point-mass manipulators in [60]. However, because of the complexity of

forming the *upper* WFW boundaries for planar and spatial cable robots, it is not currently feasible to formulate all workspace boundaries analytically.

It was also shown how this method can be used to form a number of other workspaces, including the Force-Only Wrench-Feasible Workspace, Static Equilibrium Workspace, Controllable Workspace and Dynamic Workspace.

4. **A new workspace for underconstrained cable robots – the Specified Robustness Workspace.** This workspace consists of the set of all poses that meet or exceed a specified robustness value. Not only is this workspace a new concept, it can also be calculated analytically using the techniques developed for the Wrench-Feasible Workspace.

In addition, much of this work was performed using the "intermediate space." This space provided a novel approach for examining twists and wrenches that solves the problem of mixed-dimensionality while still maintaining physical meaning through the concepts of kinetic energy and acceleration energy.

In summary, the proposed research discussed here will greatly extend the theoretical framework for underconstrained cable robots. Key issues of disturbance robustness, wrench-feasibility and workspace generation were examined systematically, resulting in insight that can be used to more effectively design cable robots.

6.3 Future Work

The work presented in this thesis opens up several areas of potential future work. Section 4.8 details several areas where future work on disturbance robustness could lead. One possibility is to investigate the effects of curvature of the constraint surfaces on the response of the manipulator to external disturbances. Because curvature of constraint surfaces is used in some work in grasp stability, it may be possible to leverage the work that has already been done in this area. Because of the

similarity between cable-robots and grasping (due to the uni-directional constraints), the disturbance robustness measure could also possibly be extended to an equivalent measure for underconstrained grasped objects. Investigation of disturbances causing a manipulator to transition to a different static equilibrium pose could lead to a measure of the "transition energy" of the pose. The investigation of the effects of disturbances on the end-effector pose could also lead to a control strategy for actively causing the manipulator to return to its original pose.

Section 5.9 lists some of the potential future work in Wrench-Feasible Workspace generation. One of these areas is formulation of the upper workspace boundaries. Because of the complexity of forming the upper WFW boundaries for planar and spatial cable robots, it is not currently feasible to formulate all workspace boundaries analytically. Thus it would be advantageous to develop a more effective method for formulating the upper workspace boundaries. It would also be desirable to incorporate the effects of cable interference, which reduces the effective workspace. Based on the expressions for the WFW boundaries, it would also be possible to determine workspace properties and workspace geometry trends similar to what was done for point-mass manipulators in [60]. This would allow design guidelines to be synthesized for obtaining a WFW of a desired geometry. Also, the Available Net Wrench Set can be used as described in Section 5.7.3 to calculate time-optimal sway-free paths and trajectories. Based on the results of such an analysis it would be possible to generate design guidelines for selecting optimal paths and trajectories for certain classes of cable robots.

Based on the knowledge gained from these two areas of research, general guidelines can be developed for maximizing manipulator robustness and achieving desired geometries of the WFW. This would allow more systematic development of optimized cable robot architectures. To date, most planar and spatial architectures are chosen in a somewhat ad-hoc manner. The tools developed here allow a more systematic

optimization of motor placements and end-effector geometry.

Lastly, it may be of interest to incorporate the effects of cable sag and stretch. Cable sag and stretch affects both the analysis of disturbance robustness and wrench-feasibility. Incorporating cable sag into this workspace generation approach is expected to be very difficult. However, the effect of cable sag could be reduced for the generation of the WFW by requiring non-zero minimum tension values (i.e. using $t_{i,max} \geq t_i \geq t_{i,min} \geq 0$ when forming NW_{avail} in (13)). This adjustment is suggested in [78], where maintaining a minimum tension in each cable reduces the effect of cable sag.

APPENDIX A

PROOF OF THEOREM IN SECTION 4.4.4

Theorem **:**

Given two uni-directional twists that positively span a constraint surface. Then the magnitude of the acceleration of the end-effector due to gravity while moving along one of the uni-directional twists will be less than or equal to the magnitude of the acceleration of the end-effector due to gravity while moving along the constraint surface.

Proof **:**

Given two n-dimensional uni-directional twists $\$_b^t$, $\$_c^t$ that positively span a planar constraint surface CS. That is, any twist $\$^t$ along CS can be written as $\$^t = d_1\$_b^t + d_2\$_c^t$, where $d_1, d_2 \geq 0$. Let these twists be mapped to the generalized velocities $\hat{v}_b$ and $\hat{v}_c$ in the intermediate space.

Let Z be the vertical axis in the intermediate space (i.e. parallel to $\hat{f}_{grav}$) and $\hat{z}$ be a unit vector in the positive Z direction (upwards). Then for any generalized velocity $\hat{v}$, if θ is the angle between $\hat{v}$ and horizontal then

$$\sin\theta = \frac{\hat{v} \cdot \hat{z}}{\parallel \hat{v} \parallel}. \tag{205}$$

Note that in the situation considered here, $0 < \sin\theta \leq 1$ because the pose considered is an equilibrium pose. This is because $\sin\theta = 0$ corresponds to a bi-directional twist, which we are assuming are not present, and $\sin\theta < 0$ corresponds to a constraint surface that has a negative slope, which would cause the end-effector to move away from this pose under the influence of gravity, which cannot be the case for a static equilibrium pose. Thus for all equilibrium poses $0 < \sin\theta \leq 1$ along any

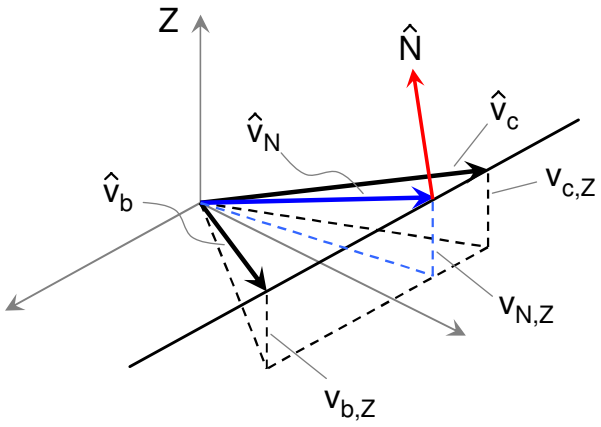

Figure 43: Decomposition of generalized velocities that positively span a constraint surface.

unconstrained generalized velocity.

From equation (205) it is also clear that multiplying $\hat{v}$ by a positive scalar will not change the result for $\sin\theta$, thus without loss of generality we can scale $\hat{v}_b$ and $\hat{v}_c$ to have the same vertical component, as shown in Figure 43. A vector $\hat{N}$ normal to the constraint surface can be constructed such that $\hat{N}$ and the Z axis are coplanar. If a generalized velocity $\hat{v}_N$ tangent to the constraint surface is constructed *in this plane* (the plane that contains $\hat{N}$ and the Z axis), the angle θ_{cs} between the constraint surface and horizontal is the same as the angle between $\hat{v}_N$ and horizontal. Without loss of generality, we can scale $\hat{v}_N$ to have the same vertical component as $\hat{v}_b$ and $\hat{v}_c$. Because the Z axis points vertically, let us denote the vertical component of a vector with a subscript Z resulting in $v_{N,Z} = v_{b,Z} = v_{c,Z}$. Thus,

$$\sin\theta_b = \frac{v_{N,Z}}{\| \hat{v_b} \|}$$

$$\sin\theta_c = \frac{v_{N,Z}}{\| \hat{v_c} \|}$$

$$\sin\theta_N = \frac{v_{N,Z}}{\| \hat{v_n} \|}.$$

Now construct a line that passes through the endpoints of $\hat{v}_b$ and $\hat{v}_c$ and let the origin of $\hat{N}$ be placed at the tip of $\hat{v}_N$ as shown in Figure 43. Because the line passes

through the endpoints of $\hat{v}_b$ and $\hat{v}_c$, which are at the same height, the line must be perpendicular to the Z axis. Also, because $\hat{v}_b$ and $\hat{v}_c$ are tangent to the constraint surface, they are both perpendicular to $\hat{N}$. Thus this line through the endpoints of $\hat{v}_b$ and $\hat{v}_c$ is perpendicular to the plane that contains the Z axis and $\hat{v}_N$. Because $\hat{N}$, $\hat{v}_N$ and the Z axis are constrained to be coplanar, the line between $\hat{v}_b$ and $\hat{v}_c$ must also be perpendicular to $\hat{v}_N$.

Because $\hat{v}_N$ is perpendicular to this line, it represents the shortest distance between the origin and the line. Thus

$$\| \hat{v}_N \| \leq \| \hat{v}_b \| \tag{206}$$

and

$$\| \hat{v}_N \| \leq \| \hat{v}_c \| . \tag{207}$$

Recall $v_{N,Z} = v_{b,Z} = v_{c,Z}$. Let $v_{N,Z} = d$. Then,

$$\sin\theta_b = \frac{d}{\| \hat{v_b} \|} \tag{208}$$

$$\sin\theta_c = \frac{d}{\| \hat{v_c} \|} \tag{209}$$

$$\sin\theta_N = \frac{d}{\| \hat{v_N} \|}. \tag{210}$$

Thus applying (206) and (207) results in:

$$\sin\theta_N \geq \sin\theta_b \tag{211}$$

and

$$\sin\theta_N \geq \sin\theta_c. \tag{212}$$

Recall that the vertical acceleration for motion along a uni-directional generalized velocity is $\overline{a}_{vert} = \overline{g}\sin^2\theta_{uni}$ while the vertical acceleration for motion along a constraint surface is $\overline{a}_{vert} = \overline{g}\sin^2\theta_{cs}$. Thus for any uni-directional twists that positively span a constraint surface the acceleration along the uni-directional twists will be less than the acceleration along the constraint surface because $\sin\theta_{cs} \geq \sin\theta_{uni}$ for each uni-directional twist. Q.E.D. $\square$

APPENDIX B

SIMULATION OF A CABLE ROBOT WITH NON-IDEAL CABLES

B.1 Motivation

In Chapter 4 a method was shown for calculating the robustness measure, $\mathcal{R}$. This method assumes ideal cables that are massless and do not stretch or sag. The purpose of this brief study is to: 1) verify that the smallest static disturbance wrench, $\$^w_{min}$, is found correctly for the case of ideal cables, and 2) investigate the effects of non-ideal cables that stretch and sag.

This study is performed in computer simulation using VisualNastran4D software, a software package meant for modeling and simulation of the motion of bodies. This study is chosen to be performed in simulation in order to avoid the time and cost of setting up a physical experimental test bed.

It is also anticipated that the effects resulting from non-ideal cables may vary depending on the robustness of the pose (found using the assumption of ideal cables). Thus two poses of a manipulator are considered here, one with relatively high robustness and one with relatively low robustness. Each of these poses are considered with both ideal and non-ideal cables.

B.2 Test Set-Up

The manipulator considered for this study is a 3-cable, planar cable robot as shown in Figures 44 and 45. The end-effector geometry is chosen (arbitrarily) to be a $0.4\,\mathrm{m} \times 0.16\,\mathrm{m}$ rectangle of uniform thickness and density with a mass of $20\,\mathrm{kg}$. The

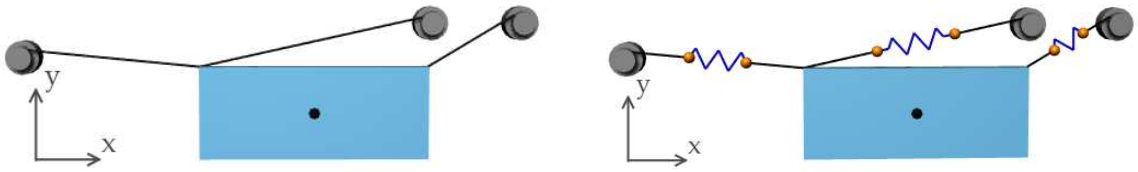

(a) Test manipulator with ideal cables.

(b) Test manipulator with non-ideal cables.

Figure 44: High robustness pose of the test manipulator.

resulting rotational inertia of the end-effector is $0.3093\,\mathrm{kg}\cdot\mathrm{m}^2$. Note that in Figures 44 and 45 the center of gravity is represented by a black dot. The pose of the manipulator is $(x, y, \theta)^T$, where the $+x$ direction is to the right and the $+y$ direction is upward, as shown in Figures 44 and 45. θ is positive in the counter-clockwise direction.

Motor 1 is located at $(-0.3\,\mathrm{m}, 0.19\,\mathrm{m})^T$, motor 2 is located at $(0.4\,\mathrm{m}, 0.25\,\mathrm{m})^T$ and motor 3 is located at $(0.55\,\mathrm{m}, 0.25\,\mathrm{m})^T$, where the motors (and cables) are numbered from left to right. Cables 1 and 2 are chosen to be attached to the upper-left corner of the end-effector and cable 3 is chosen to be attached to the upper-right corner of the end-effector. Thus the vectors from G to the attachment points are $\overline{c}_1 = \overline{c}_2 = (-0.2\,\mathrm{m}, 0.08\,\mathrm{m})^T$ and $\overline{c}_3 = (0.2\,\mathrm{m}, 0.08\,\mathrm{m})^T$ (for $\theta = 0$). The two poses of the manipulator that are considered here are $(0.2\,\mathrm{m}, 0.08\,\mathrm{m}, 0\,\mathrm{rad})^T$ (shown in Figure 44) and $(0.2\,\mathrm{m}, -0.6\,\mathrm{m}, 0\,\mathrm{rad})^T$ (shown in Figure 45).

The modeling and simulation software includes ideal cable elements, which were used to construct the manipulators with ideal cables that are massless and do not stretch (in Figures 44(a) and 45(a)). Because the software does not include non-ideal cable elements, the non-idealities of the cables must be introduced manually. This was accomplished by dividing each cable into three parts of equal length (as shown in Figures 44(b) and 45(b)). The distributed mass of the cables was approximated by two discrete masses placed at the two divisions between the three cable segments. The stretch in the cables was approximated by replacing each middle cable segment

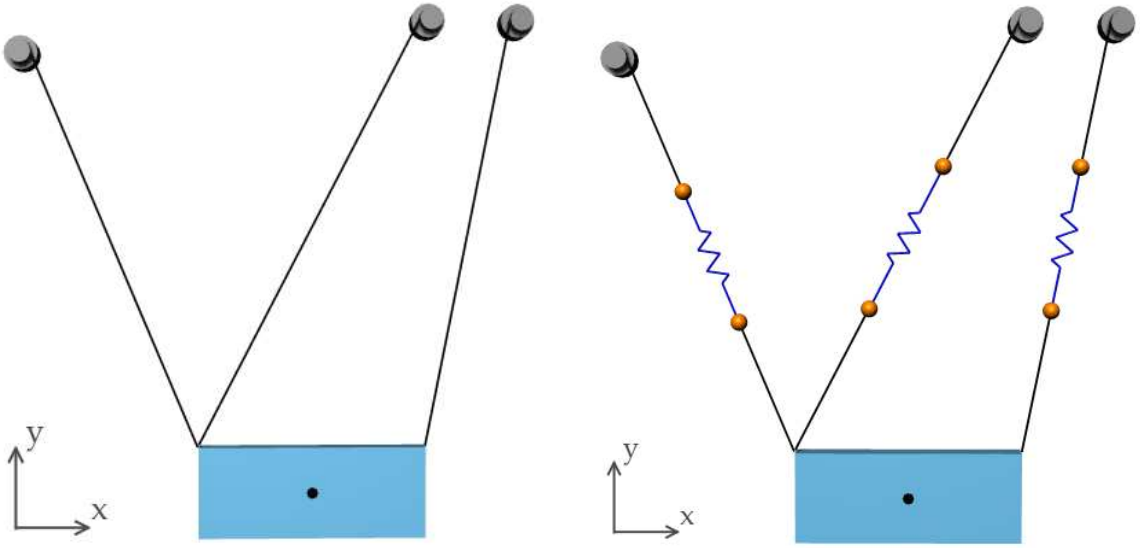

(a) Test manipulator with ideal cables.

(b) Test manipulator with non-ideal cables.

Figure 45: Low robustness pose of the test manipulator.

by a linear spring. While this approximation is somewhat crude, it is sufficient for the purpose of this initial study.

The mass of cable i can be found using:

$$m_i = \pi R^2 \rho L_i \tag{213}$$

where R is the effective radius of the cable, ρ is the density of the cable and L_i is the unstretched length of the cable. For a manipulator such as this, 2.5 mm diameter steel cables would be more than adequate to support the end-effector. For steel $\rho \approx 7870 \, \frac{\text{kg}}{\text{m}^3}$, resulting in $m_i = 0.0386 \, \frac{\text{kg}}{\text{m}} \cdot L_i$. The cables used in this example are relatively short, and the effect of cable sag becomes more pronounced for manipulators with longer cables, thus in order to accentuate the effect of cable sag the mass of each cable was increased to $m_i = 1.0 \, \frac{\text{kg}}{\text{m}} \cdot L_i$. Because the distributed mass of the cable is being approximated by two discrete masses, each discrete mass was given half the total mass of the associated cable.

The stiffness of cable i, k_i, can be calculated as shown in [53] as:

$$k_i = \frac{\pi R^2 E}{L_i} \tag{214}$$

where R is the effective radius of the cable, E is the modulus of elasticity of the cable and L_i is the unstretched length of the cable. Assuming 2.5 mm diameter steel cables are used, $E \approx 200\,\text{GPa}$, resulting in $k_i = 982\,\text{kN} \cdot \frac{1}{L_i}$. Again, the cables used in this example are relatively short. The effect of cable stretch becomes more pronounced for manipulators with longer cables, thus in order to accentuate the effect of cable stretch the stiffness of each cable was reduced to $k_i = 100\,\text{kN} \cdot \frac{1}{L_i}$.

B.3 Calculations

For the two poses considered $((0.2\,\text{m}, 0.08\,\text{m}, 0\,\text{rad})^T$ and $(0.2\,\text{m}, -0.6\,\text{m}, 0\,\text{rad})^T)$, we must now calculate the robustness measure and the corresponding smallest disturbance wrench for each pose. All robustness calculations were performed in MATLAB and the results are shown with the numerical precision of the MATLAB results. The MATLAB code used for this example is included in Appendix C. The inertia matrix is:

$$\boldsymbol{M} = \begin{bmatrix} 20\,\text{kg} & 0 & 0 \\ 0 & 20\,\text{kg} & 0 \\ 0 & 0 & 0.3093\,\text{kg}\cdot\text{m}^2 \end{bmatrix}.$$

The motor locations are:

$$\overline{\mathbf{m}}_1 = \begin{pmatrix} -0.3\,\text{m} \\ 0.19\,\text{m} \end{pmatrix} \qquad \overline{\mathbf{m}}_2 = \begin{pmatrix} 0.4\,\text{m} \\ 0.25\,\text{m} \end{pmatrix} \qquad \overline{\mathbf{m}}_3 = \begin{pmatrix} 0.55\,\text{m} \\ 0.25\,\text{m} \end{pmatrix}.$$

The vectors from G to the attachment points are:

$$\overline{c}_1 = \overline{c}_2 = \begin{pmatrix} -0.2\,\text{m} \\ 0.08\,\text{m} \end{pmatrix} \qquad \overline{c}_3 = \begin{pmatrix} 0.2\,\text{m} \\ 0.08\,\text{m} \end{pmatrix}.$$

Table 1: Cable parameters for the pose shown in Figure 44(b).

	Cable Length (m)	Total Cable Mass (kg)	Cable Stiffness (kN/m)
Cable 1	0.302	0.302	332
Cable 2	0.410	0.410	244
Cable 3	0.175	0.175	572

Pose 1:

For the first pose, $(x, y, \theta) = (0.2\,\text{m}, 0.08\,\text{m}, 0\,\text{rad})^T$, the lengths of the cables are found by:

$$L_i = \parallel \overline{\boldsymbol{m}}_i - ((x, y) + \overline{c}_i) \parallel . \tag{215}$$

Applying the cable properties chosen previously, the mass and stiffness of each cable can be found. The results are shown in Table 1. The unit vectors along the cables are found by:

$$\overline{u}_i = \frac{\overline{\boldsymbol{m}}_i - ((x, y) + \overline{c}_i)}{\parallel \overline{\boldsymbol{m}}_i - ((x, y) + \overline{c}_i) \parallel} \tag{216}$$

resulting in:

$$\overline{u}_1 = \begin{pmatrix} -0.9950\,\text{m} \\ 0.0995\,\text{m} \end{pmatrix} \qquad \overline{u}_2 = \begin{pmatrix} 0.9756\,\text{m} \\ 0.2195\,\text{m} \end{pmatrix} \qquad \overline{u}_3 = \begin{pmatrix} 0.8575\,\text{m} \\ 0.5145\,\text{m} \end{pmatrix}.$$

The Jacobian matrix is found using:

$$\boldsymbol{J} = \begin{bmatrix} \overline{u}_1 & \overline{u}_2 & \overline{u}_3 \\ det[\overline{c}_1\ \overline{u}_1] & det[\overline{c}_2\ \overline{u}_2] & det[\overline{c}_3\ \overline{u}_3] \end{bmatrix}^T . \tag{217}$$

resulting in

$$\boldsymbol{J} = \begin{bmatrix} -0.9950 & 0.0995 & 0.0597\,\text{m} \\ 0.9756 & 0.2195 & -0.1220\,\text{m} \\ 0.8575 & 0.5145 & 0.0343\,\text{m} \end{bmatrix}.$$

The three modified Jacobian matrices are then:

$$\boldsymbol{J}_{mod,1} = \begin{bmatrix} 0.9756 & 0.2195 & -0.1220\,\text{m} \\ 0.8575 & 0.5145 & 0.0343\,\text{m} \end{bmatrix}$$

$$\boldsymbol{J}_{mod,2} = \begin{bmatrix} -0.9950 & 0.0995 & 0.0597\,\mathrm{m} \\ 0.8575 & 0.5145 & 0.0343\,\mathrm{m} \end{bmatrix}$$

and

$$\boldsymbol{J}_{mod,3} = \begin{bmatrix} -0.9950 & 0.0995 & 0.0597\,\mathrm{m} \\ 0.9756 & 0.2195 & -0.1220\,\mathrm{m} \end{bmatrix}.$$

Using these three matrices the three principal twists can be found. For each modified Jacobian matrix, a nullspace vector is found such that it has a positive vertical component. The resulting principal twists are:

$$\$^t_{princ,1} = \begin{pmatrix} -0.2009\,\frac{\mathrm{m}}{\mathrm{s}} \\ 0.3945\,\frac{\mathrm{m}}{\mathrm{s}} \\ -0.8967\,\frac{\mathrm{rad}}{\mathrm{s}} \end{pmatrix} \quad \$^t_{princ,2} = \begin{pmatrix} -0.0452\,\frac{\mathrm{m}}{\mathrm{s}} \\ 0.1413\,\frac{\mathrm{m}}{\mathrm{s}} \\ -0.9889\,\frac{\mathrm{rad}}{\mathrm{s}} \end{pmatrix} \quad \$^t_{princ,3} = \begin{pmatrix} 0.0782\,\frac{\mathrm{m}}{\mathrm{s}} \\ 0.1955\,\frac{\mathrm{m}}{\mathrm{s}} \\ 0.9776\,\frac{\mathrm{rad}}{\mathrm{s}} \end{pmatrix}.$$

The principal twists are then mapped to principal generalized velocities by $\hat{v}_i = \boldsymbol{A}\$^t_{princ,i}$, where:

$$\begin{aligned} \boldsymbol{A} &= \left(\frac{1}{m}\boldsymbol{M}\right)^{\frac{1}{2}} \\ &= \begin{bmatrix} 1 & 0 & 0 \\ 0 & 1 & 0 \\ 0 & 0 & 0.1244\,\mathrm{m} \end{bmatrix} \end{aligned} \tag{218}$$

resulting in:

$$\hat{v}_{princ,1} = \begin{pmatrix} -0.2009\,\frac{\mathrm{m}}{\mathrm{s}} \\ 0.3945\,\frac{\mathrm{m}}{\mathrm{s}} \\ -0.1115\,\frac{\mathrm{m}}{\mathrm{s}} \end{pmatrix} \quad \hat{v}_{princ,2} = \begin{pmatrix} -0.0452\,\frac{\mathrm{m}}{\mathrm{s}} \\ 0.1413\,\frac{\mathrm{m}}{\mathrm{s}} \\ -0.1230\,\frac{\mathrm{m}}{\mathrm{s}} \end{pmatrix} \quad \hat{v}_{princ,3} = \begin{pmatrix} 0.0782\,\frac{\mathrm{m}}{\mathrm{s}} \\ 0.1955\,\frac{\mathrm{m}}{\mathrm{s}} \\ 0.1216\,\frac{\mathrm{m}}{\mathrm{s}} \end{pmatrix}.$$

The sine of the angle of each generalized velocity with respect to horizontal is found by:

$$\sin\theta_i = \frac{(\hat{v}_{princ,i})_y}{\parallel \hat{v}_{princ,i} \parallel} \tag{219}$$

Table 2: Cable parameters for the pose shown in Figure 44(b).

	Cable Length (m)	Total Cable Mass (kg)	Cable Stiffness (kN/m)
Cable 1	0.771	0.771	130
Cable 2	0.868	0.868	115
Cable 3	0.785	0.785	127

resulting in:

$$\sin\theta_1 = 0.8642 \qquad \sin\theta_2 = 0.7332 \qquad \sin\theta_3 = 0.8041.$$

The robustness measure is then:

$$\mathcal{R} = \min_{i\in\{1,2,3\}} \sin\theta_i = 0.7332.$$

Because the smallest $\sin\theta_i$ corresponds to $i = 2$, the smallest generalized force that disturbs the end-effector, $\hat{f}_{min}$, is parallel to $\hat{v}_{princ,2}$ and has magnitude $mg\mathcal{R}$. Thus:

$$\hat{f}_{min} = mg\mathcal{R}\frac{\hat{v}_{princ,2}}{\| \hat{v}_{princ,2} \|} = \begin{pmatrix} -33.7500\,\mathrm{N} \\ 105.4687\,\mathrm{N} \\ -91.8164\,\mathrm{N} \end{pmatrix}.$$

The smallest static disturbance wrench, $\$^w_{min}$, is then found by mapping $\hat{f}_{min}$ back to the task space via $\boldsymbol{A}^{-1}$:

$$\$^w_{min} = \boldsymbol{A}^{-1}\hat{f}_{min} = \begin{pmatrix} -33.7500\,\mathrm{N} \\ 105.4687\,\mathrm{N} \\ -11.4188\,\frac{\mathrm{N}}{\mathrm{m}} \end{pmatrix}.$$

Pose 2:

For the second pose, $(x, y, \theta) = (0.2\,\mathrm{m}, -0.6\,\mathrm{m}, 0\,\mathrm{rad})^T$, the lengths of the cables are again found by (215). Applying the cable properties chosen previously, the mass and stiffness of each cable can be found. The results are shown in Table 2. The unit vectors along the cables are found by (216), resulting in:

$$\overline{u}_1 = \begin{pmatrix} -0.3892\,\mathrm{m} \\ 0.9211\,\mathrm{m} \end{pmatrix} \qquad \overline{u}_2 = \begin{pmatrix} 0.4610\,\mathrm{m} \\ 0.8874\,\mathrm{m} \end{pmatrix} \qquad \overline{u}_3 = \begin{pmatrix} 0.1912\,\mathrm{m} \\ 0.9815\,\mathrm{m} \end{pmatrix}.$$

The Jacobian matrix is found using (217), resulting in:

$$\boldsymbol{J} = \begin{bmatrix} -0.3892 & 0.9211 & -0.1531\,\mathrm{m} \\ 0.4610 & 0.8874 & -0.2144\,\mathrm{m} \\ 0.1912 & 0.9815 & 0.1810\,\mathrm{m} \end{bmatrix}.$$

The three modified Jacobian matrices are then:

$$\boldsymbol{J}_{mod,1} = \begin{bmatrix} 0.4610 & 0.8874 & -0.2144\,\mathrm{m} \\ 0.1912 & 0.9815 & 0.1810\,\mathrm{m} \end{bmatrix}$$

$$\boldsymbol{J}_{mod,2} = \begin{bmatrix} -0.3892 & 0.9211 & -0.1531\,\mathrm{m} \\ 0.1912 & 0.9815 & 0.1810\,\mathrm{m} \end{bmatrix}$$

and

$$\boldsymbol{J}_{mod,3} = \begin{bmatrix} -0.3892 & 0.9211 & -0.1531\,\mathrm{m} \\ 0.4610 & 0.8874 & -0.2144\,\mathrm{m} \end{bmatrix}.$$

Using these three matrices the three principal twists can be found. For each modified Jacobian matrix, a nullspace vector is found such that it has a positive vertical component. The resulting principal twists are:

$$\$^t_{princ,1} = \begin{pmatrix} -0.7685\,\frac{\mathrm{m}}{\mathrm{s}} \\ 0.2577\,\frac{\mathrm{m}}{\mathrm{s}} \\ -0.5857\,\frac{\mathrm{rad}}{\mathrm{s}} \end{pmatrix} \quad \$^t_{princ,2} = \begin{pmatrix} 0.4928\,\frac{\mathrm{m}}{\mathrm{s}} \\ 0.0640\,\frac{\mathrm{m}}{\mathrm{s}} \\ -0.8678\,\frac{\mathrm{rad}}{\mathrm{s}} \end{pmatrix} \quad \$^t_{princ,3} = \begin{pmatrix} 0.0782\,\frac{\mathrm{m}}{\mathrm{s}} \\ 0.1955\,\frac{\mathrm{m}}{\mathrm{s}} \\ 0.9776\,\frac{\mathrm{rad}}{\mathrm{s}} \end{pmatrix}.$$

The principal twists are then mapped to principal generalized velocities by $\hat{v}_i = \boldsymbol{A}\$^t_{princ,i}$, where $\boldsymbol{A}$ was found in (218), resulting in:

$$\hat{v}_{princ,1} = \begin{pmatrix} -0.7685\,\frac{\mathrm{m}}{\mathrm{s}} \\ 0.2577\,\frac{\mathrm{m}}{\mathrm{s}} \\ -0.0728\,\frac{\mathrm{m}}{\mathrm{s}} \end{pmatrix} \quad \hat{v}_{princ,2} = \begin{pmatrix} 0.4928\,\frac{\mathrm{m}}{\mathrm{s}} \\ 0.0640\,\frac{\mathrm{m}}{\mathrm{s}} \\ -0.1079\,\frac{\mathrm{m}}{\mathrm{s}} \end{pmatrix} \quad \hat{v}_{princ,3} = \begin{pmatrix} 0.0782\,\frac{\mathrm{m}}{\mathrm{s}} \\ 0.1955\,\frac{\mathrm{m}}{\mathrm{s}} \\ 0.1216\,\frac{\mathrm{m}}{\mathrm{s}} \end{pmatrix}.$$

The sine of the angle of each generalized velocity with respect to horizontal is found by (219), resulting in:

$$\sin\theta_1 = 0.3167 \qquad \sin\theta_2 = 0.1259 \qquad \sin\theta_3 = 0.8041.$$

The robustness measure is then:

$$\mathcal{R} = \min_{i\in\{1,2,3\}} \sin\theta_i = 0.1259.$$

Because the smallest $\sin\theta_i$ corresponds to $i = 2$, the smallest generalized force that disturbs the end-effector,$\hat{f}_{min}$, is parallel to $\hat{v}_{princ,2}$ and has magnitude $mg\mathcal{R}$. Thus:

$$\hat{f}_{min} = mg\mathcal{R}\frac{\hat{v}_{princ,2}}{\| \hat{v}_{princ,2} \|} = \begin{pmatrix} 23.9355\,\mathrm{N} \\ 3.1093\,\mathrm{N} \\ -5.2413\,\mathrm{N} \end{pmatrix}.$$

The smallest static disturbance wrench, $\$^w_{min}$, is then found by mapping $\hat{f}_{min}$ back to the task space via $\boldsymbol{A}^{-1}$:

$$\$^w_{min} = \boldsymbol{A}^{-1}\hat{f}_{min} = \begin{pmatrix} 23.9355\,\mathrm{N} \\ 3.1093\,\mathrm{N} \\ -0.6518\,\frac{\mathrm{N}}{\mathrm{m}} \end{pmatrix}.$$

B.4 Simulation Results

In order to test that the smallest static wrench, $\$^w_{min}$, is found correctly for the case of ideal cables the simulation must show that if $\alpha\$^w_{min}$ is applied to the end-effector, it is not disturbed when $1 > \alpha \geq 0$ but is disturbed when $\alpha > 1$. Thus four different test wrenches are applied to the end-effector: $\alpha = 0$, $\alpha = 0.5$, $\alpha = (1-\varepsilon)$ and $\alpha = (1+\varepsilon)$, where ε is a small positive number. In this case the size of ε is limited by the numerical precision of the VisualNastran4D software. For the first pose

$$(1-\varepsilon)\$^w_{min} = \begin{pmatrix} -33.7\,\mathrm{N} \\ 105\,\mathrm{N} \\ -11.4\,\frac{\mathrm{N}}{\mathrm{m}} \end{pmatrix} \qquad \text{and} \qquad (1+\varepsilon)\$^w_{min} = \begin{pmatrix} -33.8\,\mathrm{N} \\ 106\,\mathrm{N} \\ -11.5\,\frac{\mathrm{N}}{\mathrm{m}} \end{pmatrix}.$$

where each term in $(1-\varepsilon)\$^w_{min}$ is simply $\$^w_{min}$ rounded down (in magnitude) to the nearest value with 3 significant figures and each term in $(1+\varepsilon)\$^w_{min}$ is simply $\$^w_{min}$ rounded up (in magnitude) to the nearest value with 3 significant figures[1]. Similarly, for the second pose

$$(1-\varepsilon)\$^w_{min} = \begin{pmatrix} 23.9\,\mathrm{N} \\ 3.10\,\mathrm{N} \\ -0.651\,\frac{\mathrm{N}}{\mathrm{m}} \end{pmatrix} \quad \text{and} \quad (1+\varepsilon)\$^w_{min} = \begin{pmatrix} 24.0\,\mathrm{N} \\ 3.11\,\mathrm{N} \\ -0.652\,\frac{\mathrm{N}}{\mathrm{m}} \end{pmatrix}.$$

where again each term in $(1-\varepsilon)\$^w_{min}$ is simply $\$^w_{min}$ rounded down (in magnitude) to the nearest value with 3 significant figures and each term in $(1+\varepsilon)\$^w_{min}$ is simply $\$^w_{min}$ rounded up (in magnitude) to the nearest value with 3 significant figures.

In order to investigate the effects of cable stretch and sag, these same static wrenches are applied to the manipulators with non-ideal cables.

Each of these wrenches was applied to the end-effector in simulation, which produced a time-varying displacement of the end-effector. The simulation was allowed to run until the steady-state pose of the end-effector was reached. The resulting displacement of the end-effector, $(\Delta x, \Delta y, \Delta\theta)$, was then measured in terms of the change of the end-effector pose from the desired pose of $(x, y, \theta) = (0.2\,\mathrm{m}, 0.08\,\mathrm{m}, 0\,\mathrm{rad})^T$ for the first pose and $(x, y, \theta) = (0.2\,\mathrm{m}, -0.6\,\mathrm{m}, 0\,\mathrm{rad})^T$ for the second pose. The results are shown in Table 3 for the first pose and Table 4 for the second pose.

B.5 Discussion

Examination of the simulation results for the manipulator with the ideal cables shows exact agreement between the simulation and the theoretical results for both poses. In both cases there was no displacement of the end-effector when the disturbance wrench

[1]Note that here $(1-\varepsilon)$ and $(1+\varepsilon)$ are not a specific number, but are used more in a notational sense.

Table 3: Simulation results for the pose shown in Figure 44.

	Ideal Cables			Non-Ideal Cables		
Applied Wrench	Δx (m)	Δy (m)	Δθ (deg)	Δx (m)	Δy (m)	Δθ (deg)
0	0.0000	0.0000	0.0000	0.0010	-0.0038	0.6780
$0.5 \cdot \$^{w}_{min}$	0.0000	0.0000	0.0000	0.0010	-0.0027	0.4170
$(1-\varepsilon) \cdot \$^{w}_{min}$	0.0000	0.0000	0.0000	0.0000	0.0006	-0.5810
$(1+\varepsilon) \cdot \$^{w}_{min}$	0.0000	0.0002	-0.0993	0.0000	0.0008	-0.6580

Table 4: Simulation results for the pose shown in Figure 45.

	Ideal Cables			Non-Ideal Cables		
Applied Wrench	Δx (m)	Δy (m)	Δθ (deg)	Δx (m)	Δy (m)	Δθ (deg)
0	0.0000	0.0000	0.0000	0.0020	-0.0010	-0.1810
$0.5 \cdot \$^{w}_{min}$	0.0000	0.0000	0.0000	0.0040	0.0000	-0.4050
$(1-\varepsilon) \cdot \$^{w}_{min}$	0.0000	0.0000	0.0000	0.0130	0.0010	-1.3000
$(1+\varepsilon) \cdot \$^{w}_{min}$	0.0000	0.0000	-0.0160	0.0130	0.0010	-1.3100

was smaller than $\$^{w}_{min}$. In both cases, when the disturbance wrench was increased to be slightly greater than $\$^{w}_{min}$ the end-effector was displaced. Thus this simulation indicates that when the cables can be modeled as ideal cables, the disturbance robustness analysis presented in this thesis produces results that are consistent with the behavior of the system.

Examination of the simulation results for the manipulator with non-ideal cables shows that there is displacement of the end-effector for each of the applied wrenches. The end-effector is displaced for an applied wrench of $\overline{0}$ due to the weight of the end-effector. We can also see that in some cases an applied load brings the end-effector closer to its desired pose (for the first pose). The displacement of the end-effector appears to be greater for the second pose, potentially indicating that a pose with low robustness may experience more displacement of the end-effector than a manipulator with high robustness. However, in order for an exact comparison of the displacements to be performed a metric of finite motions in $SE(3)$ must be chosen.

For the case of non-ideal cables, even a small disturbance wrench can change the pose of the end-effector. Thus the robustness measure developed in this thesis will not

completely describe the robustness of a pose to external disturbances for manipulators with non-ideal cables. Further research will need to be done in order to determine if a relationship can be established between the value of the robustness measure and the amount of displacement that occurs when non-ideal cables are used.

APPENDIX C

MATLAB CODE

C.1 Planar Cable Robot WFW Generation Code

This is the MATLAB code for plotting the Wrench-Feasible Workspace of a 3-cable planar manipulator as described in Section 5.5.2.3. The motor mount locations, cable attachment points (on the end-effector, with respect to the center of gravity), end-effector mass and tension limits can be specified. An arbitrary number of vertices of NW_{req} can also be specified.

```
%%%%%%%%%%%%%%%%%%%%%%%%%%%%%%%%%%%%%%%%%%%%%%%%
% Paul Bosscher
% WFW example - planar, 3 cable
% NWreq = a polygon
% produces a discretized plot of the WFW
% 6/14/04
%%%%%%%%%%%%%%%%%%%%%%%%%%%%%%%%%%%%%%%%%%%%%%%%

%   M1         M2      M3
%     \       /       /
%      \     /       /
%       \ /--------\
%        |    ee    |
%         \--------/
%
%       y |
%         L__ x

clear all
clf
warning off
```

```
% Motor locations
M1 = [-1.5,2];
M2 = [0,2];
M3 = [1.5,2];

% vectors from center of gravity (aka ee)
% to attachment points when theta = 0
c1 = [-0.3,0.0];
c2 = [0,0.05];
c3 = [0.3,0.0];

% end-effector mass*gravity
mg_ee = 20;

% mesh size
step = 0.075;

% define the required wrench set by the vertices
% (Fx, Fy, M)
F(1,:) = [0,0,0];
F(2,:) = [5,0,0];
%F(3,:) = [0,0.5,-0.5];

[vertices,void] = size(F);

% define the tension limits
tmin = 0;
tmax = 10000;

%%%%%%%%%%%%%%%%%%%%%%%%%%%%%%%%%%%%%%%%%%%%
% search through task space
% - start at bottom left of task space and
%   search -theta to +theta, left to right, bottom to top

% x limits
LeftEdge = -2;
RightEdge = 2;
sidex = step/2;

% y limits
BottomEdge = -1;
TopEdge = 2;
```

```
sidey = step/2;

% theta limits
ThetaMin = -1.5;
ThetaMax = 1.55;
sidez = step/8;
thetastep = step*2;

% initialize the ee position to the bottom left
ee = [LeftEdge, BottomEdge, ThetaMin];

hold on
for k = 1:((TopEdge-BottomEdge)/step+1)
    for j = 1:((RightEdge-LeftEdge)/step+1)
        for i = 1:((ThetaMax-ThetaMin)/thetastep+1)
            % Rotation matrix R:
            R = [cos(ee(3)) -sin(ee(3));
                 sin(ee(3))  cos(ee(3))];
            % Form the Jacobian (F = JT*t)
            Rc1 = R*(c1');
            Rc2 = R*(c2');
            Rc3 = R*(c3');
            v1 = M1' - ([ee(1),ee(2)]' + Rc1);
            v2 = M2' - ([ee(1),ee(2)]' + Rc2);
            v3 = M3' - ([ee(1),ee(2)]' + Rc3);
            v1 = v1/norm(v1);
            v2 = v2/norm(v2);
            v3 = v3/norm(v3);
            w1 = Rc1(1)*v1(2)-Rc1(2)*v1(1);
            w2 = Rc2(1)*v2(2)-Rc2(2)*v2(1);
            w3 = Rc3(1)*v3(2)-Rc3(2)*v3(1);
            JT = [v1 v2 v3;
                  w1 w2 w3];
             % Find the cable tensions and plot acceptable ee locations
            t_error = 0;
            for h = 1:vertices
                t = inv(JT)*(F(h,:)' + [0;mg_ee;0]);
                if t(1) < tmin
                    t_error = 1;
                elseif t(1) > tmax;
                    t_error = 1;
                elseif t(2) < tmin
```

```
                    t_error = 1;
                elseif t(2) > tmax;
                    t_error = 1;
                elseif t(3) < tmin
                    t_error = 1;
                elseif t(3) > tmax;
                    t_error = 1;
                end
            end
            if t_error == 0;
                plotbox(ee(1),ee(2),ee(3),sidex,sidey,sidez)
            end
            ee(3) = ee(3)+thetastep;
        end
        ee(1) = ee(1)+step;
        ee(3) = ThetaMin;
    end
    ee(2) = ee(2)+step;
    ee(1) = LeftEdge;
end
axis([LeftEdge RightEdge BottomEdge TopEdge ThetaMin ThetaMax])
xlabel('X (m)')
ylabel('Y (m)')
zlabel('Theta (rad)')
view(-20,10)
set(gca,'PlotBoxAspectRatio',[1 1 2])
```

C.2 Planar Cable Robot WFW Cross-Section Generation Code

This is the MATLAB code for generating a cross-section of the WFW of a 3-cable planar cable robot. The motor mount locations, cable attachment points (on the end-effector, with respect to the center of gravity), end-effector mass and tension limits can be specified. An arbitrary number of vertices of NW_{req} can also be specified. The analytically determined boundaries are then plotted on the same figure in order to allow comparison between the analytical and numerical results.

```
%%%%%%%%%%%%%%%%%%%%%%%%%%%%%%%%%%%%%%%%%%%%%%
% Paul Bosscher
% WFW example - planar, 3 cable
% NWreq = a polygon
%  Produces a planar section of the
%  discretized plot of the WFW and also
%  plots the analytically determined
%  boundary curves.
% 6/21/04
%%%%%%%%%%%%%%%%%%%%%%%%%%%%%%%%%%%%%%%%%%%%%%

%   M1        M2      M3
%     \      /       /
%      \    /       /
%       \ /--------\
%        |    ee    |
%         \--------/
%
%       y |
%         L__ x

clear all
clf
warning off

% Motor locations
M1 = [-1.5,2];
M2 = [0,2];
M3 = [1.5,2];

% vectors from center of gravity (aka ee)
% to attachment points when theta = 0
c1 = [-0.3,0.0];
c2 = [0,0.05];
c3 = [0.3,0.0];

% end-effector mass*gravity
mg_ee = 20;

% mesh size
```

```
step = 0.05;

% define the required wrench set by the vertices
% (Fx, Fy, M)
F(1,:) = [0,0,0];
F(2,:) = [5,0,0];
%F(3,:) = [0,0.5,-0.5];

[vertices,void] = size(F);

% define the tension limits
tmin = 0;
tmax = 100;

%%%%%%%%%%%%%%%%%%%%%%%%%%%%%%%%%%%%%%%%%%%%
% search through task space
% - start at bottom left of task space and
%   search left to right, bottom to top

% x limits
LeftEdge = -1;
RightEdge = 2.0;
sidex = step/2;

% y limits
BottomEdge = -1;
TopEdge = 2.6;
sidey = step/2;

% initialize the ee position to the bottom left
ee = [LeftEdge, BottomEdge, (pi/8)];

hold on
% Rotation matrix R:
R = [cos(ee(3)) -sin(ee(3));
     sin(ee(3))  cos(ee(3))];

for k = 1:((TopEdge-BottomEdge)/step+1)
    for j = 1:((RightEdge-LeftEdge)/step+1)
            % Form the Jacobian (F = JT*t)
            Rc1 = R*(c1');
            Rc2 = R*(c2');
```

```
            Rc3 = R*(c3');
            v1 = M1' - ([ee(1),ee(2)]' + Rc1);
            v2 = M2' - ([ee(1),ee(2)]' + Rc2);
            v3 = M3' - ([ee(1),ee(2)]' + Rc3);
            v1 = v1/norm(v1);
            v2 = v2/norm(v2);
            v3 = v3/norm(v3);
            w1 = Rc1(1)*v1(2)-Rc1(2)*v1(1);
            w2 = Rc2(1)*v2(2)-Rc2(2)*v2(1);
            w3 = Rc3(1)*v3(2)-Rc3(2)*v3(1);
            JT = [v1 v2 v3;
                  w1 w2 w3];
            % Find the cable tensions and plot acceptable ee locations
            t_error = 0;
            for h = 1:vertices
                t = inv(JT)*(F(h,:)' + [0;mg_ee;0]);
                if t(1) < tmin
                    t_error = 1;
                elseif t(2) < tmin
                    t_error = 1;
                elseif t(3) < tmin
                    t_error = 1;
                end
            end
            if t_error == 0;
                plotsquare(ee(1),ee(2),sidex,sidey)
        end
        ee(1) = ee(1)+step;
    end
    ee(2) = ee(2)+step;
    ee(1) = LeftEdge;
end
axis([LeftEdge RightEdge BottomEdge TopEdge])
xlabel('X')
ylabel('Y')

% plotting analytically determined boundaries

x = LeftEdge:step:RightEdge;
[void,length_x] = size(x);
y = BottomEdge:step:TopEdge;
[void,length_y] = size(y);
```

```
% boundaries from vertex 1

for i = 1:length_x
    y1(i) = -(3.22*x(i)^2 + 14.851*x(i) -1.214)/(-5.161*x(i)+0.574);
    y2(i) = -(1.372*x(i)^2 + 9.494*x(i)-1.082)/(-5.926*x(i)+0.574);
    y3(i) = -(4.592*x(i)^2 + 22.173*x(i)-8.423)/(-11.087*x(i));
end

plot(x,y1,'r')
plot(x,y2,'b')
plot(x,y3,'g')

% boundaries from vertex 2

% boundary 1-2
a = 3.22;
b = 16.461;
c = -5.966;
d = -5.373;
e = 1.29;
f = 5.479;

for i = 1:length_x
    y4a(i) = (-(d+c*x(i)) + sqrt((d+c*x(i))^2
             - 4*e*(a*x(i)^2+b*x(i)+f)))/(2*e);
    y4b(i) = (-(d+c*x(i)) - sqrt((d+c*x(i))^2
             - 4*e*(a*x(i)^2+b*x(i)+f)))/(2*e);
end
plot(x,y4a,'c')
plot(x,y4b,'c')

% boundary 2-3
a = 1.372;
b = 10.18;
c = -6.269;
d = -4.416;
e = 1.481;
f = 3.012;

for i = 1:length_x
    y5a(i) = (-(d+c*x(i)) + sqrt((d+c*x(i))^2
```

```
            - 4*e*(a*x(i)^2+b*x(i)+f)))/(2*e);
    y5b(i) = (-(d+c*x(i)) - sqrt((d+c*x(i))^2
            - 4*e*(a*x(i)^2+b*x(i)+f)))/(2*e);
end
plot(x,y5a,'m')
plot(x,y5b,'m')

% boundary 1-3
a = 4.592;
b = 24.469;
c = -12.235;
d = -11.087;
e = 2.772;
f = 2.466;

for i = 1:length_x
    y6a(i) = (-(d+c*x(i)) + sqrt((d+c*x(i))^2
            - 4*e*(a*x(i)^2+b*x(i)+f)))/(2*e);
    y6b(i) = (-(d+c*x(i)) - sqrt((d+c*x(i))^2
            - 4*e*(a*x(i)^2+b*x(i)+f)))/(2*e);
end
plot(x,y6a,'k')
plot(x,y6b,'k')
```

C.3 Function Code

This is the MATLAB code for the function 'plotbox'. Given a point in x-y-z, the function will plot a box centered on the point and with the lengths of the sides specified by 'sidex,' 'sidey' and 'sidez.'

```
%%%%%%%%%%%%%%%%%%%%%%%%%%%%%%%%%%%%%%%%%%%%%%%%
% plotbox function
% - for a point (x,y,z) and a box side

function void = plotbox(x,y,z,sidex,sidey,sidez)
hold on
x1 = x-sidex;
x2 = x+sidex;
y1 = y-sidey;
```

```
y2 = y+sidey;
z1 = z-sidez;
z2 = z+sidez;

X = [x1, x1, x2, x2];
Y = [y1, y2, y2, y1];
Z = [z1, z1, z1, z1];
patch(X,Y,Z,'c')
Z = [z2, z2, z2, z2];
patch(X,Y,Z,'c')
X = [x1, x1, x1, x1];
Y = [y1, y2, y2, y1];
Z = [z1, z1, z2, z2];
patch(X,Y,Z,'c')
X = [x2, x2, x2, x2];
patch(X,Y,Z,'c')
X = [x1, x2, x2, x1];
Y = [y1, y1, y1, y1];
Z = [z1, z1, z2, z2];
patch(X,Y,Z,'c')
Y = [y2, y2, y2, y2];
patch(X,Y,Z,'c')
```

The following is the MATLAB code for the function 'plotsquare'. Given a point in x-y, the function will plot a rectangle centered on the point and with the lengths of the sides specified by 'sidex' and 'sidey.'

```
%%%%%%%%%%%%%%%%%%%%%%%%%%%%%%%%%%%%%%%%%%%%%%%%%%%%
% plotsquare function
% - for a point (x,y) and a square side

function void = plotsquare(x,y,sidex,sidey)
hold on
x1 = x-sidex;
x2 = x+sidex;
y1 = y-sidey;
y2 = y+sidey;
```

```
X = [x1, x1, x2, x2];
Y = [y1, y2, y2, y1];
patch(X,Y,'c')
```

C.4 Code for Example Problem in Appendix B

The following is the MATLAB code for calculating the robustness measure and smallest static disturbance wrench for the example problem in Appendix B.

```
%%%%%%%%%%%%%%%%%%%%%%%%%%%%%%%%%%%%%%%%%%%%%%%%%%%%
% Robustness Calculation of Example Manipulator
% 11-12-04
% Paul Bosscher

% end-effector inertia matrix in moving coordinates
m = 20;
M = [m 0 0;
    0 m 0;
    0 0 1/12*m*(0.4^2+0.16^2)];

% motor locations in global coordinates
M1 = [-0.3; 0.19];
M2 = [0.4; 0.25];
M3 = [0.55; 0.25];

% cable attachment points in moving coordinates
c1 = [-0.2; 0.08];
c2 = [-0.2; 0.08];
c3 = [0.2; 0.08];

% end-effector location in global coordinates (theta = 0)
% pose 1
ee = [0.2; 0.08];
% pose 2
%ee = [0.2; -0.6];

% cable unit vectors
u1 = (M1-(c1+ee))/norm(M1-(c1+ee));
u2 = (M2-(c2+ee))/norm(M2-(c2+ee));
```

```
u3 = (M3-(c3+ee))/norm(M3-(c3+ee));

% Jacobian matrix
J = [u1 u2 u3;
    det([c1 u1]) det([c2 u2]) det([c3 u3])].';

% modified Jacobian matrices
Jmod1 = [J(2,:); J(3,:)];
Jmod2 = [J(1,:); J(3,:)];
Jmod3 = [J(1,:); J(2,:)];

% principal twists
twist_princ_1 = null(Jmod1);
twist_princ_1 = twist_princ_1*sign(twist_princ_1(2,1));

twist_princ_2 = null(Jmod2);
twist_princ_2 = twist_princ_2*sign(twist_princ_2(2,1));

twist_princ_3 = null(Jmod3);
twist_princ_3 = twist_princ_3*sign(twist_princ_3(2,1));

% intermediate space mapping
A = (1/m*M)^0.5;

% calculation of R
vel_princ_1 = A*twist_princ_1;
vel_princ_2 = A*twist_princ_2;
vel_princ_3 = A*twist_princ_3;

R1 = vel_princ_1(2,1)/norm(vel_princ_1)
R2 = vel_princ_2(2,1)/norm(vel_princ_2)
R3 = vel_princ_3(2,1)/norm(vel_princ_3)

[R,i] = min([R1 R2 R3]);
R

% calculation of smallest critical wrench
velocities = [vel_princ_1, vel_princ_2, vel_princ_3];

force_min = R*m*9.81*velocities(:,i)/norm(velocities(:,i));

wrench_min = A*force_min
```

REFERENCES

[1] Albus, J., Bostelman, R., and Dagalakis, N., "The NIST RoboCrane," *Journal of National Institute of Standards and Technology*, vol. 97, May-June 1992.

[2] Alp, A. B. and Agrawal, S. K., "Cable suspended robots: Design, planning and control," in *Proceedings of the 2002 IEEE International Conference on Robotics and Automation*, (Washington, D.C.), pp. 4275–4280, May 2002.

[3] Alp, A. B. and Agrawal, S. K., "Cable suspended robots: Feedback controllers with positive inputs," in *Proceedings of the 2002 American Control Conference*, (Anchorage, AK), pp. 815–820, May 2002.

[4] August Design, "Intelligent spreader bar." www.august-design.com.

[5] August Design, "SkyCam." www.august-design.com.

[6] August Design, "Advanced robotic crane for container handling." www.august-design.com/html/projects/prj_aacts.htm, 1999.

[7] Ball, R. S., *A Treatise on the Theory of Screws*. Cambridge University Press, 1900.

[8] Barette, G. and Gosselin, C. M., "Kinematic analysis and design of planar parallel mechanisms actuated with cables," in *Proceedings of the ASME 2000 Design Engineering Technical Conferences and Computers and Information in Engineering Conference (DETC'00)*, (Baltimore, Maryland), September 2000.

[9] Bicchi, A. and Kumar, V., "Robotic grasping and contact: A review," in *Proceedings of the 2000 IEEE International Conference on Robotics and Automation*, (San Francisco, CA), pp. 348–353, 2000.

[10] Bobrow, J., Dubowsky, S., and Gibson, J., "On the optimal control of robotic manipulators with actuator constraints," in *Proceedings of the 1983 American Control Conference*, vol. 2, pp. 782–787, 1983.

[11] Bonivento, C., Eusebi, A., Melchiorri, C., Montanari, M., and Vassura, G., "WireMan: A portable wire manipulator for touch-rendering of bas-relief virtual surfaces," in *Proceedings of the 1997 International Conference on Advanced Robotics (ICAR 97)*, (Monterrey, CA), pp. 13–18, 1997.

[12] Bosscher, P. and Ebert-Uphoff, I., "Wrench-based analysis of cable-driven robots," in *2004 IEEE International Conference on Robotics and Automation*, 2004.

[13] Bostelman, R., Albus, J., Dagalakis, N., Jacoff, A., and Gross, J., "Applications of the NIST ROBOCRANE," in *Proceedings of the 5th International Symposium on Robotics and Manufacturing*, (Maui, HI), August 14-18 1994.

[14] Bostelman, R., Jacoff, A., Proctor, F., Kramer, T., and Wavering, A., "Cable-based reconfigurable machines for large scale manufacturing," in *Proceedings of the 2000 Japan-USA Symposium on Flexible Automation*, (Ann Arbor, MI), July 2000.

[15] Bronshtein, I. N. and Semendyayev, K. A., *Handbook of Mathematics*, ch. 3. Berlin: Springer, third ed., 1998.

[16] Cheong, J.-S., Goldberg, K., Overmars, M. H., and van der Stappen, A. F., "Fixturing hinged polygons," in *Proceedings of the 2002 IEEE International Conference on Robotics and Automation*, (Washington, DC), pp. 876–881, 2002.

[17] Doty, K. L., Melchiorri, C., Schwartz, E. M., and Bonivento, C., "Robot manipulability," *IEEE Transactions on Robotics and Automation*, vol. 11, no. 3, pp. 462–468, 1995.

[18] Ebert-Uphoff, I. and Voglewede, P. A., "On the connections between cable-driven robots, parallel robots and grasping," in *2004 IEEE International Conference on Robotics and Automation*, 2004.

[19] Fattah, A. and Agrawal, S. K., "Design of cable-suspended planar parallel robots for an optimal workspace," in *Proceedings of the Workshop on Fundamental Issues and Future Research Directions for Parallel Mechanisms and Manipulators*, (Quebec City, Quebec, Canada), pp. 195–202, October 2002.

[20] Fattah, A. and Agrawal, S. K., "Workspace and design analysis of cable-suspended planar parallel robots," in *Proceedings of the ASME 2002 Design Engineering Technical Conferences and Computer and Information in Engineering Conference (DETC '02)*, (Montreal, Canada), pp. 1–9, October 2002.

[21] Gallina, P. and Rosati, G., "Manipulability of a planar wire driven haptic device," *Mechanism and Machine Theory*, pp. 215–228, 2002.

[22] Gorman, J. J., Jablokow, K. W., and Cannon, D. J., "The cable array robot: Theory and experiment," in *Proceedings of the 2001 IEEE International Conference on Robotics and Automation*, (Seoul, Korea), pp. 2804–2810, May 2001.

[23] Gouttefarde, M. and Gosselin, C. M., "On the properties and the determination of the wrench-closure workspace of planar parallel cable-driven mechanisms," in *Proceedings of the ASME 2004 Design Engineering Technical*

Conferences and Computers and Information in Engineering Conference (DETC 04), (Salt Lake City, UT), pp. 1–10, September-October 2004.

[24] Howard, W. S. and Kumar, V., "Modeling and analysis of the compliance and stability of enveloping grasps," in *Proceedings of the 1995 IEEE International Conference on Robotics and Automation*, 1995.

[25] Howard, W. S. and Kumar, V., "On the stability of grasped objects," *IEEE Transactions on Robotics and Automation*, vol. 12, pp. 904–917, December 1996.

[26] http://www.cfinflight.com/pages/skycam.asp.

[27] http://www.ent.ohiou.edu/ bobw/image/CDDR_RV.jpg.

[28] http://www.ie.psu.edu/labs/vtrl/carp.html.

[29] http://www.isd.mel.nist.gov/projects/robocrane/.

[30] http://www.panasonic.com/business/provideo/news/news04_000.asp.

[31] http://www.ritsumei.ac.jp/se/rm/ari-kawa/result/wire.html.

[32] Huey, J., "Dynamics and vibration control of large area manipulators," Master's thesis, Georgia Institute of Technology, Atlanta, GA, July 2003.

[33] Jeong, J.-W., Kim, S.-H., and Kwak, Y.-K., "Design and kinematic analysis of the wire parallel mechanism for a robot pose measurement," in *Proceedings of the 1998 IEEE International Conference on Robotics and Automation*, vol. 4, pp. 2941 – 2946, May 16-20 1998.

[34] Kawamura, S., Choe, W., Tanaka, S., and Pandian, S., "Development of an ultrahigh speed robot FALCON using wire drive system," in *Proceedings of the 1993 IEEE/ICRA International Conference on Robotics and Automation*, vol. 1, (Nagoya, Japan), pp. 215–220, May 1995.

[35] Kawamura, S. and Ito, K., "A new type of master robot for teleoperation using radial wire drive system," in *Proceedings of the 1993 IEEE/RSJ International Conference on Intelligent Robots and Systems*, (Yokohama, Japan), pp. 55–60, July 1993.

[36] Kino, H., "Principle of orthogonalization for completely restrained parallel wire driven robot," in *Proceedings of the 2003 IEEE/ASME International Conference on Advanced Intelligent Mechatronics (AIM 2003)*, pp. 509–514, 2003.

[37] Kiss, B., Levine, J., and Mullhaupt, P., "A simple output feedback pd controller for nonlinear cranes," in *Proceedings of the 39th IEEE Conference on Decision and Control*, (Sydney, Australia), pp. 5097–5101, December 2000.

[38] Kobayashi, T. and Takahashi, Y., "Vibration control for two-dimensional wire driven positioning robot," in *Proceedings of the Japanese Society of Instrumentation and Control Engineering Annual Conference*, pp. 869–874, July 1998.

[39] Kurtz, R. and Hayward, V., "Dexterity measure for tendon actuated parallel mechanisms," in *Proceedings of the 1991 International Conference on Advanced Robotics (ICAR 91)*, vol. 2, pp. 1141 – 1146, June 19-22 1991.

[40] Lin, Q. and Burdick, J. W., "Objective and frame-invariant kinematic metric functions for rigid bodies," *International Journal of Robotics Research*, vol. 19, pp. 612–625, June 2000.

[41] Lipkin, H. and Duffy, J., "Sir Robert Stawell Ball and methodologies of modern screw theory," *Journal of Mechanical Engineering Science: Proceedings of the Institution of Mechanical Engineers, Part C*, vol. 216, pp. 1–11, 2002. Special Issue Paper.

[42] Maeda, K., Tadokoro, S., Takamori, T., Hiller, M., and Verhoeven, R., "On design of a redundant wire-driven parallel robot WARP manipulator," in *Proceedings of the 1999 IEEE International Conference on Robotics and Automation*, (Detroit, Michigan), pp. 895–900, May 1999.

[43] Martindale, S., Dawson, D., Zhu, J., and Rahn, C., "Approximate nonlinear control for a two degree of freedom overhead crane: Theory and experimentation," in *Proceedings of the 1995 American Control Conference (ACC 95)*, (Seattle, Washington), pp. 301–305, June 1995.

[44] Mason, M. T., *Mechanics of Robotic Manipulation*. Cambridge, MA: MIT Press, 2001.

[45] Mason, M. T. and Salisbury Jr., J. K., *Robot Hands and the Mechanics of Manipulation*. Cambridge, MA: MIT Press, 1985.

[46] Melchiorri, C., Montanari, M., and Vassura, G., "Control strategies for a defective, wire-based, haptic interfaces," in *Proceedings of the 1997 IEEE/RSJ International Conference on Intelligent Robots and Systems (IROS 97)*, vol. 1, (Grenoble), pp. 181–187, Sept. 7-11 1997.

[47] Melchiorri, C. and Vassura, G., "A performance index for under-actuated, multi-wire, haptic interfaces," in *Proceedings of the 1998 IEEE International Conference on Robotics and Automation*, (Leuven, Belgium), pp. 1026–1031, May 1998.

[48] Merlet, J.-P., *Parallel Robots*. Kluwer Academic Publishers, 2000.

[49] Ming, A. and Higuchi, T., "Study on multiple degree-of-freedom positioning mechanism using wires (part 1) - concept, design and control," *International*

Journal of the Japanese Society for Precision Engineering, vol. 28, pp. 131–138, June 1994.

[50] Ming, A. and Higuchi, T., "Study on multiple degree-of-freedom positioning mechanism using wires (part 2) - development of a planar completely restrained positioning mechanism," *International Journal of the Japanese Society for Precision Engineering*, vol. 28, pp. 235–242, September 1994.

[51] Mishra, B., Schwartz, J. T., and Sharir, M., "On the existence and synthesis of multifinger positive grips," *Algorithmica*, vol. 2, pp. 541–558, 1987.

[52] Morizono, T., Kurahashi, K., and Kawamura, S., "Realization of a virtual sports training system with parallel wire mechanism," in *Proceedings of the 1997 IEEE International Conference on Robotics and Automation*, (Albuquerque, New Mexico), pp. 3025–3030, April 1997.

[53] Murison, M. A., "Stretching of a cable with a weight attached." http://arnold.usno.navy.mil/murison/papers/Notes/CableStretch/CableStretch.pdf, May 1999.

[54] Murray, R. M., Li, Z., and Sastry, S. S., *A Mathematical Introduction to Robotic Manipulation*. Boca Raton: CRC Press, 1994.

[55] Nguyen, V.-D., "Constructing force-closure grasps," *International Journal of Robotics Research*, vol. 7, no. 3, pp. 3–16, 1988.

[56] Okamura, A. M., Smaby, N., and Cutkosky, M. R., "An overview of dexterous manipulation," in *Proceedings of the 2000 IEEE International Conference on Robotics and Automation*, (San Francisco, CA), pp. 255–262, 2000.

[57] Osumi, H., Utsugi, Y., and Koshikawa, M., "Development of a manipulator suspended by parallel wire structure," in *Proceedings of the 2000 IEEE/RSJ International Conference on Intelligent Robots and Systems (IROS 2000)*, pp. 498–503, 2000.

[58] Papastavridis, J. G., *Analytical Mechanics: A Comprehensive Treatise on the Dynamics of Constrained Systems: for Engineers, Physicists, and Mathematicians*. Oxford University Press, 2002.

[59] Park, F., "Distance metrics on the rigid-body motions with applications to mechanism design," *Transactions of the ASME Journal of Mechanical Design*, vol. 117, pp. 48–54, March 1995.

[60] Riechel, A. T., "Design and control of cable robots with moving attachment points," Master's thesis, Georgia Institute of Technology, Atlanta, GA, April 2004.

[61] Riechel, A. T. and Ebert-Uphoff, I., "Force-feasible workspace analysis for underconstrained, point-mass cable robots," in *2004 IEEE International Conference on Robotics and Automation*, 2004.

[62] Rimon, E. and Burdick, J. W., "Mobility of bodies in contact - part I: A 2nd-order mobility index for multiple-finger grasps," *IEEE Transactions on Robotics and Automation*, vol. 14, pp. 696–708, October 1998.

[63] Roberts, R. G., Graham, T., and Trumpower, J. M., "On the inverse kinematics and statics of cable-suspended robots," in *Proceedings of the IEEE International Conference on Systems, Man, and Cybernetics*, pp. 4291 – 4296, October 1997.

[64] Shen, Y., Osumi, H., and Arai, T., "Manipulability measures for multi-wire driven parallel mechanisms," in *Proceedings of the IEEE International Conference on Industrial Technology*, pp. 550–554, December 1994.

[65] Shen, Y., Osumi, H., and Arai, T., "Set of manipulating forces in wire driven systems," in *Proceedings of the 1994 IEEE/RSJ/GI International Conference on Intelligent Robots and Systems (IROS 94)*, vol. 3, pp. 1626–1631, September 1994.

[66] Shiang, W.-J., Cannon, D., and Gorman, J., "Dynamic analysis of the cable array robotic crane," in *Proceedings of the 1999 IEEE International Conference on Robotics and Automation*, (Detroit, MI), pp. 2495–2500, May 1999.

[67] Tadokoro, S., Murao, Y., Hiller, M., Murata, R., Kohkawa, H., and Matsushima, T., "A motion base with 6-DOF by parallel cable drive architecture," *IEEE/ASME Transactions on Mechatronics*, vol. 7, pp. 115–123, June 2002.

[68] Tadokoro, S., Verhoeven, R., Hiller, M., and Takamori, T., "A portable parallel manipulator for search and rescue at large-scale urban earthquakes and an identification algorithm for the installation in unstructured environments," in *Proceedings of the IEEE/RSJ International Conference on Intelligent Robots and Systems*, pp. 1222–1227, 1999.

[69] Takahashi, Y. and Tsubouchi, O., "Tension control of wire suspended mechanism and application to bathroom cleaning robot," in *Proceedings of the 39th SICE Annual Conference*, (Iizuka, Japan), pp. 143–147, July 2000.

[70] Thomas, F., Ottaviano, E., Ros, L., and Ceccarelli, M., *Advances in Robot Kinematics*, ch. Uncertainty Model and Singularities of 3-2-1 Wire-Based Tracking Systems, pp. 107–116. Kluwer Academic Publishers, 2002.

[71] Thompson, C. J. and Campbell, Jr., P. D., "Tendon suspended platform robot." U.S. Patent No. 5,585,707, 1996.

[72] Trinkle, J. C., "On the stability and instantaneous velocity of grasped frictionless objects," *IEEE Transactions on Robotics and Automation*, vol. 8, pp. 560–572, October 1992.

[73] Trinkle, J. C., Farahat, A., and Stiller, P., "Second-order stability cells of a frictionless rigid body grasped by rigid fingers," in *Proceedings of the 1994 IEEE International Conference on Robotics and Automation*, pp. 2815 – 2821, 1994.

[74] Trinkle, J. C., Farahat, A., and Stiller, P., "First-order stability cells of active multi-rigid-body systems," *IEEE Transactions on Robotics and Automation*, vol. 11, pp. 545–557, August 1995.

[75] Verhoeven, R. and Hiller, M., "Estimating the controllable workspace of tendon-based stewart platforms," in *Proceedings of the ARK '00 7th International Symposium on Advances in Robot Kinematics*, (Protoroz, Slovenia), pp. 277–284, 2000.

[76] Verhoeven, R. and Hiller, M., "Tension distribution in tendon-based stewart platforms," in *Proceedings of ARK '02 8th International Symposium on Advances in Robot Kinematics*, (Caldes de Malavella, Spain), 2002.

[77] Verhoeven, R., Hiller, M., and Tadokoro, S., "Workspace of tendon-driven stewart platforms: Basics, classification, details on the planar 2-dof class," in *Proceedings of the 4th International Conference on Motion and Vibration Control*, vol. 3, pp. 871–876, 1998.

[78] Verhoeven, R., Hiller, M., and Tadokoro, S., "Workspace, stiffness, singularities and classification of tendon-driven stewart platforms," in *Proceedings of the ARK '98 6th International Symposium on Advances in Robot Kinematics*, (Strobl, Austria), pp. 105–114, 1998.

[79] Webster, R., *Convexity*. Oxford: Oxford University Press, 1994.

[80] Weisstein, E., ed., *CRC Concise Encyclopedia of Mathematics*. Boca Raton, FL: Chapman and Hall/CRC Press, second ed., 2003.

[81] Williams II, R. L., "Cable-suspended haptic interface," *International Journal of Virtual Reality*, vol. 3, no. 3, pp. 13–21, 1998.

[82] Williams II, R. L. and Gallina, P., "Planar cable-direct-driven robots: Design for wrench exertion," *Journal of Initelligent and Robotic Systems*, vol. 35, pp. 203–219, 2002.

[83] Williams II, R. L. and Gallina, P., "Translational planar cable-direct-driven robots," *Journal of Initelligent and Robotic Systems*, vol. 37, pp. 69–96, 2003.

[84] Yamamoto, M., Yanai, N., and Mohri, A., "Trajectory control of incompletely restrained parallel-wire-suspended mechanism based on inverse dynamics," *IEEE Transactions on Robotics*, vol. 20, pp. 840–850, October 2004.

[85] Yanai, N., Yamamoto, M., and Mohri, A., "Inverse dynamics analysis and trajectory generation of incompletely restrained parallel wire mechanisms," in *Proceedings of the 2001 IEEE International Conference on Robotics and Automation*, (Seoul, Korea), pp. 3489–3494, May 2001.

[86] Yanai, N., Yamamoto, M., and Mohri, A., "Anti-sway control for wire-suspended mechanism based on dynamics compensation," in *Proceedings of the 2002 IEEE International Conference on Robotics and Automation*, (Washington, D.C.), pp. 4287–4292, May 2002.

[87] Yang, L.-F., Mikulas Jr., M. M., and Chiou, J.-C., "Stability and 3-D spatial dynamic analysis of a three-cable crane," in *Proceedings of the 1992 AIAA/ASME/ASCE/AHS/ASC Structures, Structural Dynamics, and Materials Conference*, (Dallas, TX), pp. 2069–2076, April 13-15 1992.

[88] Zheng, Y.-Q. and Liu, X.-W., "Force transmission index based workspace analysis of a six DOF wire-driven parallel manipulator," in *Proceedings of ASME 2002 Design Engineering Technical Conferences and Computer and Information in Engineering Conference (DETC'02)*, (Montreal, Canada), pp. 1–8, 2002.